



**UNIVERSITÀ
DI TRENTO**

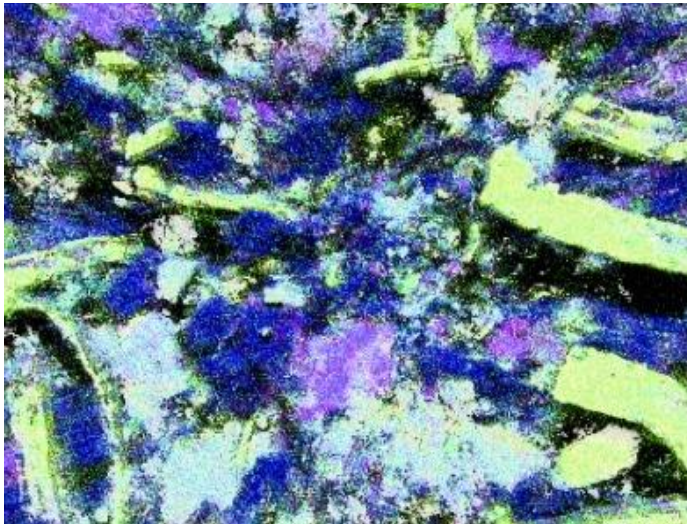
**Dipartimento di
Ingegneria Industriale**

XXXII cycle

Doctoral School in Materials, Mechatronics
and Systems Engineering

Development of novel eco-friendly friction materials for disc brake systems

Mara Leonardi



3rd April 2020

Development of novel eco-friendly friction materials for disc brake systems

Mara Leonardi

E-mail: mara.leonardi@unitn.it

Approved by:

Prof. Stefano Gialanella, Supervisor
Department of
Industrial Engineering
University of Trento, Italy.

Prof. Giovanni Straffelini,
Supervisor
Department of
Industrial Engineering
University of Trento, Italy.

Ph.D. Commission:

Prof. Massimo Pellizzari
Department of Industrial
Engineering
University of Trento, Italy.

Prof. Gian Luca Garagnani,
Department of Engineering
University of Ferrara, Italy.

Prof. Vlastimil Matějka,
Department of Chemistry
*Technical University of Ostrava, Czech
Republic.*

University of Trento,
Department of Industrial Engineering

3rd April 2020

**University of Trento - Department of
Industrial Engineering**

Doctoral Thesis

Mara Leonardi - 2020

Published in Trento (Italy) – by University of Trento

I hear. *I forget.*
I see. *I remember.*
I do. *I understand.*

Confucius

Abstract

Due to new environmental regulations, the demand for brake systems producing low polluting emissions and keeping high performance, is increasing. Therefore, a reduction in the toxic substances contained in brake friction materials is required that still meets all applicable safety standards and retaining properties such as low wear, high temperatures resistance, friction coefficient stability and consistency. Among the various ingredients used in formulations, copper has recently become the subject of different regulations on brake pad materials and will be reduced, or even prohibited, in the coming years. Recent studies have found that brake pads are major contributors to the deposit of copper in rivers and lakes, and this has a toxic impact on the environment. This metal is currently added in brake material formulations because of its good physical properties and its contribution to the formation of a uniform and stable friction layer. Its characteristics make it a constituent that is not easy to replace and an adequate substitute covering all the roles of copper has not been found as yet.

The present research aims at developing, producing and testing new formulations for brake pads without copper. A relatively wide range of friction materials was investigated, in order to understand the role that selected constituents have in friction and wear behaviour.

In the first place, an investigation on the role of copper in friction materials was performed. The study was followed by the selection of a suitable replacement for this constituent in the formulation. To do so, different friction components were studied. Additionally, other aspects relating to friction materials, such as the deterioration of the binder, were subject of investigation.

The novel formulations, produced starting from commercially available compositions, were ranked in terms of wear and friction behaviour by means of a pin-on-disc tribometer. Cylindrical specimens were produced directly from powders, so that constituents could be easily modified based on the test outcome. This is a very effective method to study the role of individual constituents in the

mixture, considering the relatively small amount of each specific composition to be prepared and the ease of processing it. In order to identify the principal wear mechanisms and their dependence on material properties and test conditions, the worn materials were analysed via scanning electron microscopy (SEM) techniques and Energy Dispersive X-Ray Spectroscopy (EDXS).

Part of the acquired knowledge from the first part of the work was used in the initial stages of the ECOPADS project (the project started during the doctoral period) to develop and manufacture real brake pads that were tested on brake dynamometers and evaluated in terms of both performance and emissions.

Contents

Variables and Abbreviations	i
1. Introduction to disc brake systems	1
1.1 General Overview	1
1.1.1 Brake Caliper	2
1.1.2. Brake Discs	3
1.1.3 Brake Pads	5
1.2 Tribology in disc-pad system	5
1.2.1 General overview of friction and wear	6
1.2.2 Role of the temperature	9
1.2.3 Tribological interface	11
2. Friction materials for brake pads.....	17
2.1 Friction material characteristics	17
2.1.1 Organic friction materials.....	17
2.2 Brake materials.....	18
2.1.1 Reinforcements	20
2.1.2 Friction modifiers	22
2.1.3 Fillers.....	25
2.1.4 Binders	26
2.3 New trends.....	28
2.3.1 Legislations	28
2.3.2 Copper	30
2.3.4 Wear particle emissions.....	32
2.4 Eco-friendly formulations	33
2.4.1 ECOPADS project.....	34
3. Materials and methodology.....	37
3.1 Materials.....	37
3.1.1 Master-batches	37
3.1.2 Constituents investigated	39
3.1.3 ECOPADS materials	47
3.1.4 Grey cast iron discs	48
3.2 Pin production.....	50
3.3 Experimental procedure.....	51

3.3.1	Pin-on-disc tests.....	51
3.3.2	Dynamometer tests	56
3.4	Characterization tools.....	60
3.4.1	Scanning Electron Microscopy (SEM) and Energy Dispersive X-Ray Spectroscopy (EDXS).....	60
3.4.2	X-ray diffractometer (XRD).....	61
3.4.3	Profilometer	62
3.4.5	Shore D Hardness.....	62
3.4.6	Compression tests	62
3.4.7	Helium gas pycnometer	62
3.4.8	Thermogravimetric (TG) analyses	63
3.4.9	Fourier-transform infrared spectroscopy (FT-IR)	63
3.4.10	Differential scanning calorimetry (DSC)	64
4.	Evaluation of pin properties.....	65
4.1	Validation of the pin production	65
4.2	Case study: pin density	66
4.2.1	Effect of density on mechanical behaviour	67
4.2.2	Effect of density on tribological properties	71
4.2.3	Main results.....	72
5.	Copper substitution	73
5.1	Copper	73
5.1.1	Background	73
5.1.2	Samples.....	74
5.1.3	Testing and characterization.....	74
5.1.4	Main results.....	78
5.2	Steel fibres.....	79
5.2.1	Background	79
5.2.2	Samples.....	79
5.2.3	Testing and characterization.....	79
5.2.4	Main results.....	83
5.3	Barite.....	84
5.3.1	Background	84
5.3.2	Samples.....	84
5.3.3	Testing and characterization.....	85
5.3.4	Main results.....	93
5.4	Cu-free formulation.....	93

5.4.1	Samples.....	93
5.4.2	Testing and characterization.....	94
5.4.3	Main results.....	98
5.5	Commercial Cu-free friction materials.....	98
5.5.1	Cu-free master-batch.....	98
5.5.2	Cu-free pads.....	100
5.5.3	Main results.....	103
6.	An eco-friendly formulation	105
6.1	Samples	105
6.2	Testing and validation.....	106
6.2.1	Pin-on-disc tests.....	106
6.2.2	Dyno tests.....	112
6.2.3	Car test.....	113
6.3	Final considerations.....	114
7.	Different constituents in FMs	115
7.1	Graphite.....	115
7.1.1	Background	115
7.1.2	Samples.....	116
7.1.3	Testing and characterization.....	117
7.1.4	Concentration of graphite	126
7.1.5	Main results.....	128
7.2	Mineral fibres.....	129
7.2.1	Background	129
7.2.2	Samples.....	129
7.2.3	Testing and characterization.....	130
7.2.4	Main results.....	132
7.3	Phenolic resin	133
7.3.1	Background	133
7.3.2	Degradation	133
7.3.3	Main results.....	136
8.	Conclusions and future perspectives.....	139
	References.....	143
	Appendices.....	159
I.	List of publications.....	161
II.	Participation to Workshops, Schools and Congresses	163
III.	Acknowledgments.....	165

Variables and Abbreviations

Symbol	Description	Unit
μ	Coefficient of friction	-
K_a	Specific wear coefficient	m^2/N
P	Contact pressure	MPa
v	Sliding velocity	m/s

Abbreviation	Description
FM s	Friction Material(s)
PoD	Pin on Disc test
RT	Room Temperature (<100°C)
HT	High Temperature (300°C or 400°C)
FL	Friction Layer
PP	Primary Plateaus
SP	Secondary Plateaus
SEM	Scanning Electron Microscopy
EDXS	Energy dispersive X-ray spectroscopy

Chapter 1

1. Introduction to disc brake systems

1.1 General Overview

A brake is a mechanical device which hinders motion. Automotive brakes are designed to slow and stop a vehicle by transforming kinetic (motion) energy into heat energy. As the brake linings get in contact with the drums/rotors, they create friction which produces heat. The heat budget, absorbed and dissipated by the brake parts, is proportional to the vehicle speed, the weight of the vehicle, and the quickness of the stop.

Brakes not only have to be capable of stopping a vehicle but must stop it in as short a distance as possible. The modern high-speed vehicles require well designed and powerful brakes. They must be able to decelerate a vehicle at a faster rate than the engine can accelerate, and they must control a greater power than that developed by the engine. There are many types of brake system designs in use on vehicles. Regardless of the design, all systems require the use of rotating and non-rotating units. Each of these units houses one of the braking surfaces, which, when forced together, produce the friction of braking action. Two major braking systems are used in automobiles: drum brakes and disc brakes.

A drum brake unit consists of two brake shoes mounted on a stationary backing plate. When the brake pedal is pressed, a hydraulically activated wheel cylinder pushes the shoes out to contact a rotating drum which creates friction and slows the vehicle. As the pedal is released, return springs retract the shoes to their original position.

A disc brake (Fig. 1.1) has a disc that turns with the wheel. The disc is straddled by a caliper, hosting small hydraulic pistons operated by pressure developed by the master cylinder (a device that converts force, from the driver's foot, into hydraulic pressure). The pistons press on friction pads that clamp against the disc from each side to slow or stop it.

Most modern cars have disc brakes on front wheels and drum brakes on rear wheels and some wheels have disc brakes on all four wheels.

The main advantages of disc brakes over drum brakes include:

- better fade resistance;
- self-adjustment capability;
- better cooling;
- water and dirt resistant;
- less maintenance;
- greater surface area for a given weight of brake.

Moreover, a recent investigation suggests that frictional behaviour of disc brake is more reliable than drum brake, which presents sudden variations in friction coefficient [1].

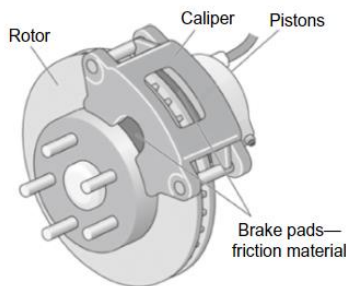


Fig. 1.1. Sliding disc brake [2].

1.1.1 Brake Caliper

Disc brake calipers contain brake pads and hydraulic pistons that press the pads against the rotor surfaces. There are different kinds of calipers that differ in material, structural design and piston arrangement. The two-basic type of calipers are: fixed and floating (Fig. 1.2). The first one has one or two pistons on both sides of the disc, moving relative to the disc, both pistons move and push the brake pads. Whereas a floating

caliper usually has one piston on one side of the disc only, it is mounted in a way that the piston moves the inner brake pads. When the pad contacts the disc, caliper moves in the opposite direction so that also the outer pad contact the disc.

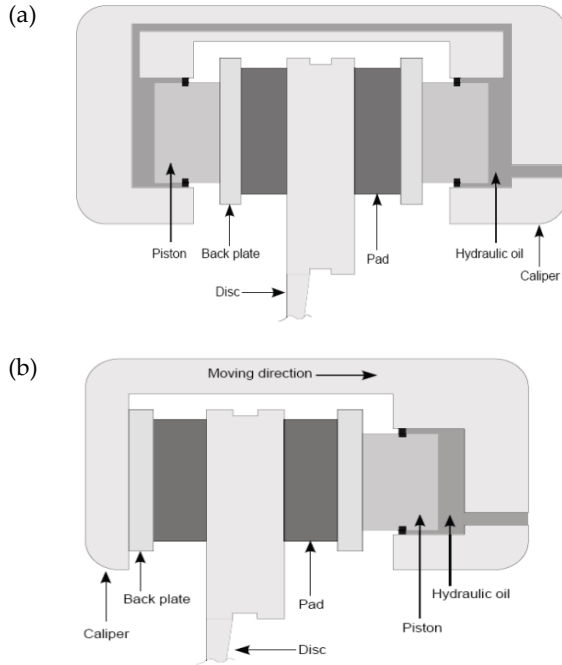


Fig. 1.2. Schematic representation of a fixed (a) and floating (b) caliper [3].

1.1.2. Brake Discs

Brake disc is fixed to the axle, so it rotates with the same speed as the wheel. An efficient brake should be able to bear thermal fatigue and should absorb and dissipate, as soon as possible, the heat generated during braking otherwise the temperature of the disc might rise and affect the performance of a disc brake.

Brake discs could be solid or ventilated brake discs (Fig. 1.3). A solid brake disc consists of a single solid disc, whereas in a ventilated disc, there are two annular discs separate with vanes that provide a passage for the air to flow. This design is to reduce the risk of brake fade in demanding applications. Different configurations of vanes are used in

ventilated brake discs, each configuration gives a unique airflow pattern. Both designs, solid and ventilated, are constructed with or without a mounting bell, useful to increase the distance from the friction surface to axle (Fig. 1.3).

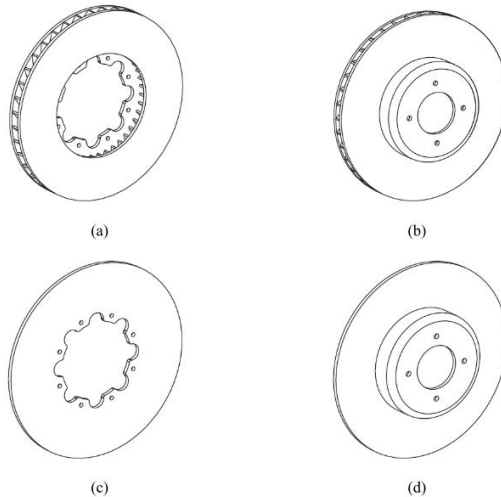


Fig. 1.3. Schematic representation of ventilated brake discs without (a) and with bell (b), and solid brake discs without (c) and with bell (d) [3].

Brake discs are typically made of grey cast iron with a predominantly pearlitic matrix [4]. Gray cast iron has good thermal conductivity due to the graphite phase, which is an excellent thermal conductor. Moreover, this material has a good castability, machinability and lower cost.

To reduce the weight further, lighter materials with suitable properties are used in specific applications. Alternative materials to cast iron are aluminium-based metal matrix composite that offer good wear and corrosion resistance, the main drawbacks are the higher coefficient of thermal expansion and limited temperature resistance as compared to cast iron [5]. Another choice for brake discs are ceramic matrix composites [6] based on carbon fibres and matrices of silicon carbide. They are being used in high performance automobiles, but their prices are currently very high as compared to cast iron discs.

1.1.3 Brake Pads

A brake pad is an assembly of the friction material mounted on a backing plate (usually a steel plate). In order to attach the friction material to the steel plate adhesive bonding or mechanical retention are used.

In addition, pads present other different parts each responsible for a specific task [7]. The piston in the brake caliper does not bear directly against the brake pad but there is a laminate of metal and viscoelastic material, the shim, attached on the backing plate. The shim is supposed to dampen the vibrations in the disc-pad system. Moreover, an additional layer of material, the underlayer, is placed between friction material and backplate with the aim of thermally insulating the backing plate, limiting the transmission of vibration and noise.

A brake pad can also have slots and chamfers on its face (Fig. 1.4), mainly to avoid cracks and to reduce squeal noise [8].

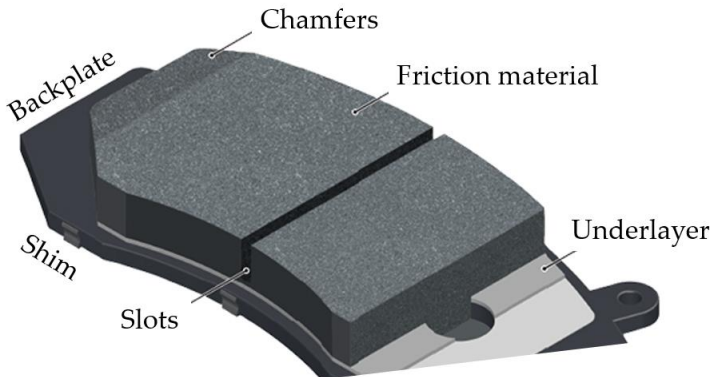


Fig. 1.4. Schematic representation of a brake pad.

1.2 Tribology in disc-pad system

The transformation of the kinetic energy of a vehicle into thermal energy occurs at the interface of pad and disc in air. This represents a tribological system, characterised by the frictional force and wear of the contacting surfaces.

The sliding surfaces are made of different materials, in fact friction materials are a mix of different constituents (metals, ceramics,

polymers). This makes the understanding of the tribological phenomena very complex. Tribological properties are altering to oxygen and humidity that react with elements of the sliding surfaces. Another important issue is the roughness. The surfaces of friction materials and discs are rough, and their conditions evolve during friction due to several intervening processes: plastic deformation, fractures, wear, chemical reactions and material transfer.

1.2.1 General overview of friction and wear

Friction exists when two contacting surfaces are involved in a relative sliding motion or at least are trying to slide one against another. The resistance to sliding is called friction force. This force acts on the contact points of sliding surfaces in a direction opposite to movement. The surface of a solid contains irregularities in the form of protrusions (asperities) and depressions (valleys). When one solid is pressed against another one, contact occurs at discrete contact spots. The sum of the areas of all contact spots is the real area of contact and this is usually only a small fraction of the apparent area of contact.

Friction is a complex phenomenon results of a simultaneous action of various mechanisms at different hierarchy and scale levels (molecule, asperity, surface). The main mechanisms of dry friction are: adhesion, deformation of asperities, fracture of asperities, the so-called ratchet and third-body mechanisms [9].

These various mechanisms result in a dissipative process, which can often be characterized by only one single parameter, the coefficient of friction (μ), given by the following equation (Eq. 1.1):

$$\mu = F_t/F_n \quad (\text{Eq. 1.1})$$

where F_t is the tangential force and F_n is the normal force.

It is important distinguish between the coefficient of static friction (μ_s) and the coefficient of dynamic friction (μ_d). In the first case, the tangential force is insufficient to cause motion, it is clear in this case (through application of Newton's First Law) that the friction force at the interface must be exactly equal and opposite to tangential force.

Whereas, in the other situation the tangential force is sufficient to cause sliding. In general, μ_s is greater than μ_d .

Coefficient of friction may depend on F_n and on the properties of the mating surfaces, while it is independent from the nominal area of contact; whereas it can increase with an increase of the real area of contact [9]. Dynamic friction may also depend on the sliding speed.

Dry friction causes the wear of the surfaces of the friction partners. The characteristics of the relative motion between the bodies in contact define the wear processes. If the bodies slide one over the other, the resulting wear process is sliding wear. Then there is rolling wear if the bodies roll one over the other, rolling-sliding wear if there are both types of motion and others.

A wear process is determined by the action of a predominant wear mechanisms [10][11]: adhesive, abrasive, tribo-oxidative and wear by contact fatigue.

Adhesive wear takes place when two bodies are sliding one over each other, and fragments are pulled off one surface to adhere to the other. This wear occurs because of the adhesive bond, at the contact points, is stronger than the cohesive bond of the weaker material of the pair. Normally, adhesion occurs when two similar chemical composition metals are in contact or contact surfaces are free from oxide layer.

Abrasive wear occurs due to hard particles, slides on a softer surface, and ploughs a series of grooves in it (two-body type). Three-body abrasion is also possible, in which the hard particles, at least 20–30 % greater than that of the weakest surface, are trapped between two contacting surfaces and are quite free to rotate.

Tribo-oxidative wear is given by a combination of oxidative and mechanical actions at the contacting asperities. It occurs in an environment that contains oxygen. A surface oxide layer acts as a solid lubricant and reduces friction and wear.

Wear by contact fatigue occurs during repeated sliding or rolling over track. This type of wear is a typical fatigue failure. The repeated loading and unloading cycles may induce the formation of cracks, which could result in the break-up of the surface with the formation of large fragments.

To compare different materials the Archard's wear law is used to correlate data from wear experiments. According to this law wear rate is proportional to the normal force and sliding distance.

The Archard relationship is used to describe the wear volume loss for adhesive wear in ductile materials, it is expressed as (Eq. 1.2) [12]:

$$W = \frac{V}{s} = K_{ad} * A_r = K_{ad} * \frac{F_n}{H} \quad (\text{Eq. 1.2})$$

where V is the wear volume, K_{ad} the wear coefficient for adhesive wear, F_n the nominal contact force, s the sliding distance of the two surfaces and H the hardness of the softer material.

The law could be generalized in order to describe the wear behaviour in the case of dry sliding as (Eq. 1.3):

$$W = K * \frac{F_n}{H} = K_a * F_n \quad (\text{Eq. 1.3})$$

where K_a is the specific wear coefficient. The value of K_a is representative of the prevailing wear mechanism. The wear of the components is mild if the main mechanism is the tribo-oxidative wear, severe if the adhesive and/or abrasive wear are predominant. The transition between the mechanisms is influenced by the loading conditions that generate different contact temperature.

1.2.1.2 Typical sliding conditions

The brake discs are typically made of pearlitic grey cast iron, whereas the friction pads are usually made of organic friction materials. The thermal conductivity of the disc (about 52 W/mK) is higher than the conductivity of the pads (about 1 - 2 W/mK), so most of the frictional heat is dissipated by the rotating disc. The temperature reached on the surface of the breaking components depends from many factors, like the material composition, the geometry of the system and the braking conditions. These factors also influence the prevailing wear mechanism at the disc-pad interface, that can be adhesive, abrasive and tribo-oxidative. The abrasive and the adhesive wear are favoured

by low contact stresses and low sliding velocities while the tribo-oxidation is promoted by moderate loads and high sliding speeds. In Table 1.1 are reported the typical sliding conditions in an automotive brake system.

Table 1.1. Typical automotive braking conditions [13].

	Braking condition	
	Normal (urban)	Heavy (sport drives)
Decelerations during braking	< 2 m/s ²	> 5 m/s ²
Nominal contact pressure	0.2 – 1.5 MPa	1.1 – 4 MPa
Average surface temperature	< 300°C	> 300°C
Pad wear, K_a	5*10 ⁻¹⁵ – 4*10 ⁻¹⁴ m ² /N	↑ with T
Coefficient of friction, μ	0.35 – 0.55	↓ with T

1.2.2 Role of the temperature

Temperature is one of the main parameters that influence the wear of the pad/disc system.

In general, the heat generated from the sliding between two surfaces pressed together, i.e. pads and disc, can be evaluated as (Eq. 1.4) [14]:

$$q = \frac{\mu * F * v}{A_n} \quad (\text{Eq. 1.4})$$

Where F is the normal force, v the relative velocity, μ the coefficient of friction and A_n the nominal contact area. The heat flows into the two contacting solids, partitioned between them in a way which depends on their geometry and thermal properties.

Ashby et al. [14] studied and identified two characteristic temperatures in a sliding system:

- the average surface temperature (T_s), T of the regions right beneath the asperities; T_s decreases across the bulk until reaching the starting temperature of the body (T₀);

- the flash temperature (T_f), high-localized temperature generated at the asperity tips.

The flash temperature is usually higher than T_s since the average radius of the asperities is small and can strongly influence the mechanical behaviour of concerned materials. Kennedy et al. [15] reports that such temperature can be responsible for oxide formation, spot weld, thermoelastic instabilities, thermomechanical failure, and wear.

The flash temperature is difficult to predict. Ashby et al. [14] propose a relationship (Eq. 1.4) for the estimation of the T_f of two bodies sliding over each other, assuming that the heat flux entering the bodies is linear and uniformly distributed on the nominal contact area. The relationship is:

$$T_s - T_0 = \frac{\mu F_N v}{A_n} \frac{1}{\frac{k_1}{l_1} + \frac{k_2}{l_2}} \quad (\text{Eq. 1.5})$$

Where k_1 and k_2 are the thermal conductivities of the two bodies, l_1 and l_2 are the lengths of the heat paths inside the two bodies. Relationships for the estimation of l_1 and l_2 are reported in [14].

In an experimental approach, proposed by Sutter et al. [16] to quantify the T_f of two bodies in sliding contact at high velocities, was deduced that the flash temperature can exceed 1100°C over an area of about 100 μm in diameter.

Not only flash temperatures influence the wear of the system, but also the surface temperature reached on the sliding bodies determine the wear conditions, e.g. the braking action can be classified as mild if the surface contact temperature is lower than 300°C, or heavy if the temperature is higher.

Verma et al. [17] found that, in a low metallic friction material during a pin-on-disc test, above 250°C the wear rate increases, reaching the typical values of the severe wear regime. The increase in wear was associated with the thermal decomposition of the organic binder and components inside the friction material formulation.

1.2.3 Tribological interface

Wear plays an important role in the disc/pad tribological system. Particles of varying sizes, detached from the surfaces of disc and pad, are crushed and milled down to smaller particles while they are trapped between the contact surfaces [18]. The mixing of these particles and oxidation creates a new layer on the tribological interface called the third body or friction layer [19].

Hard particles retain their original size, whereas soft particles are milled together in a very small grain size [20]. The friction layer can consist of all the elements of the tribological system and may also contain their oxides [21]. Part of the new layer remain in the contact area while part of it is released from the system as wear debris or fine airborne emissions [22]. Obviously, the chemical composition of wear debris and friction layers depend on the formulation of pad materials. Moreover, the chemical composition is influenced by the loading and environmental conditions of the brake applications [23].

The contact surfaces are extensively investigated in the literature after the brake operation to investigate the evolution of the pad/disc interface.

Eriksson et al. [19][24][25] related the brake performance to the dynamic equilibrium between the formation and disruption of the contact plateaus (Fig. 1.5). The reinforcements of the friction materials (metal fibres and hard particles), start protruding from the pad surface, as it starts wearing out, and form the primary plateaus. These plateaus are important for the growth of the secondary plateaus. These are made of wear debris blocked and compacted against the primary plateaus so to form continuous patches. Then, the shear and abrasive stresses generated by the sliding may damage secondary plateaus, as well as, cause a detachment of the primary plateaus.

As in all sliding contact situations, the friction forces are transferred by the area of real contact. In brake pads, the area of real contact is confined within the contact plateaus (Fig. 1.6).

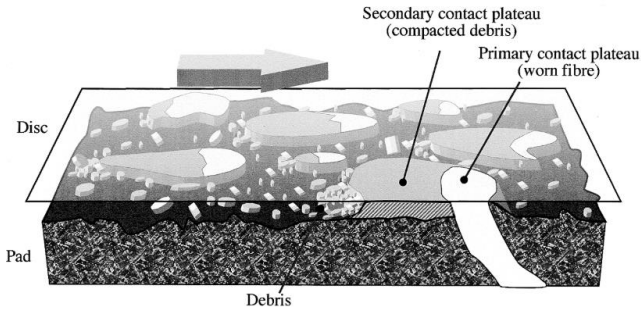


Fig. 1.5. Schematic presentation of the contact situation between an organic brake pad and a brake disc, involving contact plateaus: primary and secondary [19].

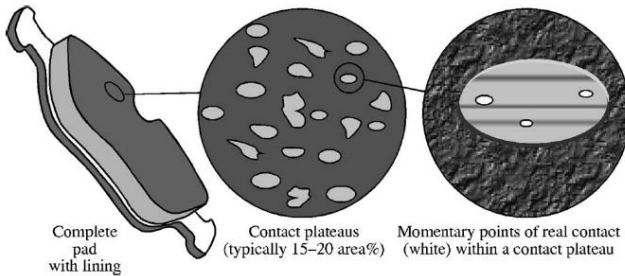


Fig. 1.6. Schematic representation of the area of real contact confined in the contact plateaus.

Other studies have also related the brake performance to the third body layers formed during brake application [23][20]. The pad and the disc are separated by a layer of third body, although not always visible after braking, which consists of fine-grained wear debris with some coarse particles, Fig. 1.7. Several studies reported the presence of films produced by the compaction of the debris. Jacko et al. [26] were the first to observe evidence of films produced by debris compaction from polymer composites sliding against a metal surface. Iron oxide was then identified as a major constituent of surface films of brake pads and discs [27][28]. Other authors, Filip [23] and Blau and Meyer [29], identified mixtures of oxides and carbonaceous products in films and wear particles, respectively.

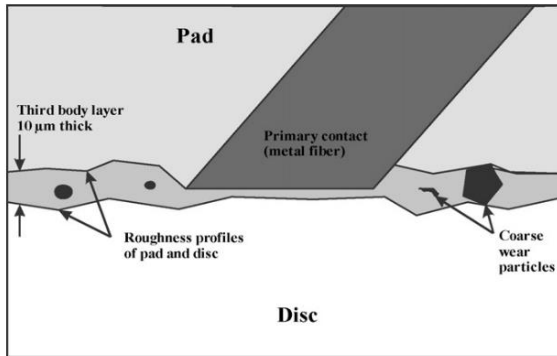


Fig. 1.7. Schematic presentation of the contact situation between an organic brake pad and a brake disc, involving the formation of a third body [20].

1.2.3.1 Friction characteristics

The surfaces are renewed by wear process, anyway the history of the surfaces (e.g., temperatures achieved, powder dissipated) influence the tribological interface.

Two situations may characterize the interface:

- running-in;
- steady state.

The initial running-in is associated with an increase in the coefficient of friction, Fig. 1.8. It is due to the removal of less wear resistant material from pad surface, which results in direct contact of more wear resistant constituent with the disc (typically reinforcing ingredients). It ends when the conformal contact between the surfaces is attained; which means that the polishing of the disc surface is accomplished, and the contact plateaus are in a dynamic equilibrium of formation and degradation (steady-state).

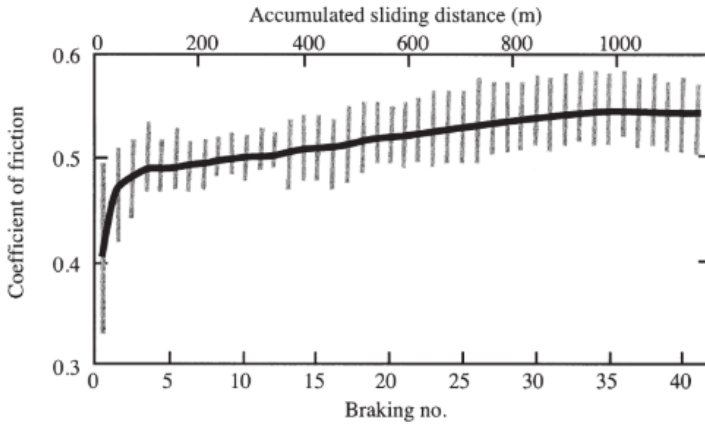


Fig. 1.8. Schematic representation of evolution of coefficient of friction during a running-in sequence. The black line is the average μ , the grey line represents each stop [19].

Many studies reported the influence of the temperature on friction coefficient [30][23][17][31]. Initially, CoF increases with increasing temperature, this behaviour can be attributed at two phenomena:

- the viscoelastic properties of the resin at high temperature;
- the growing of the secondary plateaus due to the greater sinter capacity of the wear fragments.

Above a certain temperature (about 300°C), a decrease of CoF is observed and can be attributed to the thermal decomposition of the resin and the detachment of reinforcing constituents (primary plateaus).

In literature is also reported the influence of normal force and velocity on the friction coefficient [32][33][34]. In general, it can be states that CoF decreases with increasing velocity, the reported explanation is that there is less time for asperities contact resulting in a reduction of real area of contact.

Whereas, the influence of CoF with increasing load present a mixed trend. An increase of the normal force causes an increased area of real contact, but at the same time an increase of wear of primary plateaus is observed.

A friction hysteresis is also reported by Eriksson et al. [19], Fig. 1.9. The reported curves are based on measurements with increasing pressure

followed by decreasing pressure. The solid lines are the average coefficient of friction of the measurement points, reported as plus signs and circles. In this case, lowering of the pressure caused an increase of CoF; it is explained by the relatively slow adaptation of the tribological interface. In fact, a larger contact area is created during the measurements with increasing pressure, that increase the adhesion forces, the increasing of the contact area is an irreversible process.

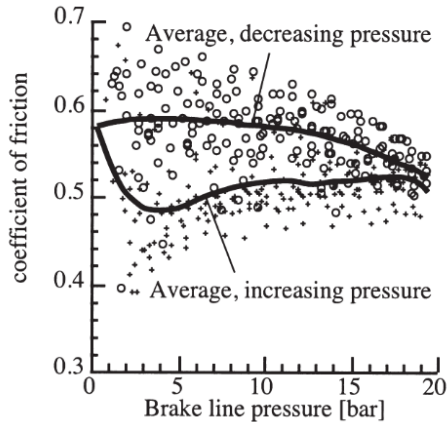


Fig. 1.9. Coefficient of friction for an organic brake pad under increasing and decreasing brake pressure. Solid lines indicate the average friction level [19].

Chapter 2

2. Friction materials for brake pads

2.1 Friction material characteristics

Nowadays, the friction materials (FMs) commonly used in automotive brakes are most of the time resin-bonded composites. They are essentially multi-component materials highly heterogenous. The basis of such formulations is usually a polymeric binder with addition of fillers and fibres.

The main characteristics that a FM must have are [35][36]:

- retaining a sufficiently high and stable coefficient of friction over a wide range of braking conditions (e.g. irrespective of temperature and humidity);
- should not wear rapidly;
- rotor friendly;
- good compressibility and mechanical strength;
- high comfort (i.e., absence of vibrations and squeal noise).

There are many different types of friction materials, each one made to emphasize particular characteristics. The ideal friction material for racing use is not the same as that for passenger-car use (the required performances are different as well as the cost versus budget).

2.1.1 Organic friction materials

Most brake friction materials on the market for light and commercial vehicles are organic. Other class of friction materials (e.g. carbon-carbon, carbon-ceramic, sintered materials) used for specific applications such as railways, aircraft or top-class cars brakes have not been studied and considered in this work. Organic friction materials

are commonly classified into one of these basic categories based on its ferrous and nonferrous metal content [37]:

- NAO (Non-Asbestos Organic);
- Low-met (Low-metallics);
- Semi-met (Semi-metallics).

NAO materials (also called ceramic) contain less than 10% of steel fibres and non-ferrous metals. Low-met materials have a content of metallic phases between 50% and 70%. Finally, semi-met materials contain more than 50% of metals. Some of the main characteristics of these categories are given in Table 2.1 [7].

Table 2.1. Organic friction material categories: main characteristics.

	Friction (μ)	Characteristics
NAO	Low/ medium-high 0.33-0.40	+ Excellent wear at $T < 200^{\circ}\text{C}$. - Poor wear under heavy duty conditions.
Low-met	medium-high 0.35-0.5	+ Good fade and high-speed performance. - High pad/rotor wear.
Semi-met	low to medium 0.28-0.38	+ Good fade characteristic, excellent wear at $T > 200^{\circ}\text{C}$. - High μ variation.

2.2 Brake materials

There are more than 100 different raw materials that are used in friction material design for brake pads [38]. The constituents vary from metallic particles/fibres, fibres of rockwool, minerals, carbon, and lubricants, different types of abrasives and fillers all held together by a polymeric binder which is normally a thermosetting polymer.

Some raw materials and its functional roles are listed in Table 2.2, these information are copied from the reference [38]. It is fundamental to understand the functional role of the constituents, such as the influence on:

- friction and wear;
- noise;
- judder;

- fade and recovery;
- sensitivity to speed, pressure, and temperature.

Table 2.2. Specific functional role of some constituents in brake friction materials [38].

Ferrous-ferric oxide	Higher porosity, bad wear and higher μ at high speed. Highly sensitive for friction property with very sharp increase noticed even with minute ratio changes.
Potassium titanate fiber/whiskers	Relatively stabilizing μ and wear improvement at high temperatures (> 250°C). Significant increase in higher temperature friction even with higher binder contents. No pronounced effect on the low temperature friction.
Ceramic pulp	Higher μ at medium speed 80 km/h, cleaning rotor, and improves rotor wear.
Barium sulfate	Thermal stability, improves wear, lowers friction level, increases density.
Bronze fibre	Higher strength at high μ and at high speeds.
Unburnt vermiculite	Slightly higher μ , cleaning rotor.
Burnt vermiculite	Slightly higher μ , lower wear.
Premixed cashew dust	Lower wear, lower noise, good fade.
Calcium hydroxide	Increase in pH, preventing rust.
Zirconium silicate	Higher μ .
Synthetic graphite	Lower wear and adjusting μ , lower fade.
Natural graphite	Lower wear, lower μ , low temperature effectiveness.
Molybdenum disulphide	Lower μ , low temperature lubrication at 100 °C free of abrasives.
Kevlar	Higher strength/lower wear, good preformability.
Aralkyl modified phenolic resin	Excellent fade/low wear at high temperature.
Epoxidized cashew modified resin	Binder, better for noise than straight resin. Lowers wear under stable friction.

Phenolic resins	Reduce delamination, improves thermal stability, and delays fade until higher temperatures, reduced swell, and growth
Copper oxide	Not kind to the opposing surface.
MgO	Thermal stability of resin.
Fused MgO	Is hard and improves friction level.
Magnesium silicates	High elevated friction $Mg_3Si_2O_5(OH)_4$
Calcined Kyanite	Elevates friction levels.
Brass >4 %	Control friction.
Petroleum coke	Instead of graphite, low ash, high carbon content, thermally stable.
Antimony trisulphide	Lower μ especially at >100 km/h, high temperature lube.

Anyway, due to the complexity of the mixtures, it is not always possible to predict the end property that a constituent has in a specific mixture. Moreover, other aspects, like the metallic counter-face, influence the overall behaviours.

The exact compositions of commercial friction materials are almost never published in the open literature. The compositions of commercial and experimental brake friction materials may vary a lot, although some constituents are commonly used in almost all formulations.

The constituents are commonly subdivided into the following main groups [39][24]: reinforcements, friction modifiers, fillers and binders. More details are given in the next paragraphs.

2.1.1 Reinforcements

The reinforcement provides mechanical strength. They are mainly fibres which give structural integrity, thermal stability and frictional property [40].

The National Institute of Occupational Safety and Health has defined a fibre as a particulate that has a physical dimension longer than 5 μm and a length-to-diameter ratio of 3 to 1 or greater.

Fibre dimension and concentration play a critical role in good adhesion of fibres with the matrix since there would be excessive wear of the

friction material, if there is not enough interfacial bonding between the constituent and the matrix [37].

Many fibres are used as reinforcing agent, organic and inorganic. Organic fibres are divided into synthetic (e.g., aramid fibres and polyacrylonitrile fibres) and natural (derived from vegetable source) [41][42][43]. The main properties of organic fibres are listed in Table 2.3.

Table 2.3. Main properties of organic fibres.

Organic Fibres	Pros	Cons
Synthetic	Weight Strength Toughness	Thermal conductivity Resistant to compression Porosity
Natural	Cost Renewable source Modulus/specific gravity ratio	Thermal resistance Variable mechanical properties

Inorganic fibres can be divided into ceramic and metallic [44][45].

Many ceramic fibres are available on the market. The crystalline fibres can be made from glass, rock and minerals [46]. Mineral and synthetic fibres have to demonstrate the non-toxicity in terms of human health to be used for current friction material formulation. Fibre dimensions established in the 1960s for the measurement of asbestos fibres are used to denote which fibres should be counted for occupational safety: these are: fibre length > 5 μm , fibre diameter < 3 μm and aspect ratio > 3 [47].

Generally, also the ceramic crystalline materials, such as boron nitride, silicon carbide, silicon nitride, alumina, zirconia and mullite, can be used as high-temperature reinforcement, in form of fibres or whiskers [48][49]. However, since their production cost and material toxicology strongly limit the use of ceramic crystalline fibrous reinforcements, they are mainly used in other shapes. Despite the toxicological aspect two crystalline ceramic reinforcements still be used for the manufacturing of friction materials due to their high cheapness and properties: potassium titanates and wollastonite [7][50].

Constituents with other than fibre shape, e.g., particles, plates and flakes, can be also used as reinforcement, if they increase the mechanical performance, like toughness and strength of the composite material, with respect to the matrix alone [51][52].

Metallic fibres with short length are widely used in friction materials. They are mainly made of steel, aluminium, copper and its alloys [53][54]. In Table 2.4 the main features compared with ceramic fibres are listed.

Hardness, expected adhesion with cast iron, thermal diffusivity and expected behaviour in temperature are the main parameters to consider in metal fibres choice [7].

Table 2.4. Main features of ceramic and metallic fibres.

Fibres	Pros	Cons
Ceramic	Higher melting Heat and chemical resistant	Stiffer Brittle
Metallic	Strength Toughness Thermal diffusivity	Wear of the disc Rust

2.1.2 Friction modifiers

Friction modifiers influence the coefficient of friction as well as the wear rate of the brake material. They are divided into two main categories [55][56]:

- abrasives, which increase friction coefficient and improve wear resistance of friction material.
- lubricants, which reduce the friction level but also stabilize it over different testing conditions.

Abrasives increase the friction coefficient increasing also the wear rate of the counter-face material, they remove iron oxides from the disc. Higher concentration of abrasives content result in an increased friction coefficient variation (instability).

Abrasives are used as a blend of different types, hard and soft: they have to be hard enough to abrade the counter friction material. There

are many different abrasives with different hardness, mild abrasives such as quartz have a hardness of around 500HV, zirconium ceramics range from 1000 to 1400HV, alumina is around the 1750HV mark and silicon carbide around 2600HV [35].

Due to the fact that brake disc Mohs hardness is around 5.5, it can be considered that are hard-abrasives all the materials with hardness equal or higher than 7, mild-abrasives materials with hardness included from 5 to 7 and low or non-abrasives or fillers all the materials the materials with hardness lower than 5 [7].

A few examples of commonly used abrasives include particles of metal oxides, silicates, carbides, e.g., zirconium oxide, zirconium silicate, aluminium oxide, chromium oxide, silicon carbide and boron carbide [57]. Table 2.5 listed some of the main features of the abrasives of oxides and carbides categories.

The thermal and chemical stability, the price/benefit ratio and the environmental and human health risk assessment, are other important parameters to be taken in account during raw materials selection. An example of a largely used abrasives in friction materials, now limited in all its forms, due to health risk for humans, is quartz [58]. In 1997, IARC classified inhaled silica in the form of quartz or cristobalite as carcinogenic to humans (Group 1) [59].

Table 2.5. Main features of abrasives of metal oxides and carbides.

Carbides	Oxides
Hardness	Low cost
Thermal conductivity	High resistance to temperature
Thermal shock resistance	in oxidizing environment
Resistance to chemicals	

As already seen in Chapter 1, a desired effect in a brake system is the formation of a friction layer, that protects the components from wear, provide smooth sliding and a stable COF within a wide range of stress and environmental conditions. Lubricants are generally used to fulfil these purposes [60]. Two main mechanisms are employed in dry lubrication for brake systems: soft films and exfoliating solids [61].

The first method is based on high temperature resistant polymers, metal oxides and fluorides, which are suitable to form a tribofilm [62]. The formation of a “soft” layer interposed between two hard surfaces (pads and disc for brake systems) is the ideal situation for friction coefficient reduction [61].

Metals and oxides can be used as lubricant through soft film mechanism. For example, copper and copper alloys have been largely used in friction materials. Copper and its alloys provide ductility and toughness to the friction layer and native oxides which are not so abrasives [63]. However, it should be considered that copper will be strongly limited by law in future. Moreover, most of soft metal oxides, e.g., lead, antimony, boron, arsenic oxides etc., are not suitable for friction materials due to their toxicity.

The second method requires solids with structure that tend to exfoliate, like lamellar solids, once placed between sliding surfaces. The bonding force between the lamellae determines if they are lubricants (low bonding force) or can be considered as mild abrasives (high bonding force) [64]. Example of lamellar solid lubricants are graphite and metals sulphides [65][66].

Graphite is the most widely used solid lubricant for all kinds of applications including friction composites. Furthermore, it is present in almost every disc brake system in the form of graphite flakes, as constituent of the cast iron rotor. Low-friction behaviour in graphite is traditionally ascribed to the low resistance to shear between atomic layers bonded by weak van der Waals force [67]. Friction and wear behaviour of graphite are correlated with structural order/disorder, contaminants and environmental conditions. At high loading range, friction induces a phase transformation in the graphite resulting in a significant increase of the friction coefficient [68]. The main problem of most of lamellar lubricants is their behaviour over 500°C, since they can oxidize losing their lubricant properties.

Metal sulphides, similarly to graphite, show lubricant properties according to their lamellar lattice structure [7]. Some metal sulphides, like lead and antimony sulphides, are nowadays avoided for potential health hazards or environmental issues [69]. Tin sulphides are currently regarded as the most promising candidates for antimony

replacement in brake pad formulations [70]. A strategy in sulphide-based lubrication is to use a cheap material, like FeS, blended with metals, e.g., tin, that can replace Fe in sulphide structure during the braking, generating metal sulphide in-situ [71].

Another widely used sulphide layered structure is the molybdenum disulphide (MoS_2) [72]. Contrary to graphite, it has been shown that the friction coefficient decreases when condensable vapours are removed from the atmosphere, indeed water penetrating in MoS_2 layers increasing their shear strength.

The concentration of solid lubricant must not exceed a certain limit (~ 10 vol.%), because otherwise, the COF might drop too low. A combination of more lubricants is commonly used to have satisfactory results. Frequently, a combination of graphite and one of the soft metal sulphides is the best choice [60].

2.1.3 Fillers

The materials that have a minimum impact on friction performance, i.e., they do not act as abrasive or lubricant, are considered as fillers. The fillers improve the processability and reduce the cost of friction material [73]. Moreover, are considered fillers all the materials which provide specific properties to final product such as noise suppressors, corrosion inhibitors, etc., in this case, they are called 'functionalizes'.

The specific filler to be used depends on the type of friction material as well as on the present constituents. For example, if a metallic pad requires noise suppressor fillers like cashew and mica will do; whereas for a semi-metallic brake pad molybdenum trioxide is used to prevent the lining cracking caused by the different thermal expansion of constituents [35].

Main properties of fillers, e.g., high thermal stability and low cost, are found in mineral materials, like sulphates and carbonates. In order to have a minimum impact on friction performance, the Mohs hardness has to be between 3 and 4.5 [7]. Two of the more commonly used fillers are barium sulphate, that imparts heat stability, and calcium carbonate that improves the friction material's brake fade properties [74][75][37].

Fillers are also used to improve comfort in terms of noise, vibration, and harshness (NVH) [76]. A strategy to reduce noise in friction materials is using particles with porous structures, since the porosity works as sound absorption reducing the noise [77][78].

Mica is another commonly used filler. It is able to suppress low-frequency noise due to its plane net-shape structure and decrease density [79]. Vermiculite is a phyllosilicate mineral-like mica and can also suppress noises generated during braking, it has low thermal conductivity and good abrasion resistance [80].

Rubbers are also used in composite materials to increase elasticity and reducing thermal diffusivity on the final compound [81]. Typically, they follow the vulcanization process or are additives, e.g., carbon black, to increase the thermomechanical resistance [82].

Other fillers are used as corrosion protectors. To prevent the oxidation at the disc-pad interface can be used a cathodic protection by addition of metallic zinc or tin to friction material formulation. Moreover, compounds like calcium hydroxide, are used as pH modifiers giving alkaline nature to the composite, this help to reduce the cast iron oxidation rate [37].

2.1.4 Binders

The binder is used to hold the components of the brake pad together, ensuring their structural integrity under mechanical and thermal stresses. Its properties determine to a large extent the process conditions for the manufacture of composite materials and the important operating conditions, e.g., working temperature and fatigue strength [35].

Phenolic resin, in unmodified or modified form, is the most common resin binder used in brake friction materials [83][84]. It is formed by a condensation reaction between phenol and formaldehyde. The reaction is shown in Fig. 2.1, it starts with the electrophilic attack of formaldehyde to form hydroxymethyl groups, and then continue with the attack of hydroxymethyl to an available position of another phenol to form water.

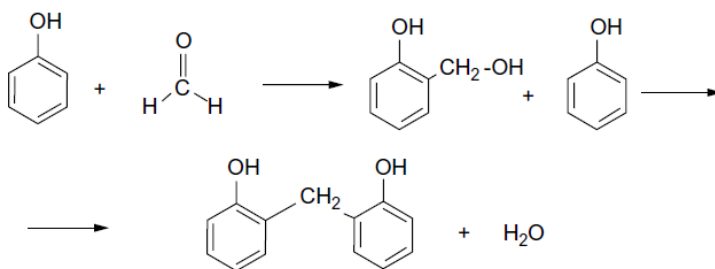


Fig. 2.1. Synthesis of phenolic resin [81].

The type of final resin, novolacs or resols, depends on the molar ratio of formaldehyde to phenol as well as the type of catalyst, e.g., acidic or basic. The most used phenolic resins in the friction field are novolacs, which are powder resins [81]. Instead, resole is a liquid resin used as wetting agent [85]. Novolacs are obtained with a formaldehyde to phenol molar ratio less than 1 and are catalyzed by either organic or inorganic acids, such as: oxalic acid, sulfuric acid, phosphoric acid, etc. When the phenolic resin mixed with the constituents is cured, through temperature and pressure, it forms a densely, cross-linked thermoset matrix.

Phenolic resins offer many useful properties, such as high mechanical strength, long-term thermal and mechanical stability, high resistance to various solvents, acids, and water and excellent thermal insulating capability. Because of its aromatic structure, phenolic resin offers flame- and smoke-resistance [86]. Although many other materials are superior to phenolic resin in some properties, phenolic resin provides a well-balanced overall performance at a relatively low cost.

However, these resins are sensitive to humidity and heat. In high-energy braking application or emergency stop, the temperature induced can be high enough to decompose the resin. Phenolic resins carbonize at approximately 450 °C, the decomposition process decreases the density of the brake friction material and increases the porosity, compromising the structural integrity. Moreover, this decomposition into fumes is likely to release its constituents. According to the Occupational Health and Safety Administration of the US Department of Labor, formaldehyde is classified as human

carcinogen, and also phenol is considered dangerous to human health [35].

Phenolic resins can be modified to improve the performance [87]. Several modified phenolic resins were used in the brake friction material, here are reported some examples.

Phenolic resin modified with cashew nutshell liquid (CNSL), containing Cardanol that improved some properties e.g. flexibility, thermal stability and the acid and alkali resistance. CNSL is an excellent natural phenol-like source for polymer synthesis, it reduces the costs and improves the ecological issue [88][89].

Boron modified phenolic resin is synthesized from phenol formaldehyde and boric acid that introduce B-O bonding in the structure, it exhibits higher thermal resistance and superior mechanical strength respect common phenolic resins due to B-O bonding [90][91].

Silicone rubber modified resin has silanol groups which introduce Si-O bond into the phenolic polymer improving thermal stability, water repellence, electrical insulation, chemical and impact resistance [92][7]. In some literature studies is reported the use of lignin, a polyphenolic macromolecule presents in the cell wall of plants, as substitute of phenol in the synthesis of lignin-modified phenol-formaldehyde [93][94].

The choice of binder depends upon the process and the required performance. Moreover, it is important a well-balanced concentration. An excessive addition of binder would lead to high fade and wear of brake pad. On the contrary, the poor concentration of binder would lead to fibre debonding from matrix which would increase the wear rate.

2.3 New trends

2.3.1 Legislations

Early organic friction materials were wood, leather or cotton impregnated with bitumen solution. Superior FMs were obtained by weaving asbestos-impregnated fibres together with organic material to glue them together [95]. The fibrous nature of asbestos as well as the

thermal stability, the mild wear and the stable coefficient of friction, have made asbestos dominant in the friction industry for a long period of time [96].

The ban of asbestos was started in the 1970s due to its hazardous nature, it was found to have a critical effect in causing lung cancer to human [97][98]. The U.S. Environmental Protection Agency required in 1986 to have non-asbestos brakes in new vehicles by 1993, and the aftermarket to convert to non-asbestos by 1996 [96].

As a result, the brake friction industry has seen the birth of different brake pads over the past decade, each with their own unique composition.

New regulations have been promulgated in some countries, the general trend is to decrease and eliminate all the hazardous and toxic elements or compounds in friction formulas. Fig. 2.2 shows the history of the changing regulations (North America) that control the chemical compounds used in the pads [99].

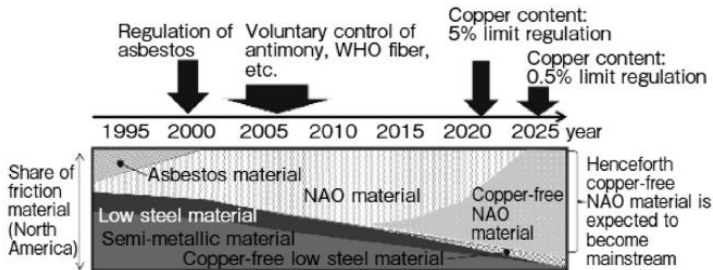


Fig. 2.2. History of changing regulations of the compounds used in North America.

In 2010, both the states of California and Washington enacted legislations that requires to lower the copper content below the limit of 5% by 2021 and 0.5% by 2025 [100]. Many brake friction materials are certified following different specifications, A, B or N (Fig. 2.3), the latter having the lower copper content in the mixture. From the data portal for the State of Washington [101], it is possible to consult the list of the certified pads. Nowadays, out of the registered 5692 friction materials, more than 50% have reached level N.




Regulation timing	Leaf Mark	Legislation Request
January 1 st , 2014		<p>LEVEL A On and after January 1st, 2014, any motor vehicle brake friction materials containing cadmium, chromium, lead, mercury, asbestos fibres (and their compounds) in an amount that exceeds the maximum concentration of 0.1 wt.% shall not be sold.</p>
January 1 st , 2021		<p>LEVEL B On and after January 1st, 2021, any motor vehicle brake friction materials exceeding 5 wt.% copper shall not be sold.</p>
January 1 st , 2025		<p>LEVEL N On and after January 1st, 2025 any motor vehicle brake friction materials exceeding 0.5 wt.% copper shall not be sold.</p>

Fig. 2.3. Brake friction material legislation requests from Washington State Legislature.

2.3.2 Copper

After asbestos was phased out of pad materials, a multitude of different brake pads have appeared on the market, each with a unique composition typically comprising reinforcing fibres, binders, fillers and frictional additives. Copper is a key element in organic friction materials, both as fibres and small particles, it is present with concentration in the 5-20% range [102].

The powders introduced as constituent normally have micrometric size. However, a literature study [63] revealed very fine copper powders (nano-size) incorporated into the friction layer that becomes denser and better adherent to the mating surfaces of the pad and disc

[21][24]. This suggests that the valuable powders are not those introduced in the initial formulation (micrometrics) but those resulting (nanometrics) from the wear process of the fibres. Moreover, inclusion of copper content led to an increase in the magnitude of μ and contributing to stabilize the friction-force [103].

Furthermore, fibres of this metal act as reinforcements engaged to reduce pad wear, as well as to provides primary contact sites for plateaus formation [104]. Its ductility ensures smooth sliding conditions and thus low noise especially at high temperatures [105][106]. In addition, copper improves the thermal conductivity of the pad and thus decreases the contact temperatures [107].

On the other hand, brake pads are regarded as the main source of copper released in the runoff from roads [108][109]. Then, due to rainfalls, larger non-airborne wear fragments of copper are washed to lakes and rivers [110], and have detrimental and toxic effects on aquatic species [111][112]. Previous studies [113] have shown high concentrations of copper originated from brake pads wear, deposited in San Francisco Bay (California), leading the U.S. government to enact legislations.

Regarding human health, the toxicity of copper has been reported to be relatively low compared with other metals, such as mercury, cadmium, lead, and chromium. However, metals in form of airborne PM₁₀ can generate Reactive Oxygen Species (ROS) and Cu is among the most effective in triggering oxidative stress into biological tissues [114][115]. Humans are exposed to copper mainly via the inhalation of PM. Exposure to PM generated by the brake wear may induce strong inflammatory reactions in bronchial branches. Particles can be retained in the alveolar tissues and increase the inflammatory responses [22][116]. Moreover, the high fraction having average particle size in the submicrometric range (ultra-fine particulate matter, UFP) renders the debris particularly dangerous, since it can directly access the deeper pulmonary regions and goes in the blood circulation [114][117]. That is why, the friction material Industry is facing a challenge to replace copper and its alloys with other substances.

2.3.4 Wear particle emissions

Currently, there is no specific regulation in the European Union that limits the use of copper in brake pads. Anyway, copper is not the only relevant environmental issue to brake materials. On a worldwide scale, some legislations for air quality standards have been adopted. In the review [118] is reported that exhaust and non-exhaust traffic-related sources are almost equally contributing to Particulate Matter (PM) emissions in cities. Many technological improvements in recent years have reduced considerably the exhaust emissions [119][120], whereas non-exhaust emissions are not currently regulated and all the studies on this theme are quite recently [121][122][123].

The disruption of the friction layer, formed on both brake pads and disc, during the braking event, generate wear debris that goes into the environment [124]. The coarsest fraction is deposited on the road, whereas the finest fractions become airborne.

The airborne particles are classified into three main classes, according to the aerodynamic diameter, defined as the diameter of a sphere of unit density (1 g/cm^3), which settles in still air at the same velocity as the particle in question:

- PM_{10} , Particulate Matter with diameter lower than $10 \text{ }\mu\text{m}$ (coarse fraction);
- $\text{PM}_{2.5}$, Particulate Matter with diameter lower than $2.5 \text{ }\mu\text{m}$ (fine fraction);
- $\text{PM}_{0.1}$, Particulate Matter with diameter lower than $0.1 \text{ }\mu\text{m}$ (ultrafine fraction).

The airborne fraction is dangerous for human because on the basis of their dimensions, the particles could interact with the human body, and penetrate deep in pulmonary regions [116]. Inhaled PM_{10} are deposited in the nose and throat, causing irritations, while fine and ultrafine particles may penetrate deep into the lungs and enter the pulmonary interstitial and vascular space, to be subsequently absorbed directly into the blood stream [125][126].

Approximately 40% of the total pad wear has been reported to be emitted as airborne material [127], and several studies regarding urban environments have reported contributions of brake wear particles to

non-exhaust PM₁₀ emissions ranging between 16 and 55 % by mass [118][128]. The concentration of PM₁₀ deriving from brake wear was estimated ranging from marginal to greater than 4 µg/m³ [129][118]. The most critical issue related to these studies is the lack of standardized procedures, that generate data and results difficult to compare. Despite the difficulties in collecting and characterize the wear particles, an increasing number of researchers have started to discuss the issue.

2.4 Eco-friendly formulations

Many recent studies have been devoted to the development of “eco-friendly” or “green” materials in the field of brake assemblies [130][131][102]. The best goal for the new generation of brake pads would be to create Cu-free friction materials that perform like Cu-full formulations. Such brake pads should include reduced PM emissions. Several replacements for the current components are required to substitute copper in the brake pad formulations. A single constituent capable of providing all the characteristics of copper has not yet been found. Moreover, with the increased standards for brakes, e.g., safety requirements and comfort, material selection becomes critical.

Instead of increasing the number of ingredients in FMs, nowadays, a more favoured trend is to improve properties of the existing constituents with the aim of preserving the tribological performance in Cu-free formulations. In fact, the properties of friction materials mainly depend on the characteristics of their components and the strength of the bonds among them.

Different studies have been performed in order to optimise the properties of constituents such as the evaluation of the best shapes, sizes and concentration of ingredients [132][133][42], employing chemical treatments [134][135][136] and considering resin modification [137][138]. Moreover, researchers are studying the possibility of utilizing either industrial or agricultural waste as a source of raw materials, e.g. banana peels [139], coconut shell and palm ash [140].

Mathematical methods have been suggested in the literature for the evaluation and optimization of new formulations [141][75][142]. However friction materials are still developed with the experience of manufacturers and through experimentation [131].

As concerns the emissions, researchers investigated brake pads, using dynamometers or pin-on-disc tribometers, enclosed in a climate chamber, to identify, quantify and characterise the brake wear and the emissions [143][144][145]. Interesting works have been conducted with the aim of studying the dependence of the size and the concentration of the particles on the brake parameters, i.e., the interface temperature, the contact pressure and the sliding velocity [146][32].

The University of Trento was involved in two projects supported by the European Union within the FP7 and H2020 programmes respectively: REBRAKE [147] and LOWBRASYS [148], this latter developing further the research started during REBRAKE. The projects successfully achieved the design of a braking system able to reduce PM emissions. In LOWBRASYS several strategies were adopted to achieve the goal; in addition to the development of advanced brake pad used against novel discs (coated and heat-treated), it was studied a particle capturing systems able to stop the wear debris and it was created a smart dashboard that communicates with the driver and gives feedback on braking behaviour.

2.4.1 ECOPADS project

The ECOPADS project [149] (Eliminating COpper from brake PADS and recycling) is supported by the European Institute of Innovation and Technology (EIT) Raw Materials and the partners of the Consortium are:

- University of Trento (UniTN);
- Royal Institute of Technology (KTH);
- Brembo S.p.A;
- Hub Innovazione Trentino (HIT).

The two main goals of the project are the following:

- To produce a 'green' copper-free brake pad, which combines excellent brake performance and reduced certified emissions.

- To study and design a specific recycling protocol for brake pads.

ECOPADS, stems from the results achieved in the REBRAKE and LOWBRASYS projects, and is being focussed on the development of a new brake pad for road vehicles, hence to anticipate the forthcoming standards and regulations concerning the limitations to the usage of copper and the emission of non-exhaust sources.

The newly developed materials were formulated adding steel fibres and barite, as a key component, in different concentrations. Barite is considered a low cost, not hazardous raw material.

The new formulations were tested in the UniTn and KTH laboratories with different PoD apparatus to evaluate friction, wear and emission behaviour. The preliminary investigation on the use of balanced concentration of barite combined with steel fibres, appeared promising especially as regards the emission behaviour of friction materials. After that, in order to validate the findings from the most promising formulations, real brake pads were manufactured and tested on a brake dynamometer to evaluate both performances and emissions. Finally, the best formulation was also tested in real car working conditions.

Chapter 3

3. Materials and methodology

3.1 Materials

A wide range of friction materials were investigated, in order to understand the role that selected constituents have on friction and wear behaviour. All the developed formulations are based on two master-batches, which were used as references in different phases of the study. Moreover, several Cu-free formulations available on the market were investigated for a comparison.

As counter-face material in tribological tests, pearlitic gray cast iron discs were used.

3.1.1 Master-batches

Two master-batches were used as reference:

- the low-met friction material **FM/1**. It is a Cu-full formulation. It was employed to investigate the role of copper in friction materials and to perform some preliminary studies on its potential substitution.
- the low-met friction material **FM/2**. It is a commercial Cu-free formulation. FM2 was taken into consideration in order to study the role of some targeted components.

The elemental compositions, as measured by energy dispersive X-ray spectroscopy (EDXS) are given in Table 3.1. The main component phases detected by X-Ray Diffraction (XRD) are listed in Table 3.2. Semi-quantitative phase composition was obtained by means of the Rietveld methodology as implemented in the MAUD software [150].

Table 3.1. Elemental composition of the two reference masterbatches used in the study. The concentration of C is not included in the table.

Element (wt.%)	FM/1	FM/2
Fe	3.8	25.6
Cu	8.3	-
Zr	27.4	-
Ti	14.0	-
Zn	4.2	8.2
Mg	1.0	7.7
Al	4.8	6.0
Si	3.1	3.2
S	2.7	4.8
Sn	-	4.8
Ca	5.3	2.1
Cr	-	1.8
K	4.2	-
Ba	2.4	
O	18.7	35.8

Due to the relative complexity of the analysis, it is possible that some low-% crystallographic phases have not been identified correctly and/or some low-% phases are missing from the picture. Moreover, some phases could be overestimated, like graphite; this is related to the presence of large number of crystallographic phases; some of which may exhibit some problems of preferential orientation, poor statistics (few particles of considerable size) and/or complicated microstructure.

Additionally, for some specific investigations the reference formulations were modified as follow:

- FM/1 was produced without copper (**FM/1-Cu**);
- FM/2 was produced without graphite (**FM/2-C**).

Moreover, three Cu-free friction materials (P/1, P/2, P/3) sold on the market were considered in order to have some information about their tribological behaviour. These materials were used to compare the Cu-free reference master-batch used in this study (FM/2). The pads are

produced from different manufacturer: TMD Friction, ITT Corporation and Federal-Mogul Corporation.

Table 3.2. Main component phases detected in the two reference master-batches by X-Ray Diffraction.

Phase (wt.%)	FM/1	FM/2
Graphite - C	27.51	34.31
Iron - Fe	4.67	20.76
Copper - Cu	16.03	-
Zirconia – ZrO ₂	23.16	-
Corundum – Al ₂ O ₃	0.26	16.23
Zinc - Zn	9.68	7.61
Barite – BaSO ₄	5.85	-
Tin Sulfide - SnS	-	1.15
Periclase - MgO	-	11.39
Zincite – (Zn, Mn)O	0.15	3.14
Sphalerite – (Zn, Fe)S	0.45	3.96
Chromite – Fe ²⁺ Cr ₂ O ₄	-	1.45
Silicates (Al,Mg)	1.17	-
Potassium Hexatitanate – K ₂ Ti ₆ O ₁₃	11.07	-

3.1.2 Constituents investigated

In order to replace copper in the master-batch FM/1, two constituents were selected, i.e., steel fibres and barite, correctly balanced in the formulation.

Moreover, other constituents have been investigated, using the master-batch FM/2, because of their interesting properties (e.g., mineral fibres) and a strategic role (e.g., phenolic resin). Others are studied because considered important in the literature for Cu-free formulations, as graphite.

3.1.2.1 Steel fibres

The morphology of the steel fibres used in the study, as observed at the SEM, is shown in Fig. 3.1. The chemical composition of the fibres is reported in Table 3.3.

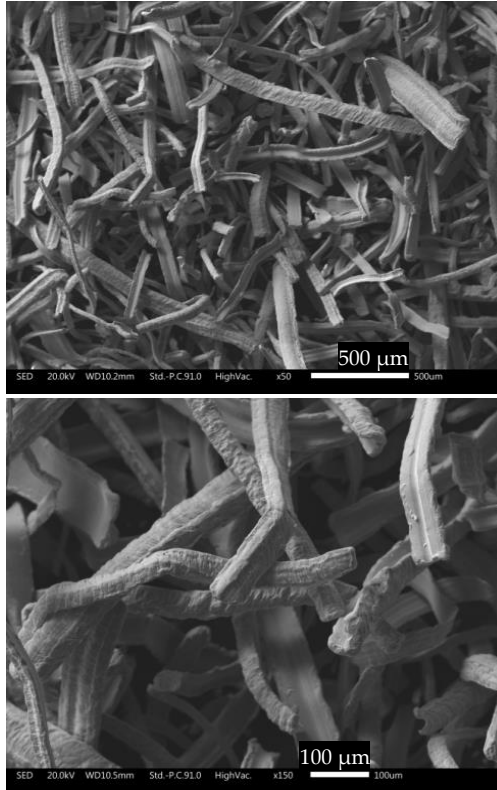


Fig. 3.1. SEM images at different magnifications of the steel fibres.

Table 3.3. Elemental composition of the steel fibres.

Element	Wt. %
Fe	96.57
C	2.27
Al	0.74
Mn	0.33
Si	0.09

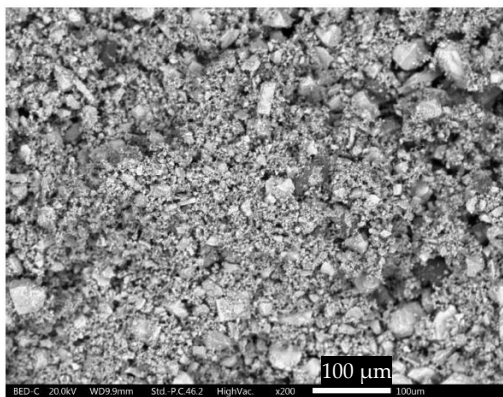
3.1.2.2 Barite

The natural barite used in the study is a fine powder of a mineral composed of barium sulfate, BaSO_4 . The purity is 96% and the main contaminants are strontium oxide (SrO), quartz (SiO_2), sodium oxide (Na_2O) and hematite (Fe_2O_3). In Table 3.4 is reported the concentration of the oxides present in the powder.

Table 3.4. Concentration of oxides presents in the barite.

Element	Wt. %
BaO	63.71
SO₃	32.06
SrO	1.56
SiO₂	2.04
Na₂O	0.52
Fe₂O₃	0.11

The morphology of the barite is shown in Fig. 3.2, the powder size is between $30\ \mu\text{m}$ and $40\ \mu\text{m}$, furthermore is present a very fine fraction with the size below the micrometre.



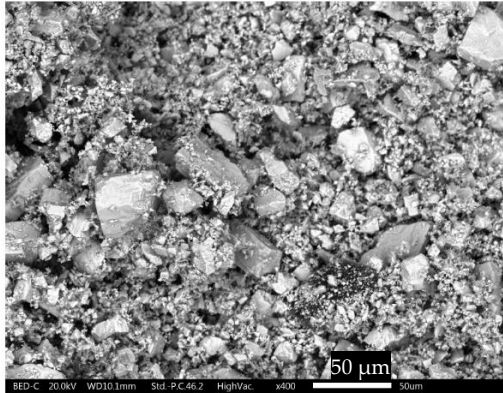
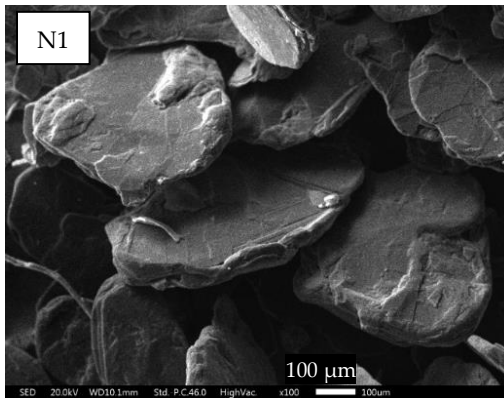


Fig.3.2. SEM images at different magnifications of the barite.

3.1.2.3 Graphite

Three different types of natural graphite, featuring a diverse particle size, were selected. In Fig. 3.3 the SEM micrographs with the morphology of the types of graphite are shown. The graphite N1 is a flake graphite with the particle size in the 300 – 425 μm range. The graphite N2 has a flake morphology, with the grain size below 100 μm. The graphite N3 is a fine granular graphite with particle size below 40 μm. The main features of the selected graphite are summarized in Table 3.5.



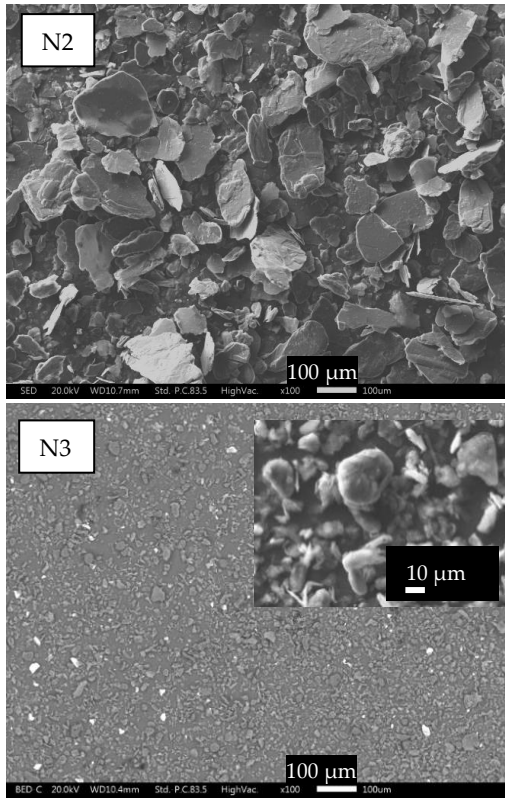


Fig. 3.3. SEM micrographs of the natural graphite (N1, N2, N3) with different particle size.

Table 3.5. Specifications of the three types of natural graphite (N1, N2, N3). d_{90} indicates that 90% of the graphite is below the specified value.

	N1	N2	N3
Content of C	94-97%	94-96%	96-98%
Graphite grade	Flake	Small flake	Very fine grinding
Particle size d_{90} (μm)	< 400	< 100	< 40

A synthetic graphite was also selected. The main features are summarized in Table 3.6. In Fig. 3.4 is shown its morphology.

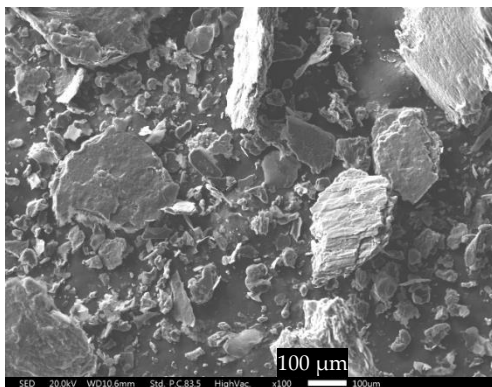


Fig. 3.4. SEM micrograph of the synthetic graphite (S1).

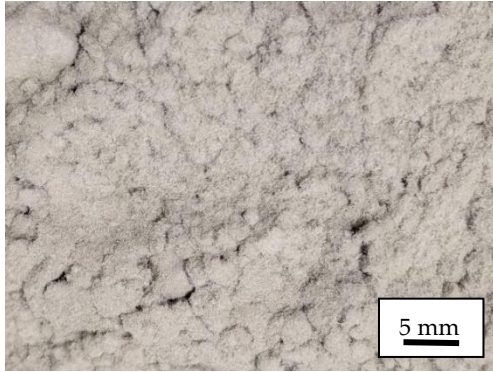
Table 3.6. Specifications of the synthetic graphite (S1). d_{90} indicates that 90% of the graphite is in the specified range.

S1	
Graphite grade	Fine powder
Particle size d_{90} (μm)	150-500

3.1.2.4 Mineral fibres

Two different types of mineral fibres were selected. The main differences of the fibres are the dimension and the agglomeration, see Fig. 3.5. Moreover, the fibres LF1 have an amino-silane/rubber surface treatment whereas fibres LF2 have no treatment. The SEM observation of the fibres is shown in Fig. 3.6. Table 3.7 shows the chemical analysis (XRF), taken from the Technical Data Sheets of fibres.

LF1



LF2

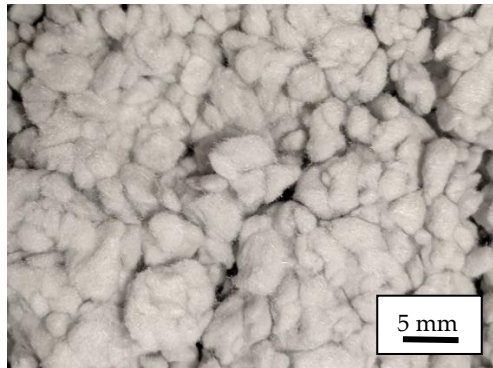
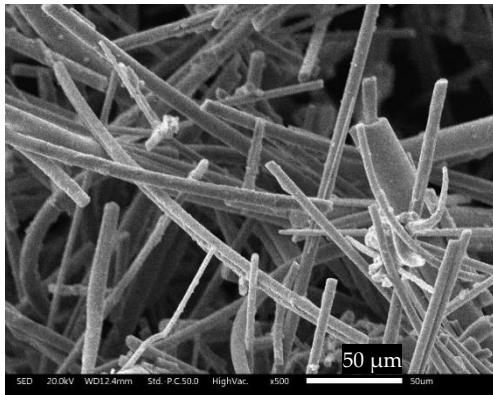


Fig. 3.5. Pictures of mineral fibers (LF1, LF2).

LF1



LF2

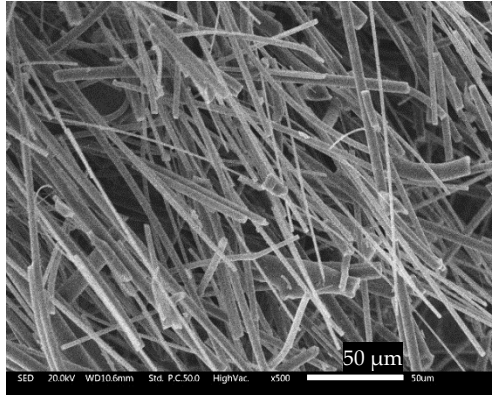


Fig. 3.6. SEM observations of mineral fibers (LF1, LF2).

Table 3.7. Chemical analysis (XRF) of mineral fibers (LF1, LF2).

Element (wt. %)	LF1	LF2
SiO₂	42.7	41
Al₂O₃	18.5	20
TiO₂	1.3	2
Fe₂O₃	7.7	6
CaO	20.6	20
MgO	6.0	5
Na₂O	2.2	3
K₂O	0.6	1
P₂O₅	0.2	0.2
MnO	0.2	0.2

3.1.2.5 Phenolic resins

Two different types of phenolic resins (codename: R1, R2) were considered to investigate the binder deterioration. Both resins are used in friction materials. The resin R1 is the binder used in the reference master-batch FM/2. It is a fast-curing resin which means that it is synthesized under a complex catalyst for increasing the curing rate and decreasing the curing temperature. The pictures of the two resins are shown in Fig. 3.7.



Fig. 3.7. Pictures of phenolic resins (R1, R2).

3.1.3 ECOPADS materials

The research work for the development of new copper-free brake pads with low emissions, started from two friction material mixture without copper (FM/2, see paragraph 3.1.1, and FM/3), used as baselines.

Moreover, two commercial friction materials were selected as benchmarks in order to compare performance:

- FM/4 is a Cu-free commercial formulation;
- FM/5 is a Cu-full commercial formulation.

Table 3.8. Elemental composition of the friction materials used in the Ecopads study. The concentration of C is not included in the table.

Element (wt.%)	FM/3	FM/4	FM/5
Fe	30.2	26.0	12.3
Cu	-	-	12.9
Zn	9.5	1.4	8.7
Mg	9.7	12.2	8.2
Al	6.1	8.1	5.8
Si	4.5	1.4	3.7
S	8.0	3.9	4.0
Sn	4.4	6.6	6.7
Ca	3.8	1.2	3.5
Cr	2.4	3.0	1.5
P	-	-	0.6
K	0.9	-	-
Ba	-	-	1.1
O	20.4	36.2	31.0

3.1.4 Grey cast iron discs

As counter-face material in tribological tests, pearlitic grey cast iron discs were used. The study was conducted using the discs referred to as D/1. Their diameter was equal to 60.0 ± 0.1 mm and the thickness was 6.0 ± 0.1 mm (Fig. 3.8). Moreover, some discs, codenamed D/2, were used for the Ecopads' tests (Chapter 6). In this case, the discs were 140.0 ± 0.1 mm in diameter and 15.0 ± 0.1 mm in height (Fig. 3.8). The average surface roughness of the discs, for both D/1 and D/2, was equal to 2.2 ± 0.2 μm . The hardness of the discs was 245 ± 20 HV30 and 216 ± 10 HV30, respectively for D/1 and D/2.

The microstructures of the two grey cast iron discs, made of graphite flakes in a pearlitic matrix, are shown in Fig. 3.9. They are both used to produce real discs for commercial vehicles.

In Table 3.9 is reported the nominal elemental composition of the pearlitic grey cast iron. The physical and thermal properties of the cast iron are instead listed in Table 3.4.

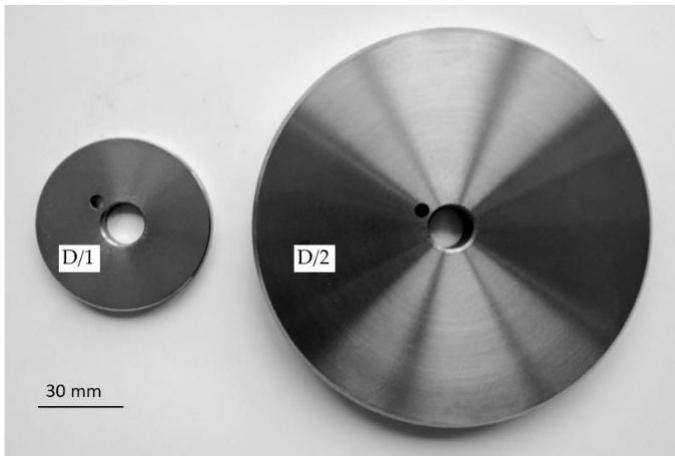
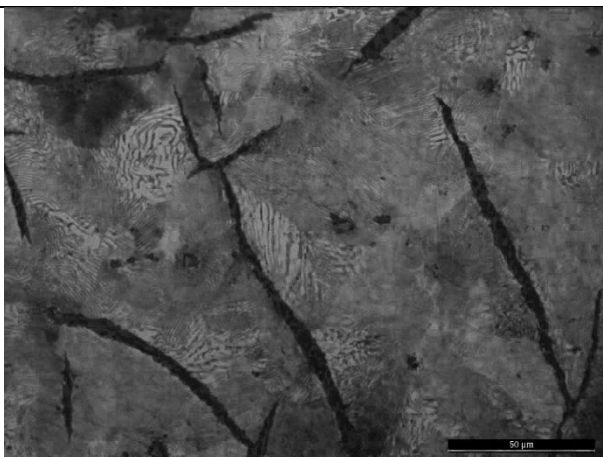


Fig. 3.8. Geometry of the disc D/1 and the disc D/2 used for the tribological tests.

D/1



D/2

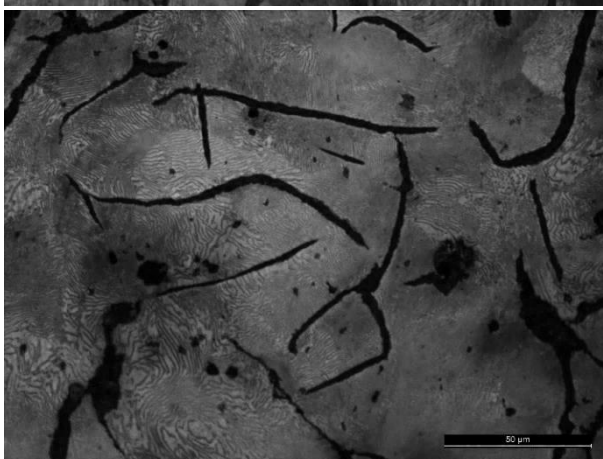


Fig. 3.9. Optical images of grey cast iron discs D/1 ad D/2 after 2% Nital etching.

Table 3.9. Nominal elemental composition of grey cast iron with flake graphite [151].

Element	(wt.%)
C	3.40
Si	2.00
Mn	0.50
S	0.05
P	0.15
Sn	0.11
Fe	Balance

Table 3.10. Properties of the grey cast iron [152].

Density	7200 kg/m ³
Thermal Conductivity	52 W/mK
Specific Heat	447 J/kgK
Elastic Modulus	98 GPa

3.2 Pin production

The production of the samples for the tribological tests was based on a net-shape powder metallurgy approach (Fig. 3.10). This approach is strategic compared to the machining of the sample from real brake pads, since it allows to have an in-house production and prepare pin samples out of limited amounts of powder with different compositions, in order to check for the effect of targeted components. The reference master-batch was mixed with the constituents under investigation by using a Turbula mixer (3-dimensional shaker). For all the samples, 100-200 g of powder mix were mixed for 15 mins to ensure a complete homogenization.

Cylindrical pins for the pin-on-disc (PoD) tests were prepared out of the diverse mixtures, by using a cylindrical mould placed in a hot-pressing, apparatus typically employed for metallographic sample preparation.

The process temperature during curing was set at about 150 °C. The pins remain under compression for 10 min at 16 MPa. Then the specimens are post-cured, in an oven, with the same cycle used for brake pads; the pins reach 200°C and remain at that temperature for 3 hours before undergoing a controlled cooling.

Initially, pins of 6.0 mm in diameter and 9.0 mm in height were produced. Subsequently the standard became bigger pins: 10 mm in height and 10 mm in diameter. The density typically ranges from 2.20 to 2.50 g/cm³.

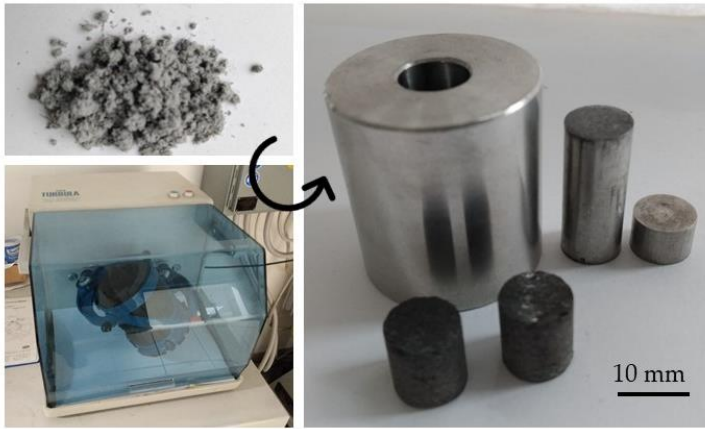


Fig. 3.10. Schematic representation of the net shape approach to produce the samples for the tribological tests.

3.3 Experimental procedure

3.3.1 Pin-on-disc tests

The tribological performance of the friction materials were investigated using a pin-on-disc tribometer. In the PoD tribometer the pin is kept stationary and pressed against the rotating surface of the disc, a schematic is reported in Fig. 3.11. This test set-up implies wear of the friction material under drag conditions (the angular velocity of the disc is kept constant).

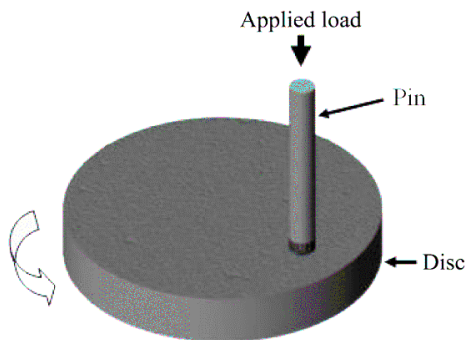


Fig. 3.11. Schematic representation of a pin-on-disc tribometer.

The PoD configuration is not designed with the intention of replicating the real brake system action, for which specific types of equipment, e.g., dyno-bench tests, are available, but rather can be useful for investigating fundamental tribological mechanisms active at the sliding interface [104][153][32].

In order to be representative of the wear mechanisms at the brake pad/disc interface, these tests should be performed under loads, velocities and temperatures that are close to those of real braking conditions. In the present research, all the tests were carried out at a sliding velocity $v = 1.5 \text{ m/s}$ and nominal contact pressure $P = 1 \text{ MPa}$. These parameters are intended to obtain mild wear sliding conditions. The duration of each test was **90 min.** (at first it was **50 min.**, but then it was extended to better follow the evolution of μ). Before each test, a **30 min.** run-in period was set to attain a stable contact between the pin and the disc. The tests were conducted at room temperature (RT) and at high temperature (HT, 300°C and 400°C).

Two different PoD test rigs were used: the Eyre/Biceri PoD (Fig. 3.12) and the Ducom PoD (Fig. 3.13). The apparatuses are equipped differently, the main features are reported below.

The Eyre/Biceri instrument displays a linear variable differential transformer (LVDT) for the evaluation of the friction coefficient (Fig. 3.12). The pin temperature is continuously monitored with a K-type (Chromel/Alumel) thermocouple during the test. The high-temperature tests are performed by heating up the disc with an electric resistance; closed-loop feedback on the disc's temperature enables accurate control on the power supplied to the electrical heaters. A thermal camera was used to control the temperature measurements of the disc.

The Ducom tribometer, more recent, is equipped with a load cell to evaluate the friction coefficient (Fig. 3.13). The disc temperature, that rise during the test, is continuously controlled with a pyrometer. The depth of wear is recorded using a linear displacement transducer. However, the measurement may also account for the wear contribution of the disc, as well as the thermal expansion of the samples. For this reason, the wear is evaluated by weighing the pin before and after each test. An inductor heats the disc during the tests

at high temperature and a closed-loop feedback keeps on controlling the temperature of the disc.

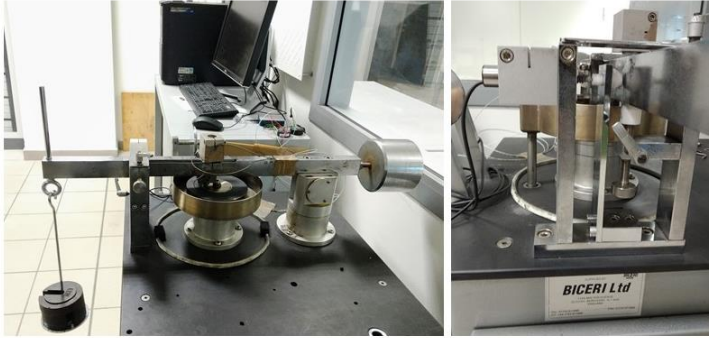


Fig. 3.12. Pin-on-disc Eyre/Biceri.



Fig. 3.13. Pin-on-disc Ducom.

In both tribometers, the friction coefficient, as well as the temperature (Eyre/Biceri: pin's temperature, Ducom: disc's temperature), were continuously recorded. While the wear was evaluated as the mass loss of the pin during the tests, which is converted in volume loss using the density of the friction material.

The wear of the disc is usually determined by obtaining the wear track profile, as measured with a profilometer.

3.3.1.1 Data analysis

The kinetic friction coefficient is determined directly during the tests by measuring the deflection of the arm that keeps the pin on the disc.

Instead, the wear rate for each sample is calculated from the volume or weight of material removed during the test.

The pin is weighted and measured before and after the test by means of an analytical scale having a 10^{-4} g sensitivity and a digital caliper (sensitivity, 0.01 mm). The wear volume of the pin (V) is calculated as (Eq. 3.1):

$$V = \frac{m_0 - m_1}{\rho} \quad (\text{Eq. 3.1})$$

where m_0 and m_1 are the pin masses before and after the test, and ρ is the bulk density calculated as the ratio between the mass and the volume. The wear volume (V) is used in the equation to calculate the wear rate (Eq. 3.2):

$$W = \frac{V_{pin}}{s} \quad (\text{Eq. 3.2})$$

where s is the sliding distance, and it is calculated by multiplying the sliding velocity with the duration of the test.

Finally, the specific wear coefficient (K_a) evaluated as (Eq. 3.3):

$$K_a = \frac{W_{pin}}{A_{pin} * P_n} = \frac{V_{pin}}{F_n * s} \quad (\text{Eq. 3.3})$$

where F_n is the nominal contact force between pin and disc, it is calculated by multiplying the nominal area (A_{pin}) by the nominal contact pressure (P_n).

The specific wear coefficient is calculated based on the Archard equation described in section 1.2.1. This parameter is indicative of the wear regime of the material. As reported in section 1.2.1.2, if K_a is in the order of magnitude of 10^{-15} (m^2/N) or lower, the wear regime is mild, if in the order of 10^{-13} , the wear is severe. The values in the order of 10^{-14} are between the two regimes (mild and severe).

3.3.1.2 Evaluation of the pin-on-disc emissions

In the ECOPADS project, the selected formulations and the reference materials were tested at KTH as regard to the emissions. The tests were performed using a pin-on-disc close in a box (climate chamber) in which the cleanness of the incoming air is controlled. In Fig. 3.14 is reported a scheme of the experimental set-up [154]. The contact pressure and sliding speed for testing are 0.6 MPa and 2 m/s, respectively.

When the test starts and the disc is rotating, the generate airborne fraction of the wear debris is well mixed to the clean air volume. The flux of air that passes through the chamber outlet is sampled by the particle instruments.

Airborne PM emitted during the sliding tests are measured by a TSI® Optical Particle Sizer (OPS) model 3330 and a DEKATI® Electrical Low-Pressure Impactor (ELPI+) at a sampling frequency of 1 Hz.

The particle measurement instruments use different working principles, herewith listed:

- **Optical Particle Sizer (OPS):** it measures the particle number concentration (PN) in the particle size range from 0.3 μm to 10 μm . The particles are divided into different counting channels according to their optical diameter. The working principle of the instrumentation is based on light scattering. The sampling flow rate in entrance, passes in an optical chamber and each particle is sampled by a laser beam. A photo-detector counts the number and the size of the particles scattered by the beam.
- **Electrical Low-Pressure Impactor (ELPI+):** this measures the particle distribution and concentration in the size range from 6 nm to 10 μm . It collects particles on 14 different stages according to their aerodynamic diameter. The instrument is a low-pressure cascade impactor. The particles are charged with a known charge level by means of a corona charger. The different stages bend the air flow differently and collect particles that deposited on the collecting substrates. Particles are classified according to their aerodynamic diameter and

inertial forces. Then, the electrical current of the collected particles is recorded by the respective electrometer channel, it is proportional to the number concentration. Moreover, chemical and physical analysis can be performed after the tests since the particles are collected on the filters, typically round shaped Al foils.

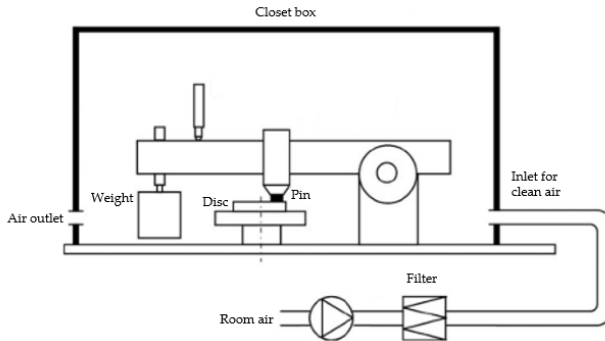


Fig. 3.14. Schematic of the pin-on-disc at KTH equipped to evaluate the emissions [154].

3.3.2 Dynamometer tests

In automotive brake testing, dynamometer tests are used in the development stage as the final verification of the brake design before the tests on complete vehicles, which are expensive and time consuming. Three different types of dynamometers are commonly used:

- chassis dynamometer, it is used to test the whole vehicle under well controlled environmental conditions [155];
- inertia dynamometers, it is used to test the single brake assembly up to the whole mechanical brake system [144][102];
- reduced-scale friction testing, it is used to generate accurate friction material data for use in brake system design and material screening, because friction materials can be tested easily without brake hardware [156].

In this work, the inertia dynamometer was used to validate some of the best formulations developed in the ECOPADS project. Pin-on-disc

tests were used as a material screening method, considering friction, wear and emission performance.

In the dyno tests are used real components of the brake system (pads, caliper and disc). The test procedures may be designed to simulate conditions like those experienced on actual vehicles.

The dyno bench set-up comprises an electrical motor that imposes the rotational speed to the brake rotor (disc). The rotor is attached to a driving shaft on which flywheels are mounted to simulate the appropriate part of the vehicle inertia and kinetic energy. The brake stator (caliper) is mounted to the 'tailstock' shaft of the machine.

The procedure used in ECOPADS and commonly accepted for the performance tests is the AK master (SAE J2522). The test cycle used for wear performance testing is referred to as Block Wear (SAE J2707). The brake system wear is evaluated measuring pads thickness and weight and disc weight, before and after the test. Instead, the emission tests were performed according to the urban city driving cycle reported in [121] (Table 3.11).

Table 3.11. Urban city driving cycle used for the evaluation of particulate emissions [121].

#	Section [specific energy]	Initial speed [km/h]	Final speed [km/h]	T, initial rotor brake [°C]	Braking deceleration [g]	Number of stops [N]
5' Cleaning						
1.1	25 J/kg	36	26	70	0.16	2
1.2		36	26	90	0.16	18
1.3		36	26	110	0.16	83
1.4		36	26	130	0.16	56
1.5		36	26	150	0.16	24
1.6		36	26	170	0.16	8
2.1	75 J/kg	52	28	70	0.23	5
2.2		52	28	90	0.23	16
2.3		52	28	110	0.23	22
2.4		52	28	130	0.23	25
2.5		52	28	150	0.23	12
2.6		52	28	170	0.23	8
3.1	125 J/kg	57	5	70	0.25	2
3.2		57	5	90	0.25	3
3.3		57	5	110	0.25	6
3.4		57	5	130	0.25	8
3.5		57	5	150	0.25	1
4.1	175 J/kg	70	17	110	0.31	1
4.2		70	17	130	0.31	2
4.3		70	17	170	0.31	1
5.1	225 J/kg	79	20	110	0.24	1
5' Cleaning						

3.3.2.1 Evaluation of the dyno emissions

An inertial dynamometer was redesigned by Perricone et al. [157] and it was used for the particulate matter collection. A schematic representation is reported in Fig. 3.15, whereas details of the set-up of the test are reported in [157] and previously are described by Alemani et al. [143].

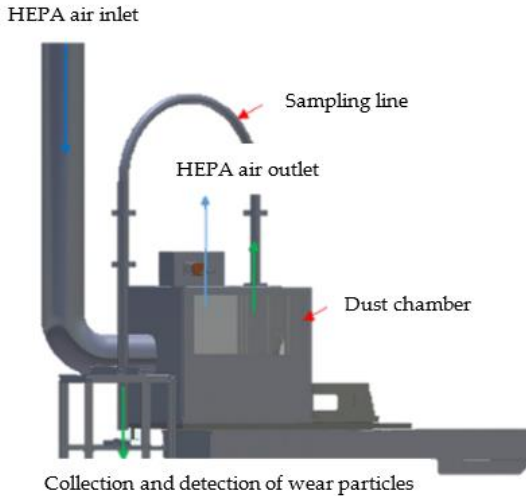


Fig. 3.15. Schematic representation of the dust chamber of dyno-bench tester [158].

The instruments used to measure particle emissions are (Fig. 3.16):

- PM10 impactor and the Filter Holder for the measure of the particle mass (PM);
- ELPI+ and CPC for the measure of the particle numbers (PN).

The main characteristics of the particle measurement instruments are here reported:

- **PM10 Impactor:** this is a three-stage cascade impactor. It determines particle gravimetric mass size distribution, the division of the particles occurs in classes of 10, 2.5 and 1 μm , making this instrument appropriate for PM10, PM2.5 and PM1.0 measurements. The filters for collection of particles are greased aluminium foils. The sticking of particles on the

specific filter is based on particle's inertia that is linked to the size of the particles.

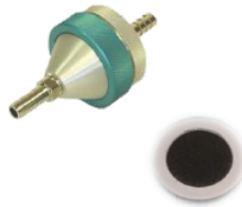
- **Filter Holder 47 mm:** this is to collect the particles with a diameter lower than $10\ \mu\text{m}$ in a unique filter, it is useful for collecting the particles for chemical analyses.
- **Electrical Low-Pressure Impactor (ELPI+):** see section 3.3.1.2.
- **Condensation Particle Counter (CPC):** this Butanol-CPC detects airborne particles down to $4\ \text{nm}$ in diameter (Max. detectable particle $> 3\ \mu\text{m}$). Butanol is vaporized and diffuses into the aerosol sample stream. The vapour pass into a cooled condenser where the butanol vapour becomes supersaturated and ready to condense on the particles present in the sample stream which serve as condensation nuclei. Particles, that become larger than a threshold value, grow into larger droplets and are counted by an optical detector.

PARTICLES MASS

PM10 impactor



Filter Holder 47 mm



PARTICLES NUMBER

Dekati® ELPI+



CPC



Fig.3.16. Emission testing set-up in dynamometer test.

3.4 Characterization tools

For the characterization of friction materials and wear samples different techniques were used. Hereafter are described the principal information on the employed experimental tools.

3.4.1 Scanning Electron Microscopy (SEM) and Energy Dispersive X-Ray Spectroscopy (EDXS)

The scanning electron microscope and the energy dispersive X-Ray spectroscopy were used to analyse and characterize the friction formulations and the worn surfaces of pins and discs.

The experimental apparatus used during this research is a JEOL IT300 equipped with the EDXS probe. This technique allows superficial analysis of the samples through the different interactions that the accelerated electron beam produces with the samples. SEM images were taken both in secondary electron (SE) mode to have a topographic contrast and back-scattered electron (BSE) mode to have phase contrast. EDXS gives compositional information by detecting the characteristic X-rays radiation deriving from the different element present on the analysed area.

Moreover, by combining SEM observations with EDXS analyses, it was possible to obtain an EDXS elemental map of the specimens, where the areas of the sample had different colours depending on their elemental composition.

The planar observation of the pin surface didn't require any preparation, and it was mainly focused on evaluating the extension of the friction layer, i.e., primary and secondary plateaus. Cross sections of the pins have been prepared by cutting the samples, embedded in a cold mounting resin (Struers Epo_x), longitudinal to the sliding direction followed by a mirror polishing of the surface, in order to evaluate the thickness and the compactness of the friction layer.

Moreover, a specific software was used to perform image analysis (ImageJ). For each evaluation of the extension of the friction layer, three different images at different locations over the worn pin's surface at a magnification of 100x were analysed.

3.4.2 X-ray diffractometer (XRD)

The crystalline phases and their composition in the reference master-batches were identified using X-ray diffraction (XRD) measurements carried out with an Italstructures IPD3000 instrument equipped with a Co anode source (line focus) operating at 40 kV and 30 mA. Diffraction spectra were acquired in reflection geometry by means of an Inel CPS120 detector over 5-120° 2-theta range (0.03 degrees per channel). XRD data were modelled by using a full-pattern approach based on the Rietveld method as implemented in the MAUD software [150]. Fig. 3.17 shows as example the XRD pattern of the master-batch FM/2.

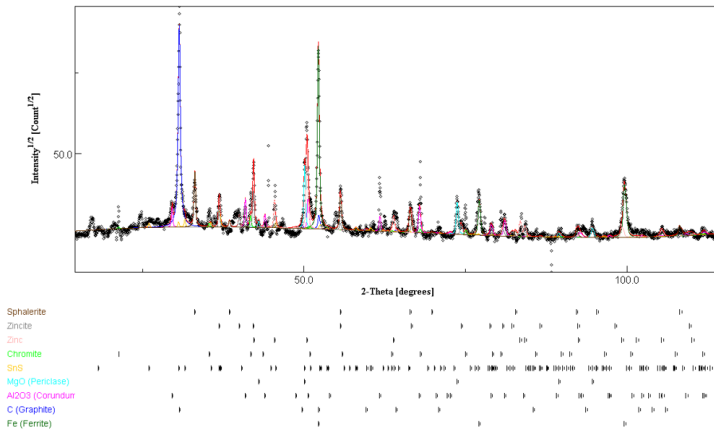


Fig. 3.17. XRD of the masterbatch FM/2. Dot: experimental points; continuous line: Rietveld simulated pattern.

Friction materials are a complex mix of different constituents, the main problems found of using XRD, especially for the quantitative analysis, were:

- the presence of a significant percentage of amorphous fraction, mainly organic;
- the presence of a considerable quantity of crystallographic phases; each of these phases presents problems of preferential orientation, bad statistics (few particles of considerable size) and complicated microstructure.

3.4.3 Profilometer

In some cases, the surface of the disc after the tribological tests was investigated with a profilometric analysis, in order to evaluate the behaviour of friction materials on the disc.

The used profilometer is a Hommel Tester T1000 stylus profilometer, with a curvature radius of the tip equal to 5 μm . The scanning length on the disc was 15 mm and the tip speed across surface of 0.15 mm/s.

3.4.5 Shore D Hardness

The hardness value is determined by the penetration of the Durometer (Hildebrand Durometer Operating Stand Model OS-2) indenter foot into the sample. Test methods used to measure Shore D Hardness are the application of a 4.550 kg mass with a 30° cone configuration (ASTM D2240). The measures are dimensionless, in the range between 0 and 100. The higher number represents the harder material.

The hardness values were measured on pins' top surfaces. The readings were carried out one second after the presser foot met the specimen, in order to avoid viscoelastic effects.

3.4.6 Compression tests

The compressive strength was evaluated through uniaxial compression tests on the pin samples using a universal testing machine Instron 5969 equipped with a load cell of 50 kN. The pins were tested at constant compressive-strain-rate by imposing a cross-head velocity of 1 mm/min.

The compressibility is an important parameter with a very significant effect on the reduction of the vibration and the squeal generation [159].

3.4.7 Helium gas pycnometer

The porosity of the pins was evaluated using a helium gas pycnometer (AccuPyc1330TC, Micromeritics). The gas pycnometer determines the density and volume by measuring the pressure change of helium in a calibrated volume. Helium molecules fill pores as small as one angstrom in diameter. This technique is non-destructive as it uses the

gas displacement method to measure volume. Analysis measures sample volume, from which density is derived automatically entering the sample weight.

The difference between the bulk density and the density evaluated with the pycnometer (apparent density) gave information about the porosity of the pins.

3.4.8 Thermogravimetric (TG) analyses

In order to determine the characteristic degradation temperature for the friction materials, thermogravimetric analysis on the phenolic resin alone (the binder) were performed, on the master-batch and on the friction material. The analyses were carried out using a Netzsch STA 409 Luxx thermal analyser with alumina sample holder. The heating rate was set to 10 °C/min in air flux. For all the specimens, a small amount of material (50 mg) was heated up to 1200°C. During the heating of the samples in the thermo-balance, if some degradation phenomena occurred the equipment detected the relative mass variation.

Moreover, the phenolic resin was isothermally heat treated in the TG analyser in air at different temperatures: 200 °C, 300 °C, 500 °C, 700 °C, 1200 °C. The thermal cycles were performed with the heating rate of 10 °C/min, with a holding time at the specific temperature of 5 min. Infrared spectroscopy analyses were then conducted on the thermal treated samples.

3.4.9 Fourier-transform infrared spectroscopy (FT-IR)

Fourier transform infrared transmission spectra were recorded with a Varian 4100 FTIR Excalibur Series spectrometer, exploiting the attenuated total reflectance (ATR) geometry using a diamond crystal as internal reflective element (IRE). The acquisition conditions were as follows:

- 4000–500 cm^{-1} wavenumber range;
- 32 scans for each acquisition;
- 4 cm^{-1} resolution.

3.4.10 Differential scanning calorimetry (DSC)

Differential scanning calorimetry was carried out with a Mettler DSC30 instrument. Heating tests were performed on phenolic resin powders of approx. 15 mg, in the temperature interval 0–250 °C, at the scanning speed of 10 °C/min, in N₂ atmosphere.

The analyses were performed to study the degradation of the phenolic resins during storage, monitoring the glass transition temperature (T_g) every two months for fourteen months. T_g is influenced by the chemical structure of the resin and an increase in the T_g value can be correlated with cross-linking phenomena.

Chapter 4

4. Evaluation of pin properties

4.1 Validation of the pin production

The methodology to produce the sample (pin) directly from the master-batch powder was validated by comparing some pins produced in laboratory (paragraph 3.2) with those extracted directly from a real pad (Fig. 4.1).



Fig. 4.1. Extraction of the pins from brake pads.

Three pins produced by powders and three pins extracted from pad (of the same formulation) were PoD tested at RT. Furthermore, some properties, like density and hardness, were compared.

In Table 4.1 the outcome of the comparison between the pins, the mean values of the evaluated parameters (density, hardness, μ , K_a), considering the uncertainty of the error, are comparable and thus representative of the material properties. Therefore, it can be stated that the procedure used for the net-shape forming of the pins can be profitably used to explore minor changes in the formulations of the

master friction materials, without the need of preparing large amount of master-batches.

Table 4.1. Comparison between the pins extracted from pads and produced by powders. Material: FM/1. Measurements: density, hardness, friction coefficient (μ) and specific wear coefficient (K_a).

	Pins from PADS	Pins from POWDERS
Density	$2.70 \pm 0.1 \text{ g/cm}^3$	$2.67 \pm 0.04 \text{ g/cm}^3$
Hardness	$80 \pm 0.03 \text{ Shore D}$	$75 \pm 0.04 \text{ Shore D}$
μ (PoD)	0.44 ± 0.02	0.43 ± 0.03
K_a (PoD)	$(6.01 \pm 2.01) *10^{-15} \text{ N/m}^2$	$(6.65 \pm 1.25) *10^{-15} \text{ N/m}^2$

4.2 Case study: pin density

The residual porosity resulting from the production process of brake pads (hot-pressing and sintering) influences the density and hence the overall performance of the friction materials. The influence of the density on mechanical and tribological properties was therefore investigated, using the master-batch FM/2. The pins for the wear testing were prepared according to the procedure describe in the paragraph 3.2. In order to obtain different densities of the pins, different initial degassing cycles and moulding pressure were used. Samples with three different densities were produced: 1.8 g/cm^3 , 2.2 g/cm^3 and 2.5 g/cm^3 . In Table 4.2, the parameters used to produce the pins of FM/2 at different densities are listed. The densities have been estimated as the ratio between the mass of the pin and its geometric volume (bulk density).

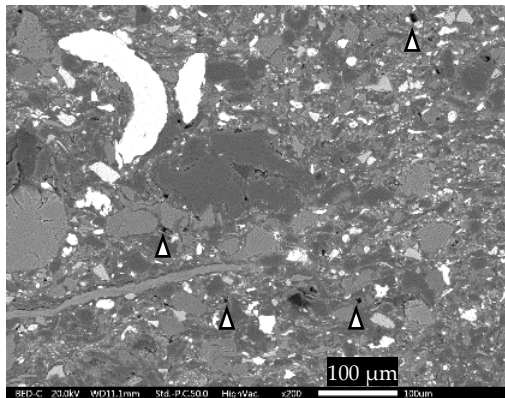
Table 4.2. Parameters used during the hot-pressing of the mixtures FM/2 to obtain the densities 1.8 g/cm^3 , 2.2 g/cm^3 , 2.5 g/cm^3 .

Density (g/cm³)	Degassing cycles (MPa)	Moulding pressure (MPa)	Moulding time (min)
1.8	1 at 2.5	-	10
2.2	1 at 7.5	2.5	10
2.5	5 at 17.5	17.5	10

4.2.1 Effect of density on mechanical behaviour

In Fig. 4.2, the SEM observations of the pin cross sections of FM/2 at different densities are shown. These images evaluate qualitatively the concentration, the dimension and the shape of the pores present in the internal structure of the samples. The arrows in the images indicate some pores. At low densities, there are many pores with small size and spherical shape. Increasing the density (2.2 g/cm^3 , 2.5 g/cm^3) there are fewer pores but in some cases, they have a larger size compared to the previous one, and also some hole near specific constituents start to appear. It is also possible to observe that the internal microstructure of the material appears more oriented as the density increases. At 2.5 g/cm^3 the pores are very elongated and similar to internal cracks (in particular at the fibre-matrix interface) probably due to the excessive moulding pressure.

1.8 g/cm^3



2.2 g/cm³



2.5 g/cm³

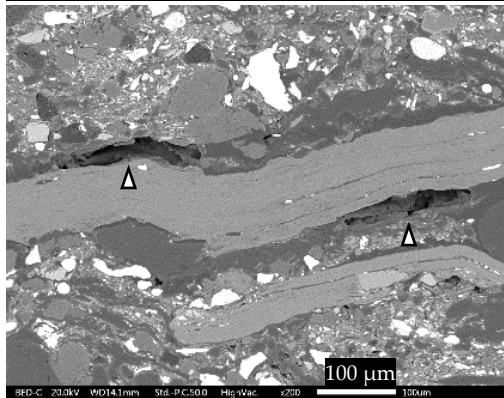


Fig. 4.2. SEM micrograph of the cross-section of the material FM/2 at different densities: 1.8 g/cm³, 2.2 g/cm³, 2.5 g/cm³. The arrows indicate some of the pores present in the cross-sections (Δ).

The values of open porosity, obtained using a helium pycnometer, are listed in Table 4.3. As expected, the porosity is strictly correlated with the density, it decreases as the density increases for both materials. In Table 4.3 the hardness (Shore D) values are also indicated. The results of the hardness are the average value of three readings for each sample, the measure was repeated on two different pins for each density. The samples with the lowest density (1.8 g/cm³) have the lowest hardness. The material hardness raises with its density even if the maximum hardness is reached at 2.2 g/cm³.

Compression tests were also conducted on materials with different densities, two repetitions were performed for each density value.

Examples of stress-strain curves for each density are provided in Fig. 4.3.

Table 4.3. Porosity (%) and Hardness (Shore D) of the material FM/2 at different densities: 1.8 g/cm³, 2.2 g/cm³, 2.5 g/cm³.

Density (g/cm ³)	Porosity (%)	Hardness (Shore D)
1.8	37	49
2.2	26	69
2.5	21	67

In Table 4.4 the values of the compressive strength are listed. The stress-strain compressive curve shown in Fig. 4.3 provides other important information on the mechanical response of the materials, i.e., the modulus of toughness (U_T). The area under the stress-strain curve is a measure of the total energy that a material can absorb before breaking. The area can be divided into two main parts. During loading, the area under the stress-strain curve is the energy absorbed by the material for the crack nucleation. Instead, the area after the maximum peak of strength is the energy for the crack growth propagation and failure. The values of the energies are listed in Table 4.4.

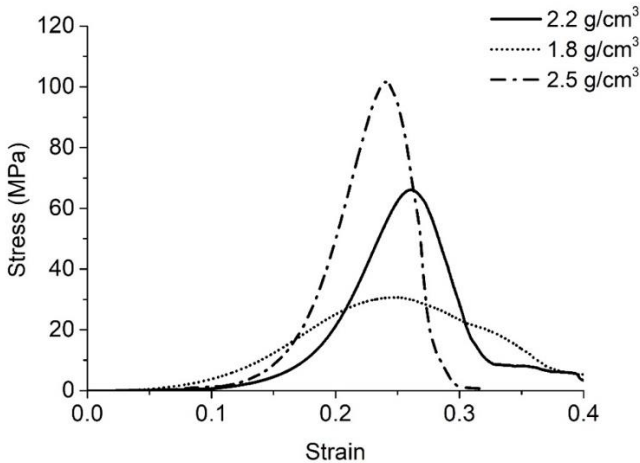


Fig.4.3. Stress-strain curves obtained by compression tests of FM/2 at different densities: 1.8 g/cm³, 2.2 g/cm³, 2.5 g/cm³.

Table 4.4. Values of compressive strength and modulus of toughness (U_T) of FM/2. U_T is divided in the energy for cracks nucleation (U_N) and the energy for cracks propagation (U_P).

Density (g/cm ³)	Compressive Strength (MPa)	U_T (KJ/m ³)	U_N (KJ/m ³)	U_P (KJ/m ³)
1.8	23	5245	3788	1457
2.2	70	5775	4578	1197
2.5	97	6583	5514	1069

In Fig. 4.4, the energy for crack nucleation and propagation for the materials of different densities are shown. The energy for the crack nucleation increases with density: this means that the pores present in the low density material (spherical geometry but a high number) contribute to a local phenomenon of damage, that leads to the formation of the cracks. For all the densities, after the crack nucleation, the energy required for the propagation is lower. Moreover, the energy for the propagation of the cracks decreases with density. This is motivated by the strong orientation of the hole observed at the interface fibres/matrix for the high-density samples, that contribute to having a faster fracture.

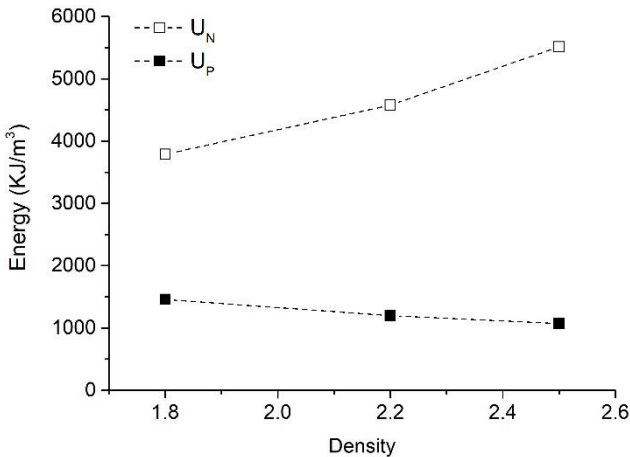


Fig. 4.4. Energy for cracks nucleation (U_N) and energy for cracks propagation (U_P) at different densities.

4.2.2 Effect of density on tribological properties

Average values of friction coefficient and specific wear coefficient (K_a) of FM/2, obtained from the PoD tests, are shown in Table 4.5. The friction coefficient raises in passing from the density of 1.8 g/cm³ to 2.2 g/cm³, then decrease for the density of 2.5 g/cm³ (Fig. 4.5). The evolution of the specific wear coefficient is also shown in Fig. 4.5: a clear reduction of K_a with the material density can be observed.

Table 4.5. Values of friction coefficient (μ) and specific wear coefficient (K_a) of the FM/2 material obtained from the pin-on-disc tests.

μ			K_a (*10 ⁻¹⁴ m ² /N)		
1.8 g/cm ³	2.2 g/cm ³	2.5 g/cm ³	1.8 g/cm ³	2.2 g/cm ³	2.5 g/cm ³
0.49 ± 0.02	0.54 ± 0.02	0.49 ± 0.03	6.43 ± 0.14	6.07 ± 0.49	3.40 ± 0.25

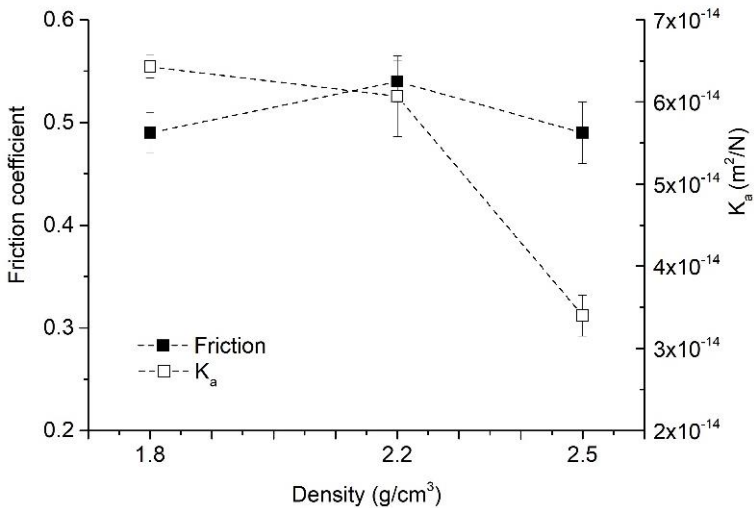


Fig.4.5. Evolution of the friction coefficient (μ) and the specific wear coefficient (K_a) with the friction material density (1.8 g/cm³, 2.2 g/cm³, 2.5 g/cm³), for the samples FM/2.

4.2.3 Main results

The production of the samples produced directly by powders, instead of machined from the pads, has proved ideal for modifying the formulations using a low amount of ingredients and has yielded representative results of the material.

The main findings of the friction material characterization are summarized below:

- The porosity decreases as the density increases.
- The hardness increases as the density increases, up to the value of 2.2 g/cm³.
- In the material featuring the higher density, due to the high pressing pressure, some cracks originate at the interface between matrix and fibres. All the friction materials exhibit a brittle fracture. After nucleation a very fast crack propagation is observed. The modulus of toughness is influenced by the presence of pores and/or cracks.
- The friction coefficient is not strictly correlated with the density.
- The wear depends on the density of the material and on the interface conditions, but not on the toughness.

Considering the results, it can be concluded that the minimum density to achieve in order to have a general improvement in friction material properties is 2.2 g/cm³.

Chapter 5

5. Copper substitution

The copper substitution started by investigating the role of copper in friction materials, in particular, its impact on tribological properties. For this purpose, the reference Cu-full master-batch was used (FM/1) which was modified by removing copper (FM/1-Cu).

Then, it was produced a Cu-free formulation with reduced wear in comparison with the reference formulation with copper (FM/1). Two procedures are adopted to do accomplish this task:

- replacement of the removed copper fibres (~ 15 wt.%) with *steel fibres* → Study of Primary Plateaus;
- addition of *barite* in different concentrations in order to reduce wear → Study of Secondary Plateaus.

The two aforementioned constituents have been balanced in the new resulting formulation to have the maximum wear performance and the friction coefficient stable.

Moreover, an investigation on some Cu-free formulations available on the market has been reported.

5.1 Copper

5.1.1 Background

Copper is added to friction materials, both in the form of fibre and powder, and has a fundamental role in tribological contact. Copper fibres act as primary plateaus. Moreover, copper particles (nano-size) enter the friction layer and work as solid lubricant contributing to stabilize the friction-force and to guarantee smooth sliding behaviour [63].

5.1.2 Samples

The investigation on the copper role in FMs starts removing copper from the master-batch FM/1. Copper is present as fibres (~15 wt.%) and powders (~1 wt.%). The new formulation is referred as FM/1-Cu (Table 5.1).

Table 5.1. Designation of samples: FM/1, FM/1-Cu

Designation	Material
FM/1	Cu-full reference friction material (see 3.1.1)
FM/1-Cu	FM/1 without copper (fibres and powders)

The mixtures were used to produce cylindrical pins for the wear testing (see paragraph 3.2).

5.1.3 Testing and characterization

Fig. 5.1 shows the evolution of the friction coefficient, μ , for the two materials as recorded during the PoD tests conducted for 50 min at RT and HT (300°C). At RT, the FM/1 specimen has higher friction coefficient compared with FM/1-Cu. At HT, the friction coefficient increased as well as the scatter for both materials. FM/1-Cu presents evident instability of friction.

In Table 5.2 the average values of the friction coefficients and the values for the specific wear coefficient (K_a) are listed. They refer to RT and HT PoD tests. For the RT tests, the FM/1 and FM/1-Cu exhibit a K_a (m^2/N) very similar, $6.65 \cdot 10^{-15}$ and $6.91 \cdot 10^{-15}$ for FM/1 and FM/1-Cu respectively. Under the HT condition, both materials display a K_a one order of magnitude higher, in the $10^{-14} m^2/N$ range, as an indication of a worst wear resistance. Moreover, material FM/1-Cu shown a higher value compared with the reference FM/1.

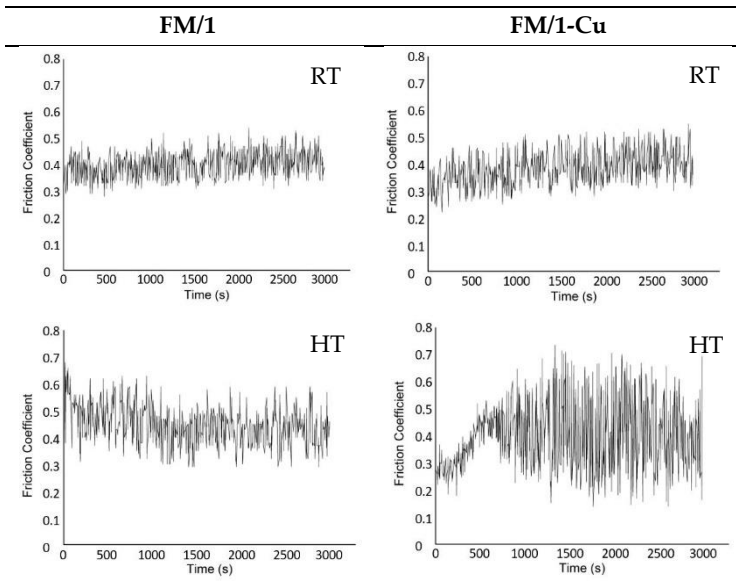


Fig. 5.1. Evolution of the friction coefficient for the materials FM/1 and FM/1-Cu recorded during the PoD tests carried out at RT and HT (300°C).

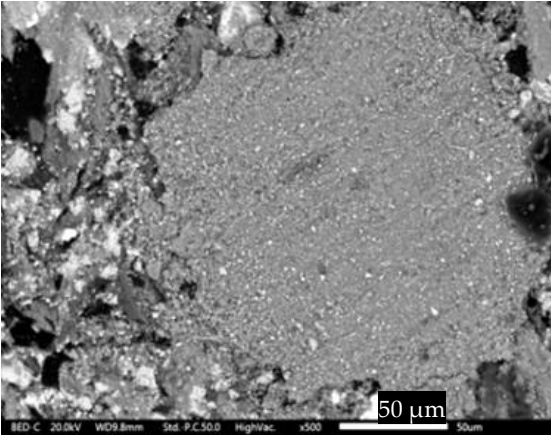
Table 5.2. Coefficient of friction (μ) and specific wear coefficient (K_a) for the PoD test carried out at RT and HT (300°C). Materials: FM/1 and FM/1-Cu.

	μ		K_a (m ² /N)	
	RT	HT	RT	HT
FM/1	0.42 ± 0.06	0.46 ± 0.07	6.65*10 ⁻¹⁵	1.68*10 ⁻¹⁴
FM/1-Cu	0.38 ± 0.07	0.40 ± 0.13	6.91*10 ⁻¹⁵	4.21*10 ⁻¹⁴

To complete the picture provided by the tribological parameters (μ and K_a), the wear tracks on the pin surface were investigated by SEM observations. Fig. 5.2 shows the top view of the friction layers that formed on the surface of the two materials at RT. The two main component parts of the friction layer are the primary plateaus (PP) and the secondary plateaus (SP). These latter are produced by the compaction of the wear debris trapped in between the two mating surfaces (the pin and the disc). The FM/1 display good compaction of the debris which forms the secondary plateaus, whereas the plateaus of the FM/1-Cu present many cracks. After the test at HT (Fig. 5.3), the

cracks tend to disappear, however, is visible the presence of coarse particles in secondary plateaus as compared to the FM/1.

FM/1



FM/1-Cu

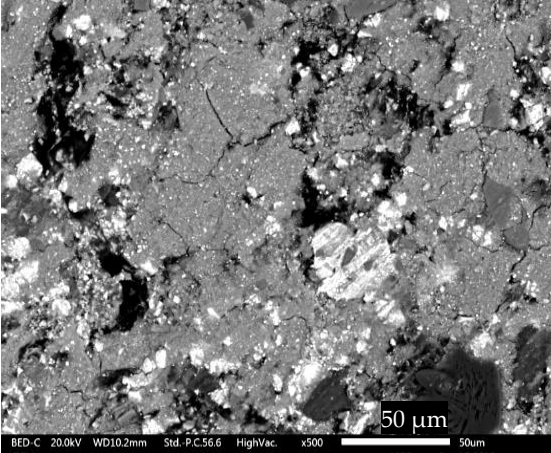
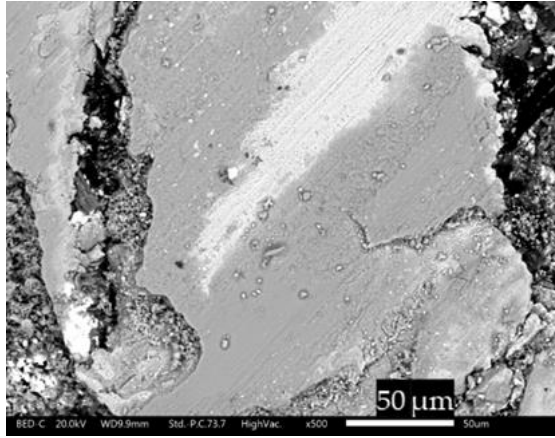


Fig. 5.2. SEM observations of the worn pins (materials FM/1 and FM/1-Cu) tested at RT.

It was observed in FM/1 that metal fibres made by steel behave the same as copper fibres as regards to the formation of primary plateaus (Fig. 5.4).

FM/1



FM/1-Cu

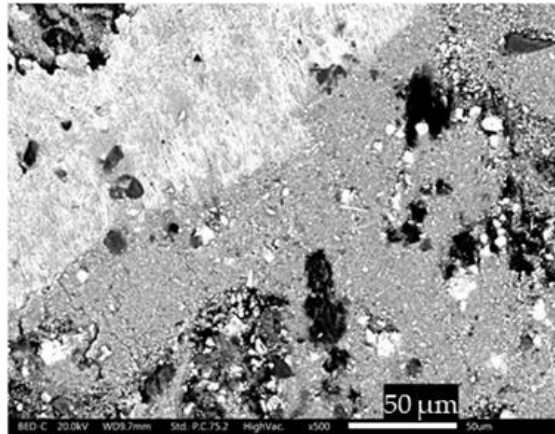


Fig. 5.3. SEM observations of the worn pins (materials FM/1 and FM/1-Cu) tested at HT (300°C).

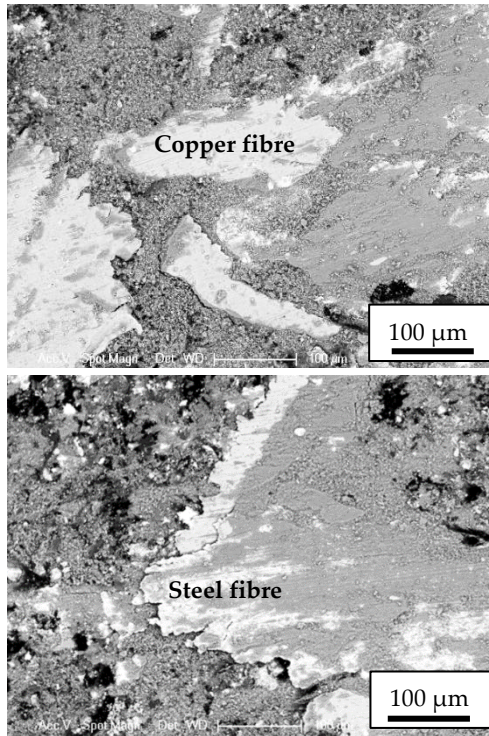


Fig. 5.4. Comparison among metal fibres (copper and steel) observed on the pin surface of FM/1 after the PoD test at RT.

5.1.4 Main results

The FM/1-Cu was compared to the original mix containing copper (FM/1) revealing a clear effect on the tribological properties. In the Cu-free formulation, a reduction of the friction coefficient and an increase of wear were observed. The friction layer formed on the worn pins' surfaces of Cu-free formulation is less compact and shows a coarser granulometry (Fig. 5.2). Fig. 5.1 shows the evolution of the coefficient of friction, for the two materials as recorded during the PoD tests. It can be seen that FM/1-Cu displays more scatter. In particular, a drastic instability of μ was noted at high temperature (Fig. 5.1). This probably also correlate with the drastic reduction in metal fibres in the formulation due to the removal of ~15 wt.% of Cu-fibres without its substitution.

5.2 Steel fibres

5.2.1 Background

As a result of the previous study on the role of copper in FMs, a good starting point for producing a novel Cu-free formulation, was the replacement of Cu fibres with steel fibres. Indeed, the formation mechanism of primary contact sites, made up of tough metallic fibres and coarse hard particles, is expected to be the same.

5.2.2 Samples

FM/1 was used as the reference material, the content of copper fibres is ~15 wt.%. The copper-free friction material (FM/1-Cu) was taken as reference to prepare the new mixture, called 15Fe/1-Cu, by adding 15 wt.% of steel fibres. The designed formulation is reported in Table 5.3.

Table 5.3. Designation of the sample 15Fe/1-Cu.

Designation	Material
15Fe/1-Cu	FM/1-Cu + 15 wt.% steel fibres

5.2.3 Testing and characterization

In Fig. 5.5 the evolution of the friction coefficient of 15Fe/1-Cu is shown in comparison to FM/1 (tests at RT). After a running-in stage (approximately 1500 s) characterized by almost a continuous increase in μ , a steady-state value is attained. The average values in the steady-state regime and the scatter of the friction coefficient recording during the tests (Table 5.4) are comparable for the two materials. Both materials have higher friction coefficient than Cu-free formulation (FM/1-Cu), thus highlighting the role that metal fibres have on μ .

As regards the wear data, the specific wear coefficients (K_a) of the materials FM/1, FM/1-Cu and 15Fe/1-Cu are included in Table 5.4. 15Fe/1-Cu presents higher K_a compared to the reference FM/1 and FM/1-Cu, however the obtained value is coherent with a mild wear regime. This could be explained considering that, especially during the early stage of the sliding process, metal fibres contribute to the tribo-

oxidative wearing out of the disc, and steel fibres that are harder than copper fibres are more aggressive towards the disc.

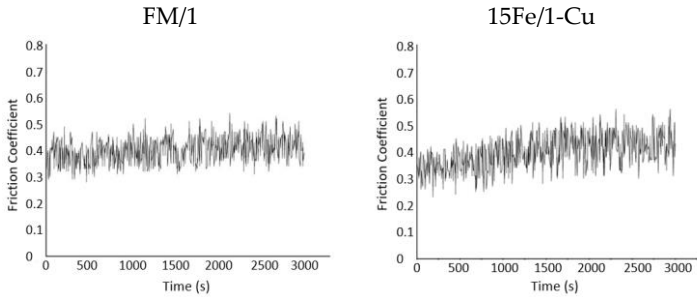


Fig. 5.5. Evolution of the friction coefficient for the samples FM/1, FM/1-Cu and 15Fe/1-Cu.

Table 5.4. Values of steady state friction coefficient (μ) and specific wear coefficient (K_a) for each material.

	μ	K_a (m^2/N)
FM/1	0.42 ± 0.06	$(6.65 \pm 0.54) \cdot 10^{-15}$
FM/1-Cu	0.38 ± 0.07	$(6.91 \pm 0.95) \cdot 10^{-15}$
15Fe/1-Cu	0.43 ± 0.06	$(8.91 \pm 0.50) \cdot 10^{-15}$

Fig. 5.6 shows the worn surfaces of the pins after the tests at lower magnification. The extension of the primary plateaus, made by metallic fibres (visible in white), was determined with image analysis. The percent extension of the primary plateaus correlates with the total content of metal fibres, that is very low in FM/1-Cu (coverage factor: 6%) and higher in FM/1 and 15Fe/1-Cu (coverage factor: 11% and 16%, respectively). The differences between FM/1 and 15Fe/1-Cu are mainly explained considering that some of the fibres acting as primary plateaus in the FM/1 material tend to be partially covered by the secondary plateaus. The reason for this behaviour can be reasonably traced back to the lower hardness of copper fibres with respect to steel fibres. This situation artificially reduces the primary plateaus that are detectable by image analysis. Furthermore, this data might suggest the presence of an excessive quantity of metallic fibres in 15Fe/1-Cu with respect to the reference (FM/1). It should be remembered that the initial

compositions of the master-batches have been estimated with analysis techniques and are indicative.

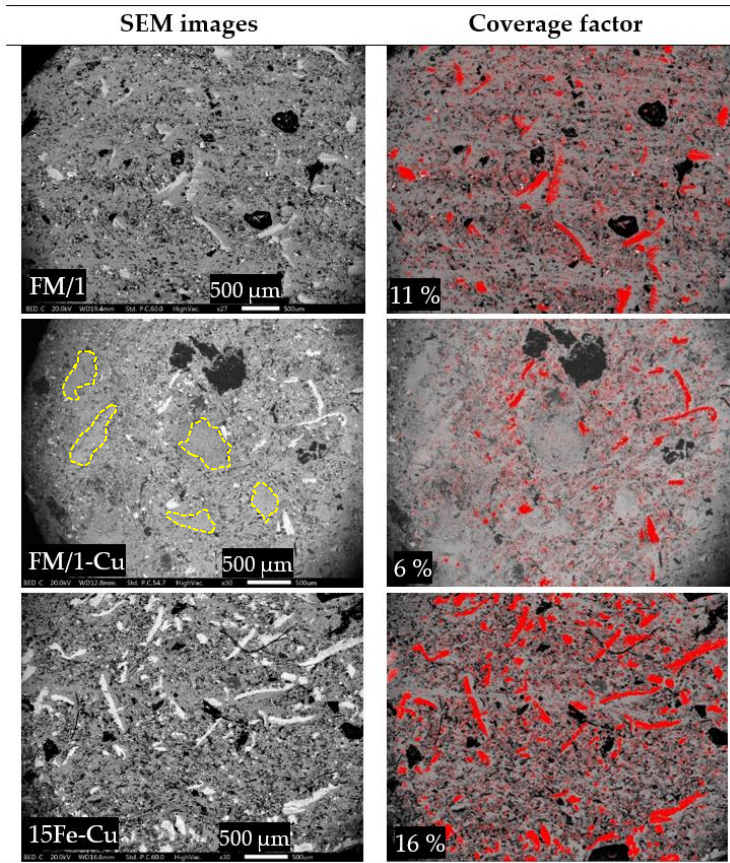


Fig. 5.6. SEM images of the pin surface after PoD tests for each material. The coverage factor (quoted in the left micrographs) represents the evaluation of the surface percentage of the primary plateaus, estimated by image analysis. In FM/1-Cu material are present large secondary plateaus (marked in yellow) not supported by primary plateaus.

Both copper and steel fibres, as primary plateaus, give support to the formation of secondary plateaus and they resist against the shear stresses. This type of SP is the standard for the materials FM/1 and 15Fe/1-Cu. FM/1-Cu shown a limited fraction of SP build up against primary plateaus. In Fig. 5.6 (market in yellow), it is evident the

presence of large secondary plateaus, forming without the support of SP. It is reported in literature [160] that these structures tend to reduce the friction coefficient.

In Fig. 5.7 the secondary plateaus planar view of 15Fe/1-Cu is shown. As for material FM/1-Cu (Fig. 5.2), some cracks are visible on the plateaus. An evaluation of the crack surface density was done on the FMs using five different SEM fields of view for each material. Plateaus were randomly selected, and the SEM magnification was kept the same throughout the measurements. The measured lengths of the cracks on the plateau were added up and then normalized to the plateau surface area, to estimate the crack surface density, expressed in $\mu\text{m}/\mu\text{m}^2$ (Table 5.5). The results confirm that at RT the two Cu-free materials, FM/1-Cu and 15Fe/1-Cu, exhibit more cracks plateaus in comparison to the FM/1. The formation of cracks can be ascribed to the absence of copper. In fact, as it is acknowledged [63], small inclusions of copper have an important role in the formation of well compacted secondary plateaus.

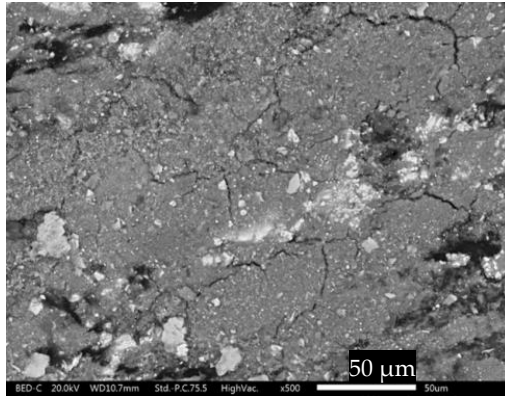


Fig. 5.7 SEM observation of the secondary plateaus in the sample 15Fe/1-Cu wear tested at RT.

Table 5.5. Crack surface density in the secondary plateaus.

Cracks density ($\mu\text{m}/\mu\text{m}^2$)	FM/1	FM/1-Cu	15Fe/1-Cu
Mean value	0.0003	0.017	0.016
Standard deviation	0.0006	0.002	0.005

The composition of the secondary plateaus was evaluated with EDXS analyses. The results are shown in Fig. 5.8. In general, all elements present in the FMs were detected, with the addition of a quite large amount of iron, showing that the wear fragments coming from the disc enter into the friction layer. The main particles are made of iron oxides, zirconium oxide and potassium titanate. As expected, the friction layer that forms on the material FM/1 contain also copper. The content of Fe is lower in FM/1-Cu compared to the other materials, on the other hand increased the content of Ti.

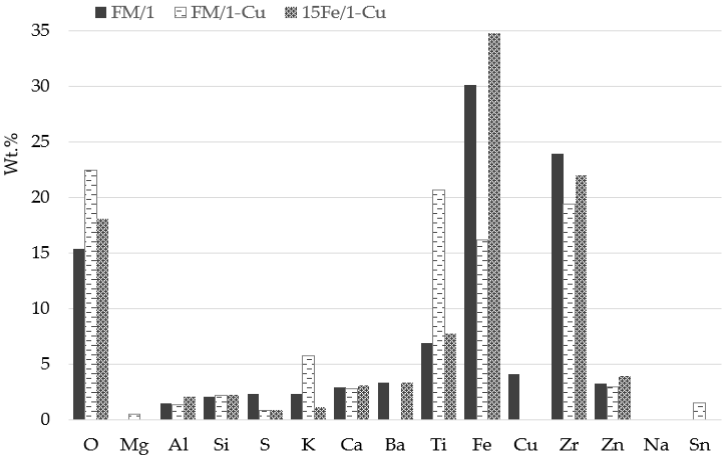


Fig. 5.8. EDXS data acquired on the secondary plateaus for FM/1, FM/1-Cu and 15Fe/1-Cu.

5.2.4 Main results

The 15Fe/1-Cu, produced by replacing copper with steel fibres, displays a friction coefficient that is comparable to the reference master-batch FM/1. The friction coefficient is dependent on the compactness and stability of the friction layer. The introduced steel fibres offer an effective contribution to the trapping and densification of the wear debris. The secondary plateaus that form in this way are more compact and adherent than those forming on the material with no replacement of copper fibres, though some cracks still remain visible on the surface like in the sample FM/1-Cu. In the latter case, the

SP that form without the support of any fibres are considerably larger and reduce the value of the friction coefficient. As regards the wear, the material with steel fibres presents the highest value of K_a in comparison to the reference master-batch (FM/1) and the Cu-free formulation (FM/1-Cu).

5.3 Barite

5.3.1 Background

Steel fibres may act as primary plateaus, but they shouldn't contribute to the cohesion of secondary plateaus in the same way as Cu fibres do. Therefore, other ingredients should be introduced within the mixture to obtain the cohesion mechanism of the secondary plateaus when copper is missing.

Interestingly, significant concentration of barium sulphate ($BaSO_4$), usually regarded as a filler in the classification of the pad formulations proposed in [81], turned out to be capable to reduce the critical copper concentration needed to lower wear through the formation of a stable friction layer [21]. The role of barite in the formation of the FL and the consequent wear behaviour of the Cu-free formulation (FM/1-Cu) was therefore explored.

The idea of using barite has been suggested by the combination of the literature studies [161] and the results obtained within the EU financed REBRAKE project.

5.3.2 Samples

New Cu-free formulations were obtained by adding barite in different concentrations to FM/1-Cu.

The reference master-batch FM/1 contains already a small amount of barite (~ 5 wt.%). The barite addition ranging from 10 wt.% to 30 wt.%, in Table 5.6 are given the designation of the samples and the total barite content.

Table 5.6. List of the barite-based friction materials: designation of the samples and total barite content.

Designation	Material	Tot. barite content %
10Ba/1-Cu	FM/1-Cu + 10 wt.% BaSO ₄	15
15Ba/1-Cu	FM/1-Cu + 15 wt.% BaSO ₄	20
20Ba/1-Cu	FM/1-Cu + 20 wt.% BaSO ₄	25
30Ba/1-Cu	FM/1-Cu + 30 wt.% BaSO ₄	35

5.3.3 Testing and characterization

The results of pin-on-disc test (50 min.) carried out with the pins containing different concentration of barite (15 wt.%, 20 wt.%, 25 wt.%, 30 wt.%) are summarized in Table 5.7. The mean values of the friction coefficient at the steady-state, show a slight increase in the barite enriched materials as compared to the FM/1 reference material, except for the material 30Ba/1-Cu which shows a slight reduction of μ .

Table 5.7. Values of friction coefficient (μ) and specific wear coefficient (K_a) for the barite-based friction materials.

	μ	K_a (m ² /N)
10Ba/1-Cu	0.46 ± 0.06	(3.28 ± 0.55) *10 ⁻¹⁵
15Ba/1-Cu	0.43 ± 0.05	(3.86 ± 1.05) *10 ⁻¹⁵
20Ba/1-Cu	0.43 ± 0.06	(3.99 ± 0.94) *10 ⁻¹⁵
30Ba/1-Cu	0.40 ± 0.05	(4.64 ± 0.78) *10 ⁻¹⁵

During the laboratory tests, it was observed that for the materials containing barite the results obtained from the 50-minute tests have to be used only as a first comparison between the materials since, in this period, the friction coefficient does not reach a steady-state condition. In order to have more reliable results, it was decided to carry out 7-hour tests.

Fig. 5.9 shows the evolution of the friction coefficient recorded during the PoD tests carried out for 7 h with the materials with the addition of barite (Table 5.6). The μ increases during the run-in period and then decreases progressively, showing an inability of the materials with

barite to maintain the friction at a stable value; this is due to the lack of PP. Moreover, it was observed that a higher concentration of barite reduces the scatter of the friction.

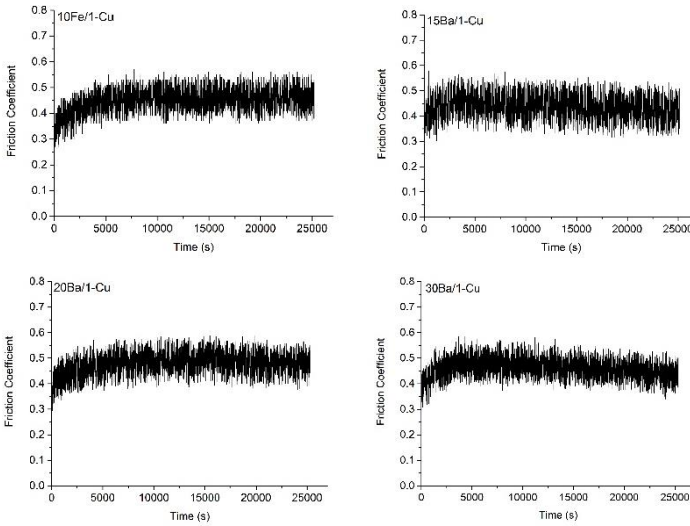


Fig. 5.9. Evolution of the friction coefficient recorded during the PoD tests carried out for 7h for the samples: 10Ba/1-Cu, 15Ba/1-Cu, 20Ba/1-Cu, 30Ba/1-Cu.

The positive feedback of the addition of barite is the reduction of the specific wear coefficient (K_a) compared to the reference formulation, as demonstrated both by the 50-minute and 7-hour tests. In Fig. 5.10, K_a of the barite enriched materials are plotted in comparison of the material FM/1. This seems to find an agreement with the outcome of an experimental study on the development of copper-free friction materials [161]. The Authors investigated the role of several new ingredients on the wear behaviour of different friction materials using barite as an inert filler [54][162]. The results suggest that wear rate is decreasing with an increasing barite content, highlighting the possibility, not investigated by the Authors, that barite might play a direct and primary role in reducing the wear rate of the materials under study.

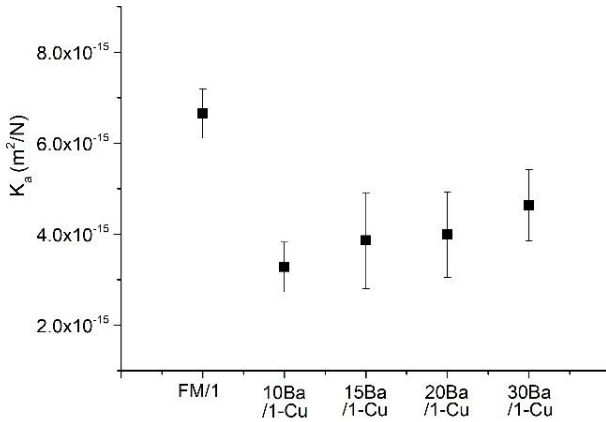
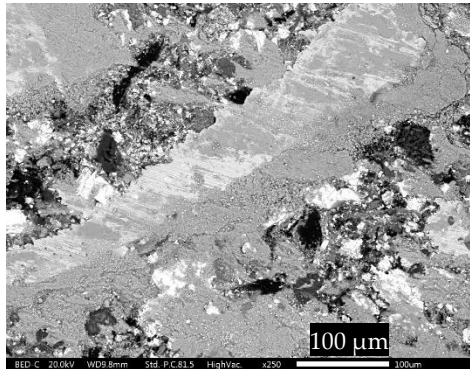


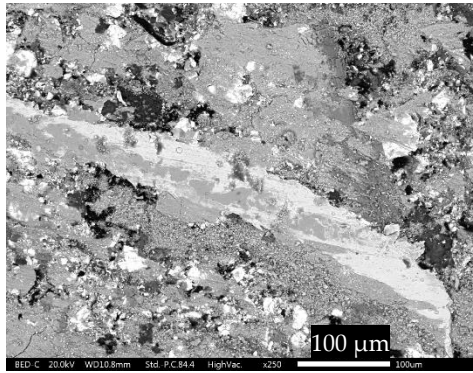
Fig. 5.10. Mean values of the specific wear coefficient (K_a) calculated for samples with different concentration of barite (10Ba/1-Cu, 15Ba/1-Cu, 20Ba/1-Cu, 30Ba/1-Cu) compared with the K_a of the reference, FM/1. Pin-on-disc tests: 50 min.

The planar views of the tested pins are shown in Fig. 5.11. It is visible the typical morphology of the friction layer formed by primary and secondary contact plateaus. The secondary contact plateaus exhibit different extension and compactness, moreover some cracks are visible on SP of 20Ba/1-Cu and 30Ba/1-Cu samples.

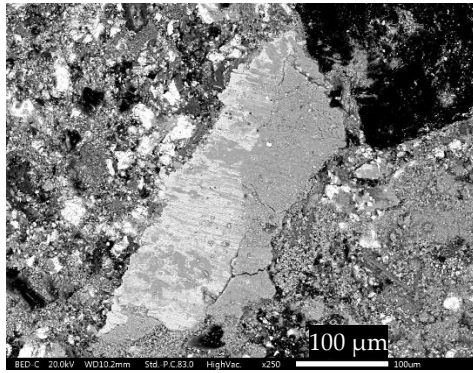
10Ba/1-Cu



15Ba/1-Cu



20Ba/1-Cu



130Ba/1-Cu

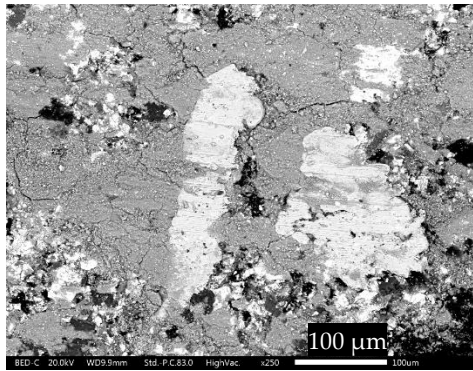


Fig. 5.11. SEM micrographs of the planar sections of the worn pin surfaces: 10Ba/1-Cu, 15Ba/1-Cu, 20Ba/1-Cu, 30Ba/1-Cu.

In some areas, there are compacted secondary plateaus not grown on metallic fibres (PP). The extension of these plateaus seems to be higher in the material 10Ba/1-Cu and 15Ba/1-Cu, where the PP areas displayed are almost completely covered by secondary contact

plateaus. An example is shown in Fig. 5.12, which refers to the 10Ba/1-Cu material.²

10Ba/1-Cu

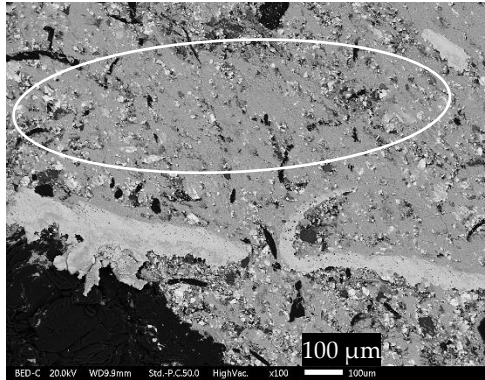
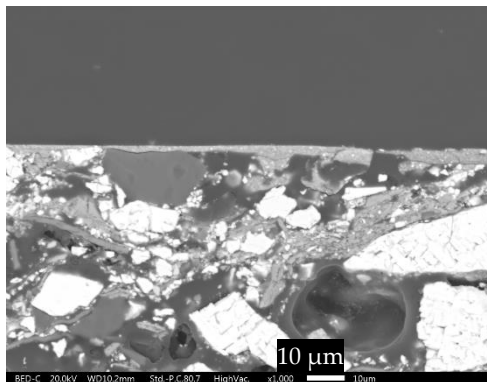


Fig. 5.12. SEM micrograph of a feature of secondary plateaus that did not form close to any primary plateaus. Sample: 10Ba/1-Cu.

The analysis of the cross sections (Fig. 5.13) indicates that samples with moderate content of barite (10Ba/1-Cu and 15Ba/1-Cu) have similar friction layers: very thin, compacted and uniformly widespread on the pin surface. Instead, in the sample 20Ba/1-Cu and 30Ba/1-Cu the friction layer shows, in some points, peculiar characteristics, much different respect to the other materials. The friction layer is thicker and locally displays concave shaped features.

10Ba/1-Cu



30Ba/1-Cu

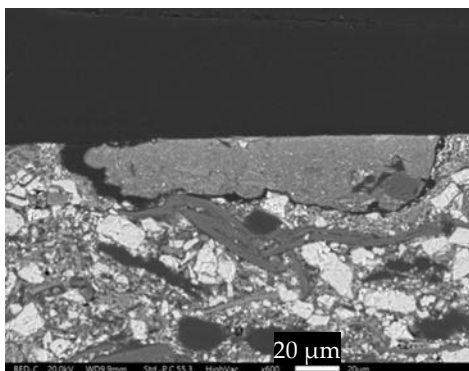


Fig. 5.13. SEM micrographs of the cross section of worn pins showing the different features of the friction layer for the material with moderate and high concentration of barite. As example, 10Ba/1-Cu and 30Ba/1-Cu have been reported.

The results of the EDXS analyses carried out on the friction layers, are summarized in Table 5.8. The main detected elements are Fe, Zr, Ba and Ti. The amount of Ba and S in the friction layers increases with the increase of the barite added to the initial master batch.

Table 5.8. EDXS of the friction layers present on the pin surface at the end of the PoD tests.

Material	Fe	Zr	Ba	S	Ti	O	Others
FM/1	25.3	24	3.6	1.6	9.5	10.0	26.0
	±1.7	±1.3	±0.7	±0.3	±0.9	±1.3	
10Ba/1-Cu	42.5	18.0	9.5	2.5	5.0	15.0	7.5
	±3.0	±1.1	±0.4	±0.3	±1.0	±2.8	
15Ba/1-Cu	42.0	15.1	11.9	3.0	4.5	14.0	10.5
	±2.8	±3.8	±1.7	±0.2	±1.6	±1.1	
20Ba/1-Cu	38.0	12.5	16.0	4.0	4.0	15.0	10.5
	±3.4	±3.4	±1.1	±0.4	±1.3	±0.9	
30Ba/1-Cu	32.0	13.0	19.1	5.2	4.5	15.0	11.5
	±1.9	±2.3	±0.9	±0.2	±1.2	±0.3	

In Fig. 5.14 the EDXS maps of the friction layer of the material 30Ba/1-Cu, it contains Fe oxides coming from the tribo-oxidation of the cast

iron disc counterface and a fine dispersion of ZrO_2 and $BaSO_4$, surrounded by a phase rich in carbon.

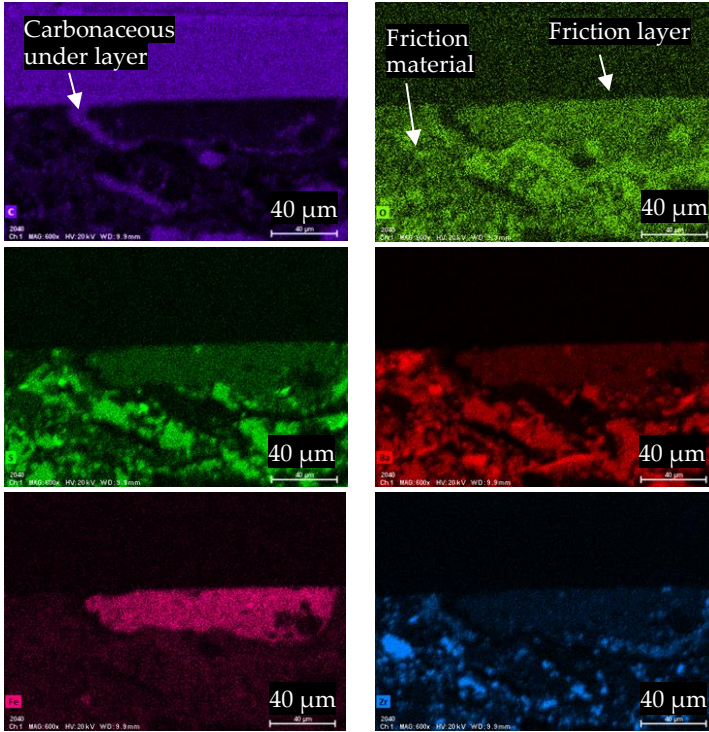


Fig. 5.14. EDXS maps of the cross-section 30Ba/1-Cu friction material after PoD test. Elements: C, O, S, Ba, Fe, Zr. In Fig. 5.12 is reported the SEM micrograph.

The friction layer is composed of extremely fine debris from the pin, mixed together with oxide particles coming from the counterface disc, which are finely milled and mixed up together by the relative sliding of the disc and pin surfaces.

In these systems mixing is promoted by Kelvin-Helmholtz shear instabilities, resulting in the formation of vortex structures [163]. The size scale of the vortices is determined by the average particle size of the debris and the size of the interface roughness and height of the obstacles, turning the laminar-like flow of the tribo-material into a turbulent one.

The dense and compacted friction layer that have been shown on the 10Ba/1-Cu pin (Fig. 5.13) result from the mechanical milling of the wear debris and their mixing up promoted by a vorticity of submicrometric size (size of the wear debris).

In the materials with higher concentration of barite (Fig. 5.13, 30Ba/1-Cu), as sliding test proceeds, the fraction of wear debris having higher concentrations of fine barite, collapse on carbonaceous components present in the FM and create step-like irregularities on the pin surface; the latter trigger the formation of large vortices (Fig. 5.15), which ground and compact the particles to form a stable friction layer structure. The mechanism is explained in Fig. 5.16.

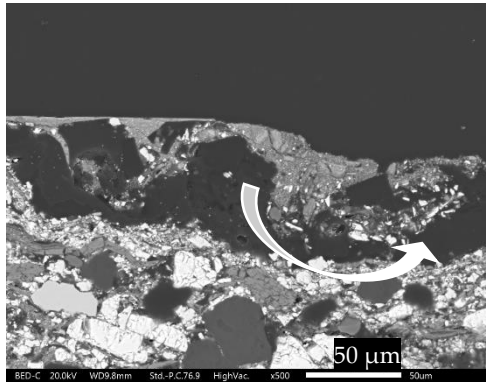


Fig. 5.15. SEM micrograph of the cross section of material 30Ba/1-Cu. It shows the vorticity rising in the FL of a material with high concentration of barite in the presence of carbonaceous particles. The arrowed line represents the trajectories of the turbulent flow of wear debris.

The characteristics of this friction layer are typical of a so-called mechanically mixed layer, often reported in tribological systems [164][165][166]. It is composed of extremely fine debris surrounded by the phases rich in carbon.

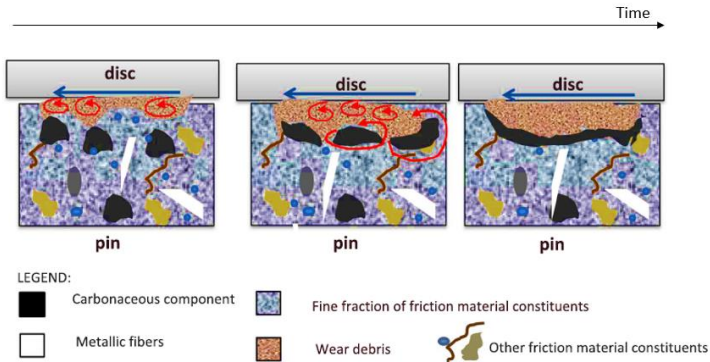


Fig. 5.16. Mechanism of formation of the friction layer on the surface of the pin with a higher concentration of barite.

5.3.4 Main results

All the barite-based friction materials have displayed a better wear behaviour than the reference FM/1. Barite helps to form a stable friction layer, characterized by good compactness. In the sample with a high concentration of barite, the friction layer, at some spots, is constituted of very fine fragments, well compacted and surrounded by a dark film (observed at the SEM). These features are typical of a mechanically mixed layer. The mechanism is explained.

Lower concentration of barite results in a slight increase in the friction coefficient whereas a higher concentration of barite reduces the scatter of the friction. The main drawback is the instability of the μ with time, this is probably correlated with a lack of PP.

5.4 Cu-free formulation

5.4.1 Samples

Steel fibres and barite powder show different evolution of friction coefficient and wear rate:

- steel fibres increase the wear compared to FM/1;
- barite reduces the wear compared to FM/1 but reduce the stability of μ .

New formulations were developed combining the two constituents with the aim of stabilizing the friction coefficient and reducing the wear. Different concentrations of barite were mixed with steel fibres. The two formulations were labelled 10Ba_Fe/1-Cu and 25Ba_Fe/1-Cu (Table 5.9).

Table 5.9. Designation of the samples 10Ba_Fe/1-Cu and 25Ba_Fe/1-Cu.

Designation	Material
10Ba_Fe/1-Cu	FM/1-Cu + 10 wt.% BaSO ₄ + 5 wt.% Steel fibres
25Ba_Fe/1-Cu	FM/1-Cu + 25 wt.% BaSO ₄ + 5 wt.% Steel fibres

5.4.2 Testing and characterization

The new formulations, combining barite and steel fibres, were obtained by adding a fixed value of steel fibres (5 wt.%). The value was decided based according to the results obtained from the PoD tests conducted on some formulations produced with different concentration of steel fibres (FM/1-Cu + 5, 10, 15 wt.% steel fibres). Fig. 5.17 show the calculated value of K_a as evaluated from PoD tests, two for each sample. The addition of 5 wt.% of steel fibres has a lower value of K_a compared to 10 wt.% and 15 wt.%.

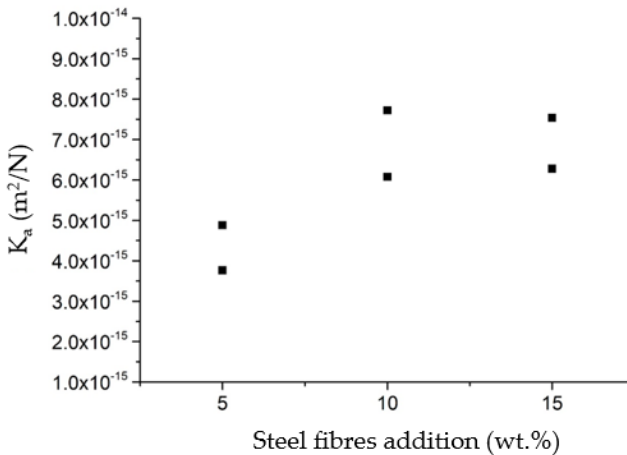


Fig. 5.17. Specific wear coefficient (K_a) calculated after the PoD tests for the material FM/1-Cu with the addition of steel fibres with different concentration (5, 10, 15 wt.%).

10Ba_Fe/1-Cu and 25Ba_Fe/1-Cu were tested at the PoD at room temperature (RT) and at high temperature (HT). In Fig. 5.18 is reported the friction coefficient recorded during the PoD tests for long time (7h). The material 10Ba_Fe/1-Cu still has instability of μ over time, whereas 25Ba_Fe/1-Cu has a stable value with a lower scatter.

The tests at high temperature (300°C) confirm the results obtained at RT. Also in these conditions, the friction coefficient of the sample 25Ba_Fe/1-Cu is stable and less scattered than the material 10Ba_Fe/1-Cu, Fig. 5.19.

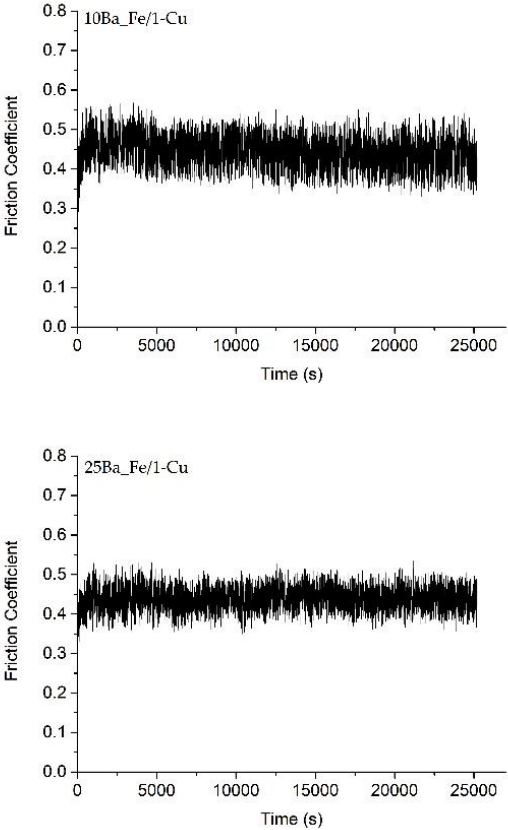


Fig. 5.18. Variations of friction coefficient as a function of time for the long PoD tests (7 hours). Materials: 10Ba_Fe/1-Cu and 25Ba_Fe/1-Cu.

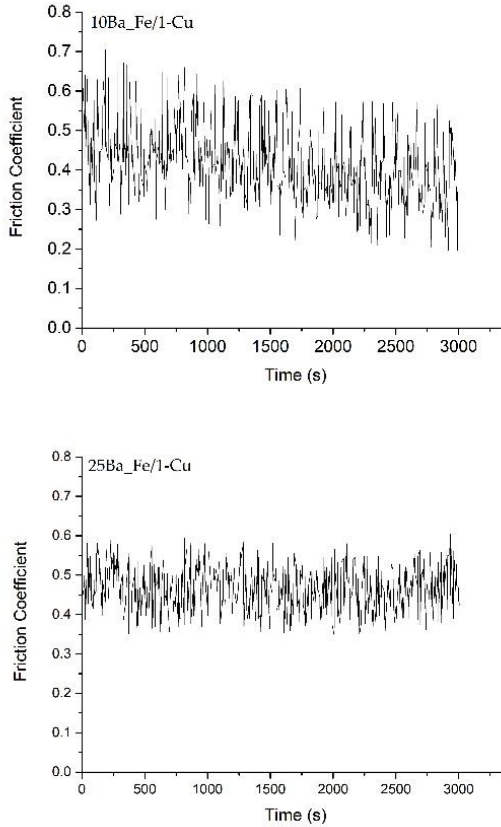


Fig. 5.19. Variations of friction coefficient as a function of time for the high temperature (300°C) tests. Materials: 10Ba_Fe/1-Cu and 25Ba_Fe/1-Cu.

The recorded average values of the friction coefficient during RT and HT tests are listed in Table 5.10; the values of the material 25Ba_Fe/1-Cu in both conditions are comparable to the FM/1 (μ : RT_7 h = 0.45 ± 0.05 , HT = 0.46 ± 0.04).

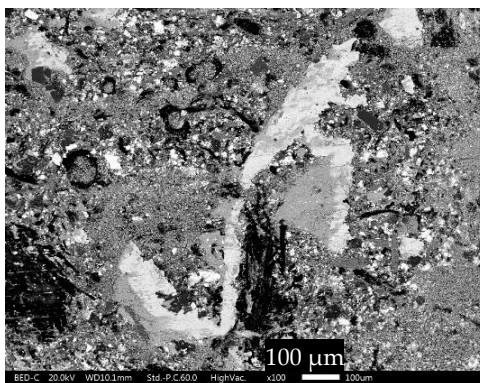
The estimated K_a values are also included in Table 5.10. The order of magnitude ($10^{-15} \text{ m}^2/\text{N}$) confirms a typical mild sliding wear regime. As expected, K_a is seen to increase with temperature ($10^{-14} \text{ m}^2/\text{N}$), while remaining in mild wear conditions. The K_a of 10Ba_Fe/1-Cu and 25Ba_Fe/1-Cu is lower than the value of FM/1 ($K_{a,HT} = 1.68 \cdot 10^{-14} \text{ m}^2/\text{N}$), especially for the sample 25Ba_Fe/1-Cu.

Table 5.10. Coefficient of friction (μ) and specific wear coefficient (K_a) for the PoD test carried out at RT and HT (300°C). Materials: 10Ba_Fe/1-Cu and 25Ba_Fe/1-Cu.

	μ		K_a (m ² /N)	
	RT	HT	RT	HT
10Ba_Fe /1-Cu	0.45 ± 0.04	0.41 ± 0.10	2.54*10 ⁻¹⁵	1.45*10 ⁻¹⁴
25Ba_Fe /1-Cu	0.44 ± 0.03	0.47 ± 0.06	2.06*10 ⁻¹⁵	1.22*10 ⁻¹⁴

Fig. 5.20 shows SEM observations of the wear surface of the pins after sliding at HT. The material containing higher quantity of barite (25Ba_Fe/1-Cu) presents larger and more compact secondary plateaus. The concentration of Ba, detected with EDXS, on the secondary plateaus of 10Ba_Fe/1-Cu and 25Ba_Fe/1-Cu is 10 wt.% and 22 wt.%, respectively. This confirms the inclusion of barite into a compact friction layer.

10Ba_Fe/1-Cu



25Ba_Fe/1-Cu

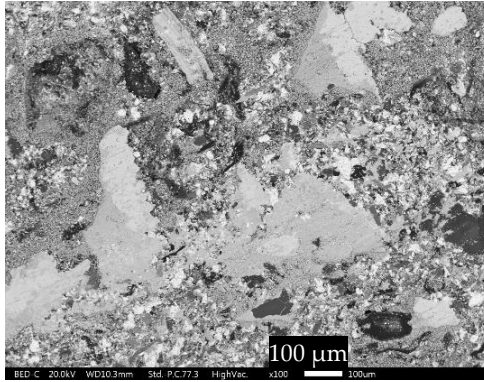


Fig. 5.20. SEM micrographs showing the top view of the worn pins after the PoD tests at HT (300°C). Materials: 10Ba_Fe/1-Cu and 25Ba_Fe/1-Cu.

5.4.3 Main results

The best results (reduction of wear and stabilization of friction) were achieved by adding to the FM/1-Cu 5 wt.% of steel fibres and 25 wt.% of barite.

The wear rate is similar to the reference material FM/1, and even lower in the severe conditions (high-temperature tests). The friction coefficient remains high and stable over time. Steel fibres act as primary plateaus and reinforcement for the friction material (low wear), whereas barite contributes to stabilizing the secondary plateaus (stable friction coefficient).

Moreover, considering that barite is fully inert and not considered of any risk for the human health [167][168], its introduction into the friction formulation in order to eliminate and substitute an environmentally critical material such as copper could be an additional advantage.

5.5 Commercial Cu-free friction materials

5.5.1 Cu-free master-batch

The commercial Cu-free formulation (FM/2) used as reference master-batch in the second part of the research activity was tested and characterized. The tribological properties were compared with the

master-batch FM/1 (Cu-full) and the developed formulation without copper (25Ba_Fe/1-Cu, paragraph 5.4).

In Fig. 5.21 the values of friction coefficient for the formulations at RT, 300°C and 400°C are shown. The material FM/2 shows higher friction values than FM/1 in all the tested conditions.

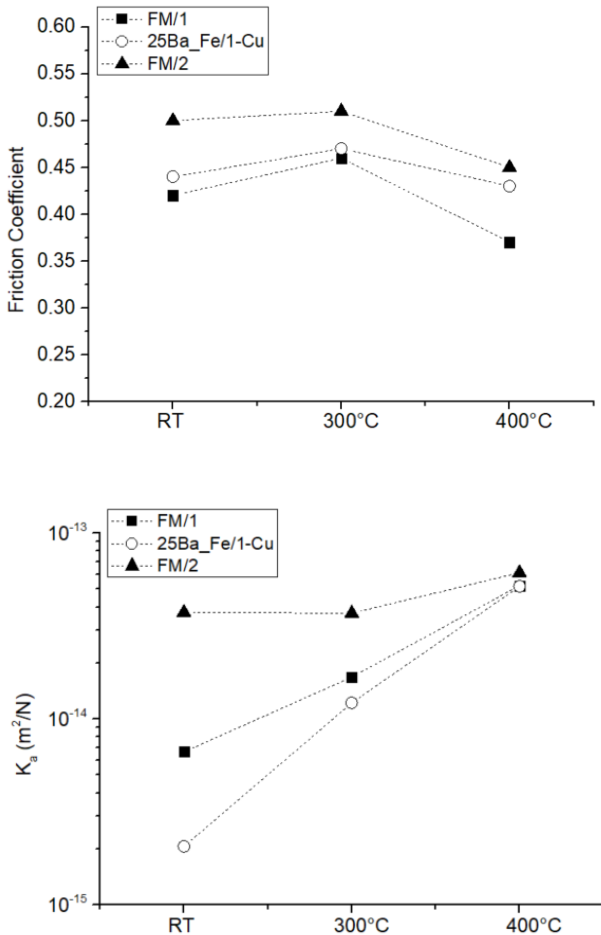


Fig. 5.21. Values of the friction coefficient and the specific wear coefficient of the materials FM/1, 25Ba_Fe/1-Cu and FM/2, tested at RT, 300°C and 400°C.

In Fig. 5.21, the specific wear coefficient (K_s) is shown, too. The wear of material FM/2 is higher at RT than FM/1. Nonetheless, it remains

more stable at high temperature, increasing in the 300°C tests. The material FM/1 and the modified formulation (25Ba_Fe/1-Cu) exhibit an evident increase moving from RT to 300°C. The disc wear was evaluated from the profilometer traces shown in Fig. 5.22. These observations confirm that, at RT, FM/2 is more aggressive on the disc than FM/1.

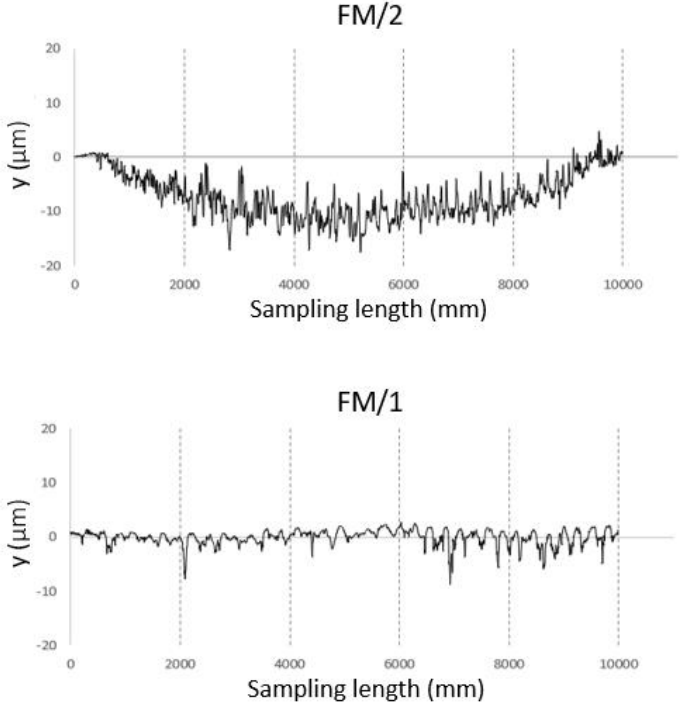


Fig. 5.22. Wear track profile present on the disc surface after room temperature PoD tests. Materials: FM/2 and FM/1.

5.5.2 Cu-free brake pads

In order to compare the master-batches used in this study with the materials present on the market, some commercial Cu-free pads were selected, and codenamed: Pad_1, Pad_2, Pad_3. Pins for tribological testing were extracted. The investigation of the Cu-free formulations

on the market is a key work to understand which properties and performance these materials have reached.

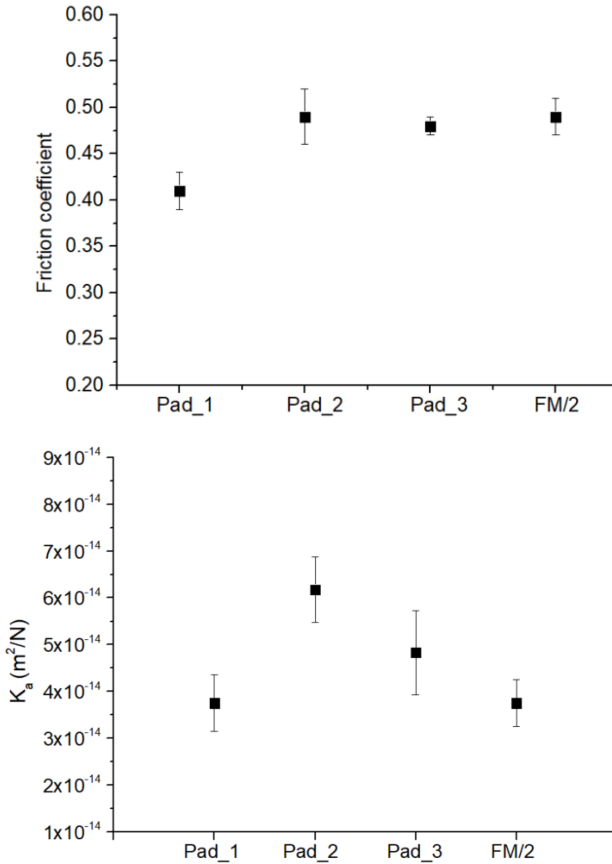


Fig. 5.23. Friction coefficient and specific wear coefficient of the material FM/2 compared with some Cu-free brake commercial materials: Pad_1, Pad_2 and Pad_3, tested at RT.

In Fig. 5.23 are reported the values of friction (μ) and wear (K_a) of the materials tested at RT. The material FM/2 presents good friction values, comparable with the other pads. As concerns the wear, the calculated values of K_a demonstrate that FM/2 has a lower wear coefficient, although close to the Pad_2 and Pad_3 formulations.

Table 5.11. EDXS analysis on the secondary plateaus of the worn pins tested at RT.

Wt.%	Pad_1	Pad_2	Pad_3	FM/2
O	9.9±0.7	9.0±0.6	15.4±2.6	7.8±1.2
Fe	81.5±0.3	64.7±2.8	66.2±3.2	82.2±0.7
Al	0.9±0.2	1.7±0.1	0.4±0.1	1.9±0.3
Si	1.5±0.1	1.5±0.1	2.6±0.4	1.4±0.6
S	1.4±0.3	1.2±0.1	-	1.5±0.1
Cr	-	1.0±0.1	0.9±0.1	0.8±0.1
Mg	-	2.9±0.4	4.2±0.6	1.0±0.2
Ti	-	1.5±0.2	-	-
Ba	5.1±0.6	-	2.8±1.1	-
Ca	-	0.6±0.1	-	-
Zn	-	-	-	2.2±0.3
Sn	-	-	-	1.4±0.1
Mo	-	-	5.5±1.5	-

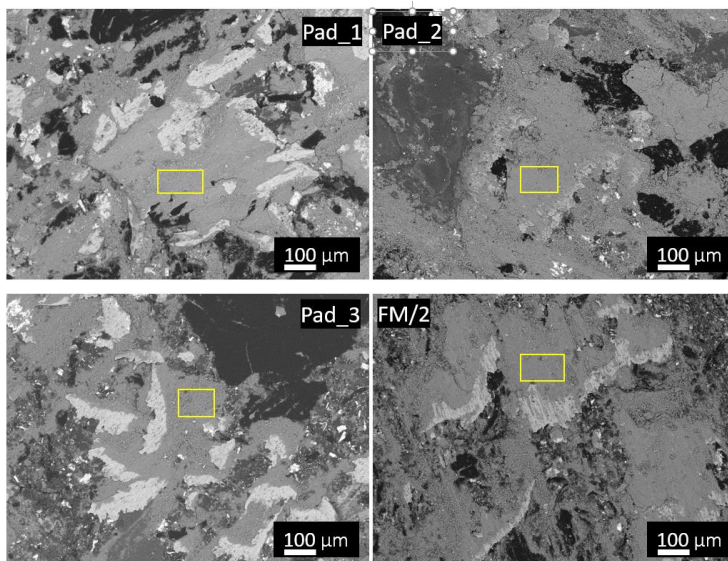


Fig. 5.24. SEM observations of the worn pins tested at RT. The yellow rectangle indicates the area of the EDXS analyses.

Table 5.11 reports the EDXS analysis carried out on the secondary plateaus found on the surfaces of worn pins tested at RT (Fig. 5.24). The concentration of Fe is in general very high in the commercial Cu-free formulations, in comparison to the formulation without Cu developed using the FM/1 master-batch.

The high concentration of iron in the secondary plateaus and values of K_a , in some cases higher than $4 \cdot 10^{-14} \text{ m}^2/\text{N}$ at RT, is an indication of high wear of the disc-pad system in commercial Cu-free formulations.

5.5.3 Main results

The master-batch FM/1 (Cu-full) has shown lower values of μ and K_a than the master-batch FM/2 (Cu-free). However, FM/2 has proved more stable with changing temperature (RT \rightarrow 300°C, 400°C).

The formulation FM/2 was also compared with the samples extracted from three Cu-free brake pads sell on the market, showing similar properties (μ e K_a). In general, in the Cu-free formulations were observed high concentrations of Fe in the secondary plateaus and high values of the K_a , suggesting that these formulations are more aggressive on the disc compared to the studied Cu-full formulation (FM/1).

Chapter 6

6. An eco-friendly formulation

The preliminary investigation on the use of a balanced concentration of barite combined with steel fibres, described in the above chapters, appeared promising especially as regards the emission behaviour of friction materials.

Over the present PhD period, the ECOPADS project was launched, it will end in March 2020. ECOPADS, starting from the results achieved in the previous EU projects (REBRAKE and LOWBRASYS) and from the indication of the reported preliminary tests, intends to take to the market a copper-free brake pad with reduced certified emissions, still retaining excellent brake performances.

In this section the story of the experimental work and the main results we have obtained from PoD and Dyno tests is reported.

6.1 Samples

Steel fibres and barite were used in the first stage of the development process. Starting from two friction material mixture without copper (FM/2 and FM/3) used as baselines, the two constituents (steel fibres and barite) were added into the mixture with different concentrations, resulting in different formulations, Table 6.1. Moreover, two commercial friction materials were selected as benchmarks (FM/4 and FM/5) in order to compare performance

The best formulation resulting from the first stage of development was then the baseline for the second development loop (Table 6.2). In the second stage three new formulations were produced adding more binder and/or abrasives. The aim was to try further optimization of the formulation.

Table 6.1. Designation of the samples produced in the first stage of development. Addition of the constituent: ↑ **Low**, ↑↑ **Medium**, ↑↑↑ **High**.

Designation	Baseline	Steel fibres	Barite
L_Ba/2	FM/2	↑	↑
M_Ba/2	FM/2	↑	↑↑
H_Ba/2	FM/2	↑	↑↑↑
M_Ba/3	FM/3	↑	↑↑

Table 6.2. Designation of the samples produced in the second stage of development. Legend: ↑ addition of the constituent, - no addition of the constituent. B = Binder, A = Abrasives, BA = Binder + Abrasives.

Designation	Baseline	Binder	Abrasives
B_Ba/2	M_Ba/2	↑	-
A_Ba/2	M_Ba/2	-	↑
BA_Ba/2	M_Ba/2	↑	↑

6.2 Testing and validation

The selected formulations and the reference materials were tested at UniTN as regards to the performance (COF and wear under drag conditions), and at KTH to evaluate the emissions. At Brembo laboratories, these formulations underwent Dyno-bench measurements by testing real pads close to real braking condition.

6.2.1 Pin-on-disc tests

In Table 6.3 the values of friction coefficient of the new formulations with the relative baselines, obtained from the PoD tests (RT), are given. In the first stage of the Project, problems relating to the surface of the discs led to have values of μ lower than the values found later in the tests. However, the tests were considered acceptable since the data are used comparatively to the baselines (FM/2 and FM/3). Moreover, the criterion for selecting the best material, in this design phase, was the wear.

Table 6.3. Values of friction coefficient for pins produced with the formulations developed in the first loop of the project and its relative baselines.

Friction coefficient	
FM/2	0.35 ± 0.02
L_Ba/2	0.38 ± 0.02
M_Ba/2	0.34 ± 0.01
H_Ba/2	0.36 ± 0.02
FM/3	0.41 ± 0.01
M_Ba/2	0.34 ± 0.01

The specific wear coefficients of the formulations are shown in Fig. 6.1. The baseline FM/2 showed better wear performance than FM/3. The K_a of the formulation M_Ba/2 is lower than those of the other new formulations, for this reason, it was selected to continue with the tests.

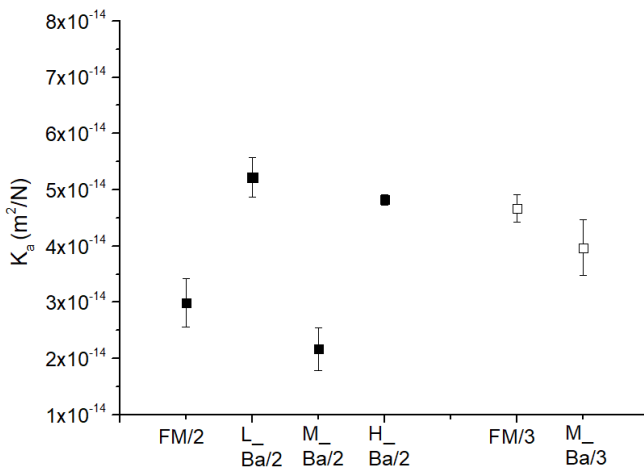


Fig. 6.1. Specific wear coefficient of baseline materials (FM/2 and FM/3) and the modified formulations.

Fig. 6.2 shows the typical curves of the PN as measured by OPS and PM10 recorded by ELPI+ of the material FM/2. The trends are representative of all the materials tested: there is a running-in period

after which there is a sort of stabilization. The values of PN and PM are calculated as the mean value and standard deviation with the data in the steady state (~ 5000 s - 7000 s).

The emission values for the material FM/2 and the formulation M_Ba/2 are reported in Table 6.4. It can be found that the FM/2 have greater PC, PM10 and PM2.5 levels than the new formulation M_Ba/2.

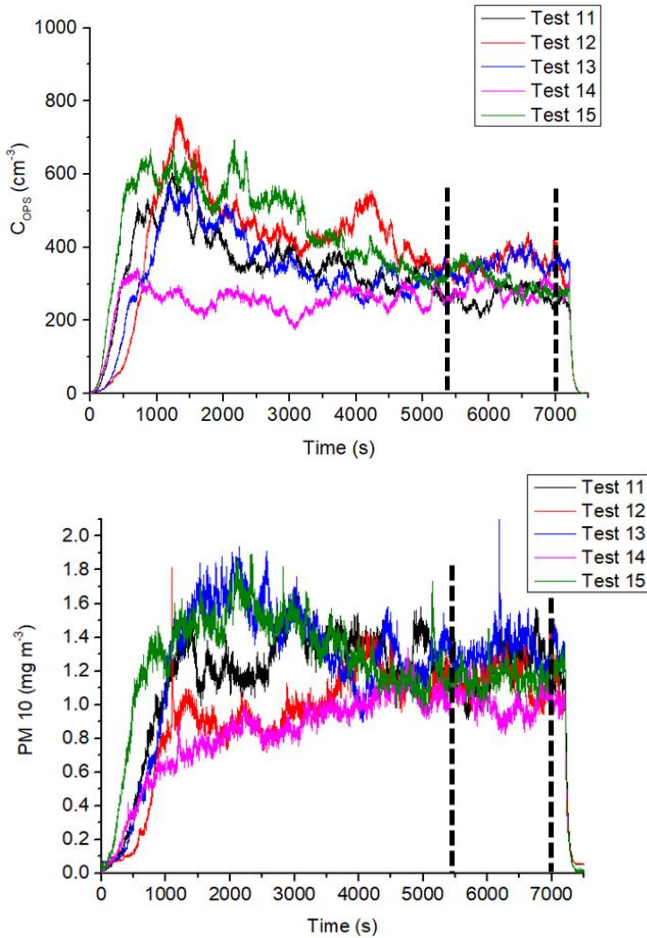


Fig. 6.2 Time history records of PN measured by OPS and PM10 measured by ELPI+. The black bars indicate the range used for the evaluation of the values.

Table 6.4. Mean value and standard deviation of PN, PM10 and PM2.5 of pins produced from master-batch powders: FM/2 and M_Ba/2.

	PN (#/cm ³)	PM10 (mg/m ³)	PM2.5 (mg/m ³)
FM/2	318 ± 45	1.18 ± 0.12	0.58 ± 0.05
M_Ba/2	264 ± 36	1.11 ± 0.16	0.42 ± 0.07

At first, the materials were tested as pins produced directly from the powders. However, some tests conducted on different pin surface status, reveal that the emission behaviour is influenced by the scorching. Scorching is a high temperature treatment conducted on pad surface for a proper surface finish. All pads normally undergo this treatment as one of the final production steps.

It was found, as shown in Fig. 6.3, that the FM/2 not scorched have greater PN and PM levels than the FM/2 scorched.

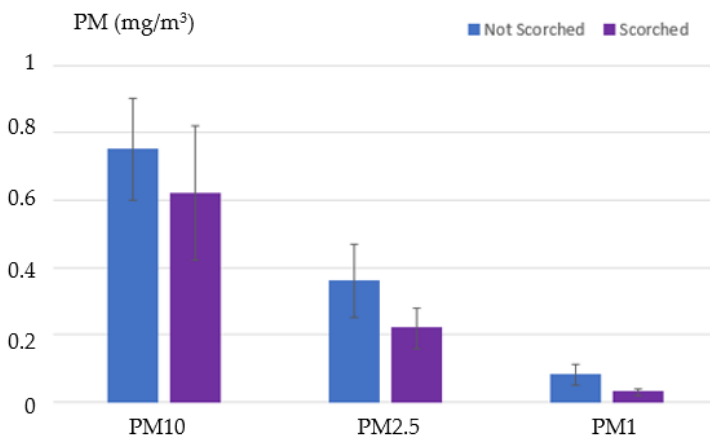


Fig. 6.3. PM10, PM2.5 and PM1 (mean value and one standard deviation) of the material FM/2 with and without scorching.

In this stage real pads for Dyno tests were produced, and because the pins produced in the laboratory do not have scorching, pins from real pads were extracted and the emission tests repeated.

In the Table 6.5 are reported the results obtained from the PoD tests related to the emissions. The new formulation M_Ba/2 emits less than

the benchmark FM/4 (Cu-free) and the reference FM/2, and slightly less/comparable than the benchmark FM/5 (Cu-full).

Table 6.5. Mean value and standard deviation of PN, PM10 and PM2.5 of pins extracted from scorched pads: FM/2, M_Ba/2, FM/4 and FM/5.

	PN (#/cm³)	PM10 (mg/m³)	PM2.5 (mg/m³)
FM/2	264 ± 36	0.62 ± 0.20	0.22 ± 0.06
M_Ba/2	95 ± 24	0.58 ± 0.22	0.18 ± 0.05
FM/4	208 ± 31	1.32 ± 0.12	0.38 ± 0.05
FM/5	91 ± 15	0.74 ± 0.09	0.20 ± 0.02

The second stage of development was conducted with the aim of increasing the coefficient of friction. In this stage, the content of phenolic resin was optimized. In fact, the introduction of barite and iron fibres into the starting reference mix had not been accompanied by the addition of a suitable percentage of binder. For the same reason, abrasives have also been optimized. Three new friction material formulations were developed, all derived from M_Ba/2: B_Ba/2 (+ binder), A_Ba/2 (+ abrasives) and BA_Ba/2 (+ binder, abrasives).

The pin-on-disc tests show an increase in the friction coefficient of the material B_Ba/2, Fig. 6.4. In addition, a slight decrease in wear was observed for material BA_Ba/2 (Fig. 6.4). These two materials were selected to be tested as concerned the emissions (PoD tests) and with the Dyno bench tests to evaluate both the performance and the emissions.

It should be noted that the new formulations were PoD tested to evaluate the emissions in the as-received pad state, which means with scorching treatment on the surface.

Fig. 6.5 illustrates the PN and PM10 of new formulations in a form of mean value and standard deviation. It can be noticed that the optimized formulations resulted in an increase in the emissions as compared to M_Ba/2.

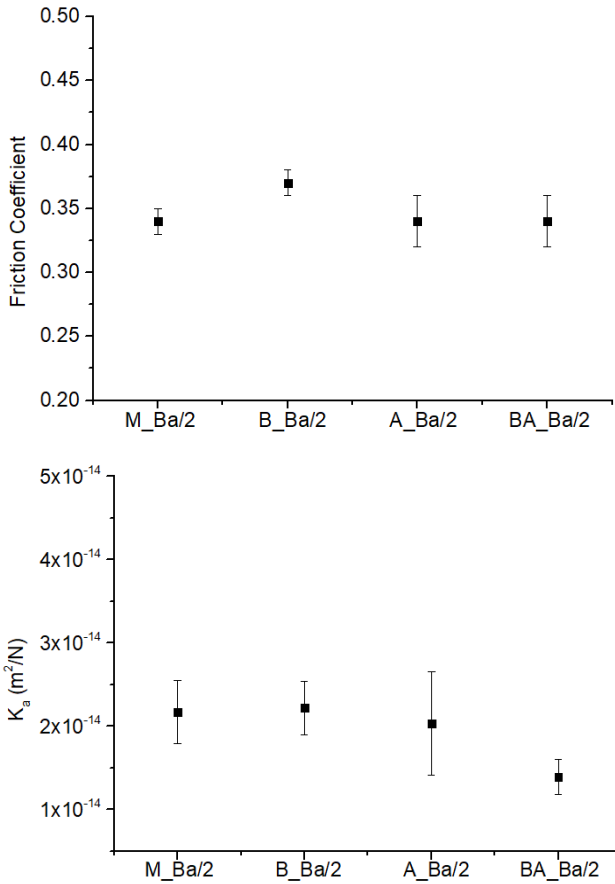


Fig. 6.4. Friction coefficient and specific wear coefficient of the materials developed in the second stage compared to the material M_Ba/2.

The optimized formulations have improved the performance (friction coefficient and specific wear coefficient), worsening the emissions. The tests displayed that the formulation M_Ba/2 developed in the first stage is the best Ecopads formulation.

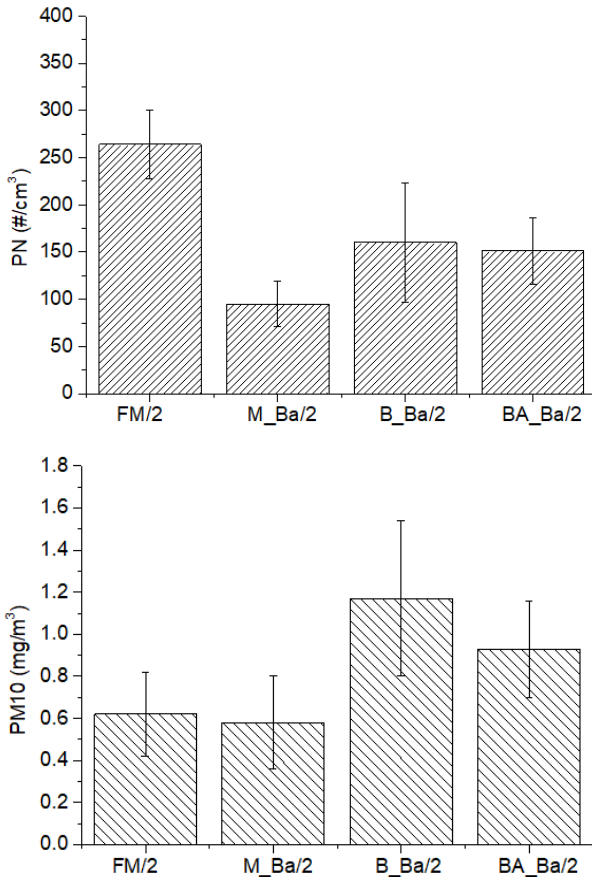


Fig. 6.5. PN and PM10 (mean value and standard deviation) of the optimized formulations (B_Ba/2, BA_Ba/2) compared with materials M_Ba/2 and FM/2.

6.2.2 Dyno tests

Full scale Dyno tests were performed on the friction materials selected at the PoD level: M_Ba/2, B_Ba/2, BA_Ba/2 and the reference materials FM/2 (Cu-free) and FM/5 (Cu-full).

Dyno tests were made for the purpose of full pads validation. Three main parameters were considered at dyno-bench level:

- friction performance;
- wear performance;
- PN and PM emission.

As concerns with the performances, all the friction materials exhibited a satisfactory behaviour, the characteristic friction coefficient range between 0.35-0.40. B_Ba/2 has the highest friction coefficient, followed by material BA_Ba/2.

The brake material M_Ba/2 exhibits the lower PN concentration between the Cu-free formulations (Fig. 6.6), although slightly higher than the Cu-full formulation (FM/5).

The PM level of material M_Ba/2 is comparable to the reference FM/2, and slightly higher than FM/5. As for the PoD tests, the formulations B_Ba/2 and BA_Ba/2 emits more than M_Ba/2.

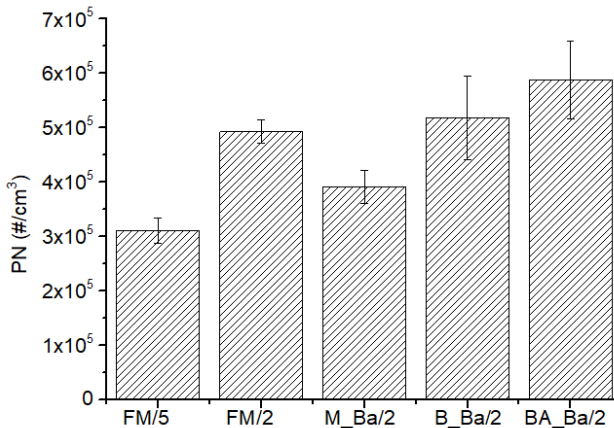


Fig. 6.6. PN (mean value and standard deviation) evaluated with Dyno tests.

6.2.3 Car test

The car test was finally conducted for the final characterization of the best performing Cu-free material, the formulation M_Ba/2.

The main parameters considered at this level are:

- run-in evaluation;
- comfort evaluation;
- fading behaviour;
- endurance.

The aftermarket sector indicates a standardized procedure (ECE R90) that can define whether a material can be commercialized or not.

The formulation M_Ba/2 met all sections of this test.

6.3 Final considerations

The best formulation developed in the project, codenamed M_Ba/2, reached the last validation step for the brake system development, the road test, giving satisfactory results.

The Ecopads project provided useful guidelines to develop and design Cu-free pads which include the emission performance.

Dyno-tests are normally the standard in the brake industry to validate new formulations. Ecopads has adopted the standard procedure introducing two novelty:

- the pin-on-disc approach at laboratory level to select new constituents and develop new formulations;
- the emission evaluation in the develops loop.

Chapter 7

7. Different constituents in FMs

It can be supposed that each ingredient influences the performances of the final product not only for its own peculiarities but also through its interactions with the polymer matrix and other components. The literature related to brake pad materials reports on the many approaches to understanding the tribological phenomena and the influence on them of the different constituents. Some Authors prepared simplified formulations [72][30] others use commercial formulation changing one or two ingredients each time [169][45].

The study conducted in this section focuses on the comprehension of the effect that some pad constituents have on the tribological properties and on the formation of the friction layer, essential for good brake performances.

Using this approach, one of the main solid lubricant used in friction material, graphite, was investigated. The same experimental approach was used to study the role that inorganic fibres (Lapinus). Finally, the binder was taken into account, as concerns the retainment of the structural integrity of the composites under mechanical and thermal stresses [35].

7.1 Graphite

7.1.1 Background

Solid lubricants are strategic since their concentration and type in the friction layers, determine conditions for friction force stabilization and influencing the sliding behaviour. Some Authors suggested to increase

the amount of graphite in a typical pad material with the aim of replacing copper.

Gilardi et al. [106] found that the addition of graphite raised thermal conductivity, depending on the graphite grade and the heat flow direction. The thermal conductivity of graphite, between 350 and 250 $WK^{-1}m^{-1}$, is close to the thermal conductivity of copper, although, the thermal conductivity of copper is far less sensitive to temperature than graphite's [81]. Moreover, as shown by Österle et al. via simulations [20], graphite particles enter the friction layer and provide a velocity accommodation between the rotating disc and the still pad. This leads to higher stability of the friction coefficient during braking.

Although graphite is regarded as a possible replacement for copper, a few research studies only have been dedicated to study graphite in Cu-free friction material formulations, and just a few of them investigated the influence of graphite on the relevant tribological properties (friction and wear) at different testing temperatures. Moreover, in comparison to synthetic graphite, only a few studies on natural graphite properties can be found in the literature.

For the above reasons, different types of natural graphite (see paragraph 3.1.2.3) were added to a Cu-free base formulation and pin-on-disc tests were carried out to correlate specific test conditions, including the temperature of the disc, to fundamental tribological mechanisms.

7.1.2 Samples

The master-batch FM/2 without graphite was used as a reference (FM/2-C). New mixtures were prepared, by adding 9 wt.% of graphite with different particle size. The selected concentration of graphite is representative of concentrations used in other studies on friction materials, with a particular focus on graphite [106][161].

The new formulations were codenamed as displayed in Table 7.1.

Table 7.1. Designation of the friction materials samples with the addition of different graphite grades.

Designation	Material
N1/2-C	FM/2-C + 9 wt.% natural graphite N1
N2/2-C	FM/2-C + 9 wt.% natural graphite N2
N3/2-C	FM/2-C + 9 wt.% natural graphite N3
S1/2-C	FM/2-C + 9 wt.% synthetic graphite S1

7.1.3 Testing and characterization

Fig. 7.1 displays the mean values of the friction coefficient at RT. The samples having smaller graphite grains, namely N2/2-C and N3/2-C, show an evident decrease in μ with respect to the reference material FM/2-C. Among these, the graphite with smaller particle size and spherical shape (N3/2-C) have a major lubricant effect. Indeed, graphite enters in the friction layer more easily and becomes more homogeneously distributed.

Moreover, the samples with finer graphite showed K_a values lower than the reference material (FM/2-C) and also of the N1/2-C sample, containing larger plate-like flakes, Fig. 7.2.

A material with the addition of synthetic graphite (S1/2-C) was also tested at RT, for a comparison with the samples containing natural graphite. The behaviour of the material S1/2-C is comparable to that of the samples N2/2-C and N3/2-C, having smaller graphite grains, in terms of friction coefficient. While, it shows larger scatter of K_a values, as evidenced by the standard deviation bars, like the materials N1/2-C and FM/2-C. This behaviour can be explained considering that the range of particle size of the selected synthetic graphite is large and includes both fine and coarse particles.

The results suggest that the particle size of graphite influences the friction and wear properties of the friction material considerably, and in particular, the friction coefficient decreases with the graphite particle size. The same trend was observed as concerns the wear coefficient.

In Fig. 7.3 the cross-sectional views of the PoD samples tested at RT are displayed. The secondary plateaus in the FM/2-C sample are made of coarse and weakly compacted particles as compared to the plateaus of

the materials with the addition of graphite. Anyway, denser and more compacted plateaus, well anchored to the pin surface, have been found on the N2/2-C and N3/2-C samples, compared to the N1/2-C and S1/2-C sample.

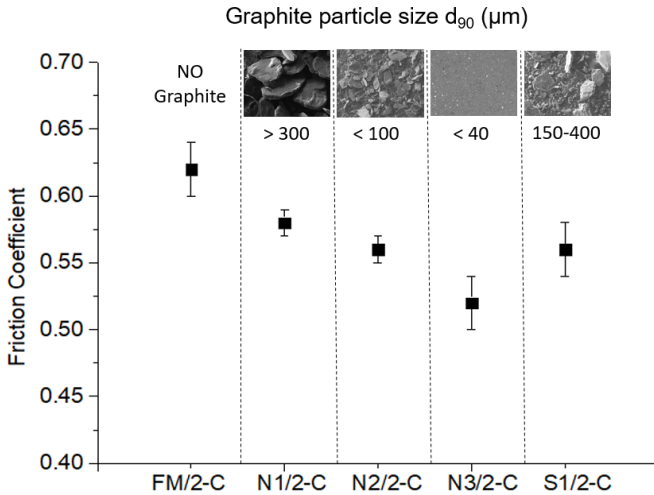


Fig. 7.1. Mean values of the friction coefficient evaluated for the pin-on-disc tests at RT. Materials: FM/2-C, N1/2-C, N2/2-C, N3/2-C, S1/2-C.

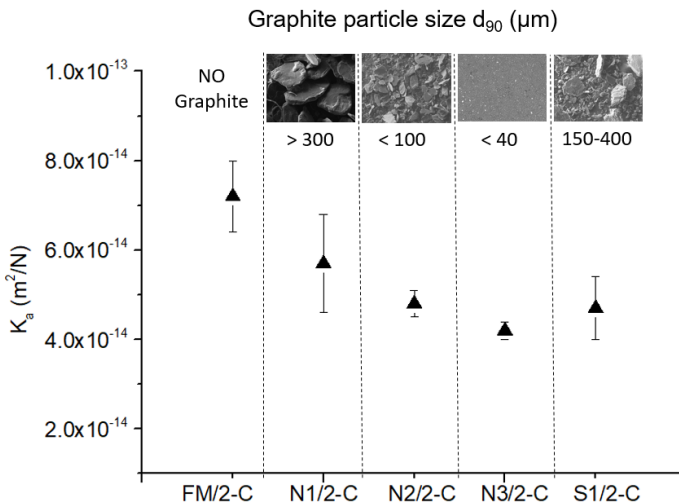
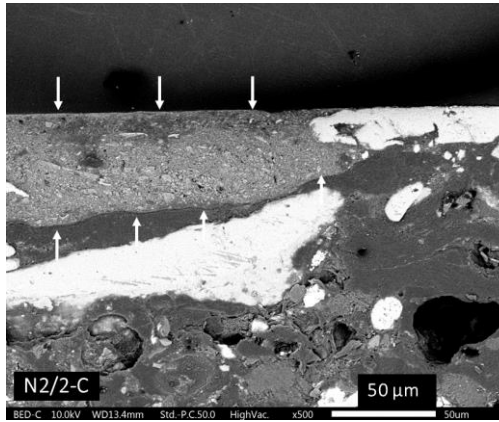
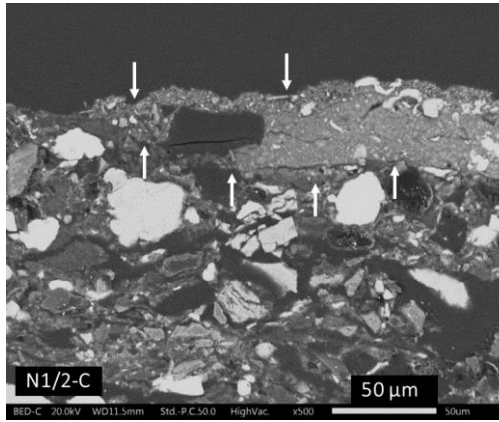
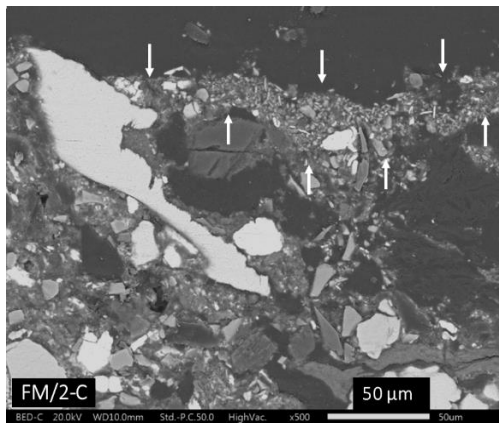


Fig. 7.2. Mean values of the specific wear coefficient (K_a) calculated for the pin-on-disc tests at RT. Materials: FM/2-C, N1/2-C, N2/2-C, N3/2-C, S1/2-C.



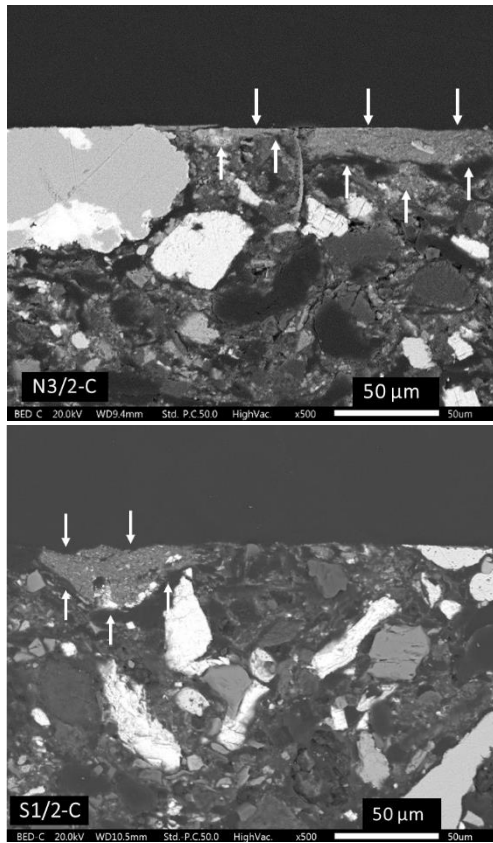


Fig. 7.3 Cross-section of the worn pins after the pin-on-disc tests at RT (sample legend in the pictures). The arrows indicate the secondary plateaus. The arrows help to identify the secondary plateaus on the pin surface.

Table 7.2 provides the compositional results of the EDXS analyses carried out on the secondary plateaus. The majority element is iron, which comes both from the disc and pin. The concentrations of the other elements in the secondary plateaus, coming mainly from the wearing out of the pin, are not so different from one sample to another. Particular attention was paid to the relative content of carbon in the plateaus of the different samples. The relative content of carbon in the plateaus of the FM/2-C and N1/2-C samples is lower (7.0 wt.%) than in the N2/2-C, N3/2-C and S1/2-C samples (8.2 wt.%, 9.3 wt.% and 8.3 wt.%, respectively). This is in agreement with literature: Yang et al.

[170] state that the presence of a relatively high concentration of graphite on the friction surface may contribute to the formation of a graphite-rich friction layer with dense and well compacted secondary plateaus, leading to a general improvement of the friction performance.

Table 7.2. EDXS analyses on the secondary plateaus tested at RT.

Wt.%	FM/2-C	N1/2-C	N2/2-C	N3/2-C	S1/2-C
Fe	61.2±2.5	62.0±1.6	58.5±2.3	55.2±0.9	57.6±1.2
O	18.1±1.2	17.7±0.9	19.4±1.1	20.1±0.8	19.7±0.5
C	7.0±0.3	7.0±0.5	8.2±0.2	9.3±0.3	8.3±0.5
Zn	3.4±0.8	3.3±2.2	3.7±1.0	3.4±0.5	3.1±0.8
Sn	2.0±0.3	2.0±0.8	2.1±0.2	2.0±0.2	2.6±0.2
Mg	2.0±0.7	1.6±0.8	1.8±0.4	2.2±0.1	2.1±0.1
Al	1.9±1.0	1.8±0.8	1.7±0.4	2.3±0.5	1.8±0.2
S	1.8±0.3	1.9±0.6	1.8±0.3	1.9±0.1	1.8±0.2
Si	1.3±0.1	1.3±0.5	1.3±0.2	2.1±1.0	1.6±0.1
Cr	0.7±0.1	0.8±0.8	0.8±0.3	0.8±0.3	0.9±0.2
Ca	0.6±0.2	0.6±0.3	0.7±0.1	0.7±0.1	0.5±0.2

The tests on the samples with natural graphite were performed also at HT (400°C), and then RT tests were conducted on the sample already tested at 400°C (RT_after HT). This was meant to investigate the recovery capability of the friction material with diverse particle size of graphite.

In Fig. 7.4 the evolution of the friction coefficient of the FM/2-C sample at HT and during the subsequent RT_after HT test is displayed.

In the test at HT, the friction coefficient has a peculiar behaviour, observed in all tests. At first, the friction coefficient increases up to a peak value and then decreases. This is related to an initial running-in, followed by the removal of the friction layer from the pin surface for the combined action of adhesion forces and thermal softening of the friction material. Successively, disc oxidation and wearing out of the pin surface determine a new rise in the friction coefficient accompanied by the formation of a new friction layer. Finally, another decrease of friction coefficient is observed, featuring the stabilization

of μ at low values. The combined effect of the friction material softening and its transfer onto the disc surface justified this reduction. This determines the progressive transition from a friction material-cast iron coupling towards a situation in which the friction layer on the pin surface is in sliding contact with the transfer layer on the disc.

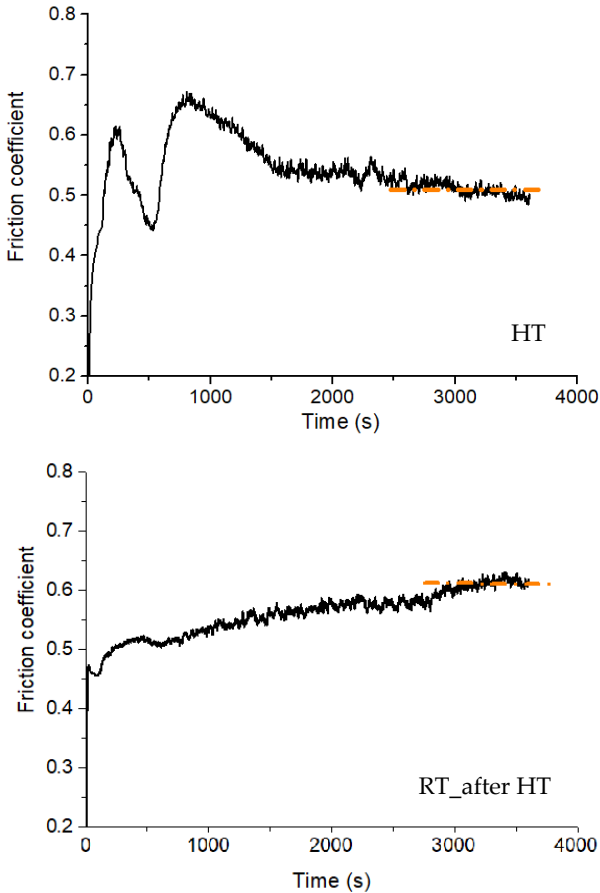


Fig. 7.4. Evolution of the friction coefficient with time for the tests at HT (400°C) and the test at RT after the HT test (RT_after HT). The data set for the material FM/2-C is shown as an example, being the behaviour of other materials quite similar.

The variations in the μ value induced by the high temperature conditions, as compared to the values measured with the tests conducted at RT, were evaluated with the following equation:

$$\% \mu_{HT} = \left(\frac{\mu_{HT} - \mu_{RT}}{\mu_{RT}} \right) \times 100 \quad \text{Eq. 7.1}$$

The comparative graph in Fig. 7.5 shows the change of μ evaluated with the Eq. 7.1. The tests at HT suggested that graphite does not significantly influence the behaviour, since all the samples tested showed a general reduction of μ and an increase in the specific wear coefficient, irrespective of the graphite grade. The oxidation phenomena of the disc and the degradation of the friction materials are predominant with respect to the beneficial contribution of graphite as solid lubricant and friction coefficient stabilizer.

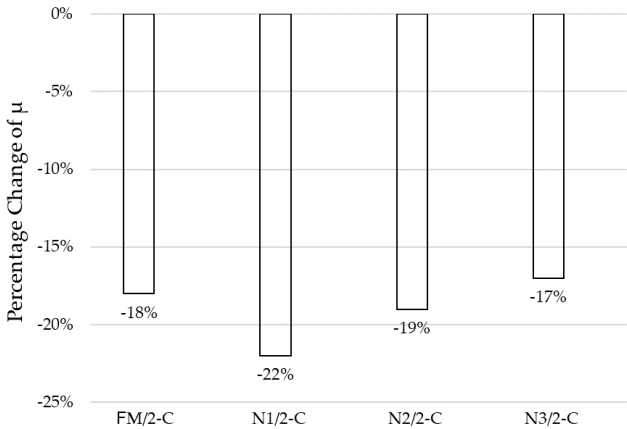


Fig. 7.5. Change in the friction coefficients, induced by the HT test as compared to the RT test, as a function of the materials.

The percent variation of the steady-state friction coefficient was also evaluated between the value at RT and these values obtained, still at RT, but after the test at HT (RT_after HT), with the Eq. 7.2:

$$\% \mu_{RT_afterHT} = \left(\frac{\mu_{RT_HT} - \mu_{RT}}{\mu_{RT}} \right) \times 100 \quad \text{Eq. 7.2}$$

In Fig. 7.6 the change of μ evaluate with the Eq. 7.2 is shown.

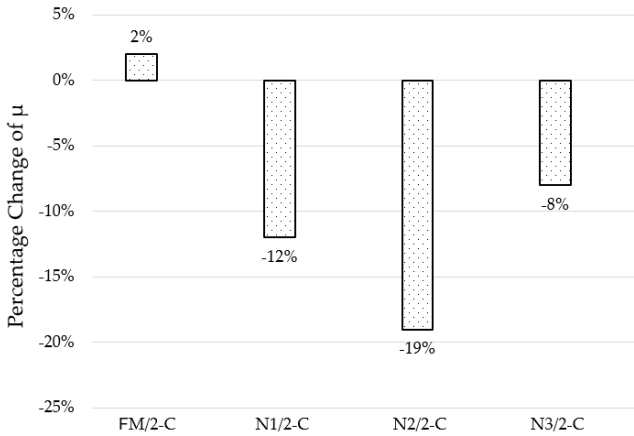


Fig. 7.6. Change in the friction coefficients, between the value at RT and these values obtained, still at RT, but after the test at HT.

Concerning the friction coefficient recovery (μ at RT after the test at HT), the FM/2-C sample recovers its μ ($\% \mu_{RT_afterHT} = 2\%$), whereas all samples with graphite additions exhibit an incomplete recovery of the friction coefficient. Among these samples, N3/2-C attained the best recovery ($\% \mu_{RT_afterHT} = -8\%$), whereas the worst behaviour was displayed by N2/2-C ($\% \mu_{RT_afterHT} = -19\%$).

The specific wear coefficient calculated for all the tested pins is shown in Fig. 7.7. FM/2-C material exhibits an increase in wear rate passing from RT tests to HT tests and to the RT tests after HT tests. The materials with graphite also exhibit an increase in wear rate passing from RT tests to HT tests. A wear rate reduction was observed instead in the RT tests conducted after HT tests. In general, materials containing graphite exhibit lower values of K_a with respect to the reference master-batch. The material N3/2-C has the best wear performance for all the tested conditions.

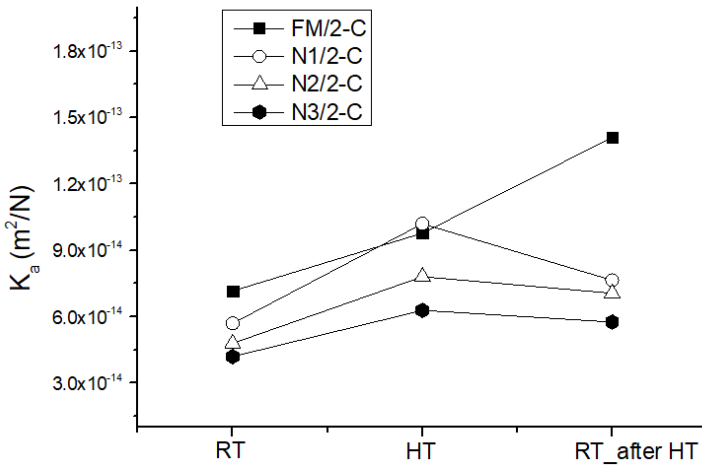


Fig. 7.7. Specific wear coefficient, K_a (m²/N), calculated for the samples tested at room temperature (RT), high temperature (HT, 400°C) and RT after the test at HT (RT_after HT).

The FM/2-C material displayed the higher specific wear coefficient, at the same time, the better friction coefficient recovery. The relevant scenario emerging from these data is the rapid restoration of the pin's pristine surface favoured by the faster wearing out of friction layer, initially present on the pin surface and produced by the HT tests (Fig. 7.8).

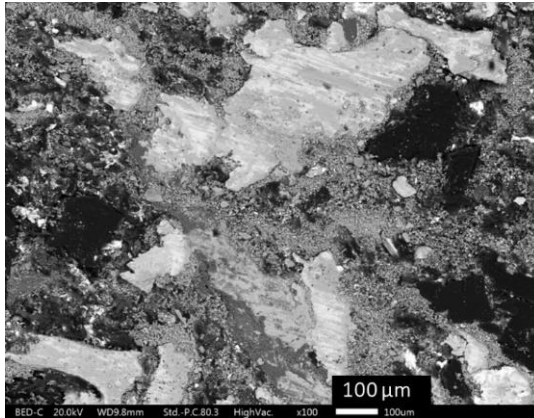
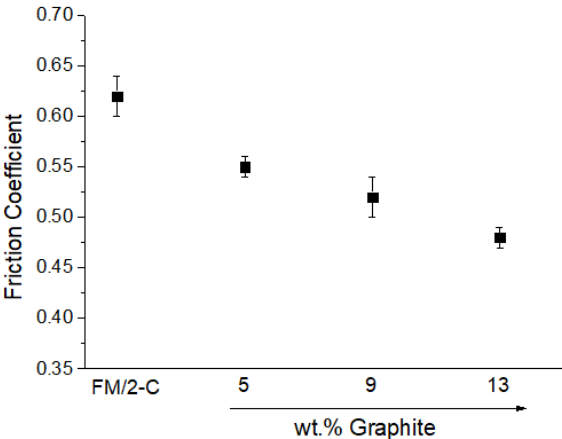


Fig. 7.8. Planar view of the FM/2-C material after the pin-on-disc tests carried out at HT (400°C).

As concerns the materials with added graphite (lower wear in the RT_after HT tests than FM/2-C), a long run-in is necessary before reaching the steady state in the new test conditions. For the finer size of added graphite (sample N3/2-C), it is easier to enter the friction layer with other constituents and re-establish the surface conditions like those attained at the end of the initial RT test.

7.1.4 Concentration of graphite

A further investigation on graphite was conducted to estimate the effect of its concentration. The graphite N3 was used to study the effect of different graphite concentrations (5 wt.%, 9 wt.%, 13 wt.%) in the material FM/2-C. Pin-on-disc tests at RT were performed, the mean friction coefficient values and specific wear coefficients are reported in Fig. 7.9. For concentrations up to 13 wt.% of graphite no drastic property losses are observed but only a proportionate reduction of μ . The wear has a similar evolution, indeed higher graphite concentrations reduce the specific wear coefficient of the material.



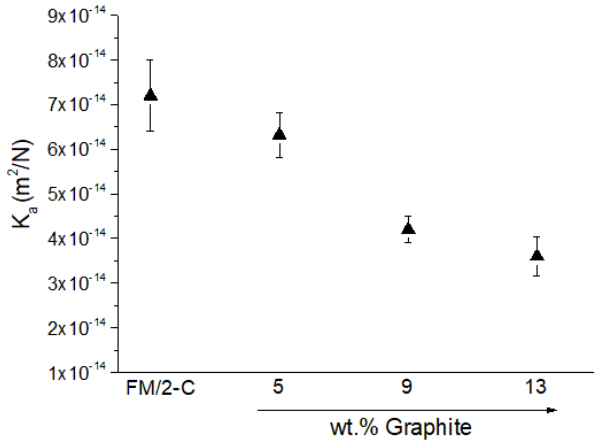


Fig. 7.9. Friction coefficient and specific wear coefficient (K_a) for the material FM/2-C with different graphite concentration (5, 9, 13 wt.%). Graphite: N3.

As concerns the friction layer, its formation too is influenced by the graphite content. For higher graphite concentrations, a greater extension of the secondary plateau is observed. These plateaus have a higher concentration of carbon than the plateaus forming for friction material compositions with lower graphite concentrations (Fig. 7.10). This observation is coherent with the investigation conducted on graphite with different particle size and underlines the active role of graphite in the formation of the friction layer. Moreover, it was found that the content of iron in the secondary plateaus is strictly correlated to the friction coefficient of the material (Fig. 7.9, Fig. 7.10). This observation has been confirmed in other reported studies [171][172].

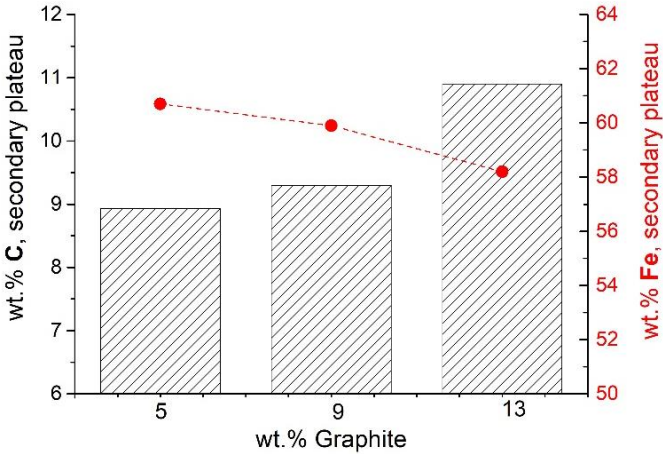


Fig. 7.10. Concentration (wt.%) of C and Fe, measured with EDXS analysis, in secondary plateaus.

7.1.5 Main results

The particle size of graphite (paragraph 3.1.2.3) impacts considerably on the friction and wear properties of the relevant friction material. The formation of the friction layer is influenced by the addition of graphite.

The best behaviour was observed in the N3/2-C sample (natural graphite N3), with graphite particle size < 40 µm; it shows a higher reduction of the friction coefficient and, in all the tests, a reduction in the wear rate. Instead, the N1/2-C sample (graphite grain size > 300 µm) presents a moderate reduction in the friction coefficient, compared to the reference master-batch without graphite (FM/2-C), and a slight wear rate reduction in the RT test; a larger reduction was observed after the recovery test (RT test after the HT test). The N2/2-C sample, (graphite grain size <100 µm), shows an intermediate behaviour.

All tested materials exhibit a negative change of friction-fade after HT tests, which is apparently not affected by the additions of graphite. On the other hand, as regards to friction-recovery ($\% \mu_{RT_afterHT}$), the material FM/2-C retains a better behaviour, correlated with the higher wear that has guaranteed a fast restore of the pin's surface.

As the concentration of graphite (N3) increases, up to 13 wt.%, a proportional decrease of the friction coefficient is observed, correlated to a proportional decrease in the wear rate.

7.2 Mineral fibres

7.2.1 Background

Mineral fibres have an effect on the micrometric scale at the surface of the brake material. The shape promotes the formation of the friction layer acting as an anchoring point for the wear debris and the chemical composition influences the friction coefficient. As a result, mineral fibres improve friction stability and wear resistance [173].

Other works in this field suggest that mineral fibres, such as Lapinus, improve the friction coefficient without increasing wear [136][174][175], a feature that deserves an in-depth investigation. Hence, two different types of mineral fibres were evaluated in a Cu-free formulation, for their friction and wear characteristics, investigating the relevant active mechanisms.

7.2.2 Samples

In order to investigate the impact of mineral fibres with different morphology in a Cu-free formulation, two different fibres, LF1 and LF2 (see paragraph 3.1.2.4), were evaluated and compared.

A fixed concentration of 5 wt.% of the two constituents were added to the reference master-batch FM/2. The designation of the samples and their compositions are given in Table 7.3

Table 7.3. Designation of the friction materials samples with the addition of mineral fibres.

Designation	Material
LF1/2	FM/2 + 5 wt.% mineral fibres LF1
LF2/2	FM/2 + 5 wt.% mineral fibres LF2

7.2.3 Testing and characterization

Both friction material compositions show an increase in the friction coefficient (Fig. 7.11). The larger increase is recorded for the material LF2/2. In Fig. 7.12, K_a values for the new materials are shown and can be easily compared to the reference master-batch. The LF1/2 material, despite the increase of μ , does not show a worsening of wear. On the other hand, the LF2/2 displays an increase in K_a . This is consistent with the EDXS analyses on the secondary plateaus, giving a higher iron content in the material LF2/2 (Fe = 68 wt.%) than in the material LF1/2 (Fe = 55 wt.%).

The worn pin surface of the material LF2/2 can be observed in Fig. 7.13. The material shows an important extension of the fibres network, in which wear fragments are trapped. A better distribution of the fibres is observed for the material LF1/2 (Fig. 7.14). LF1 fibres also act as an anchor for the wear fragments. The surface treatment with rubber improves the adhesion with the binder in the friction material and this probably contributes, together with the better distribution, to the lower wear of the material LF1/2 as compared to LF2/2.

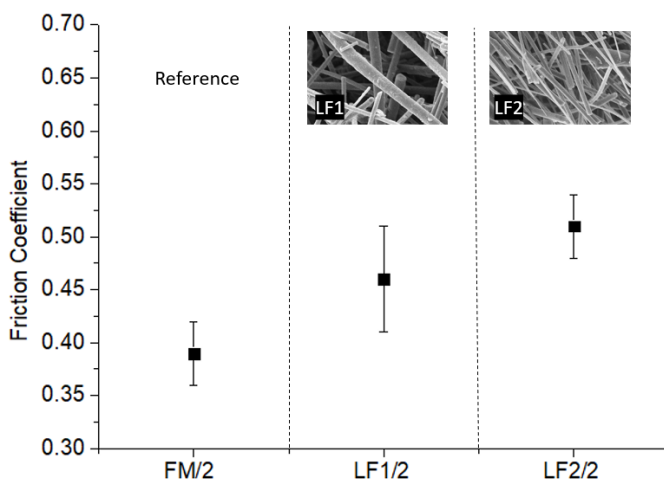


Fig. 7.11. Mean values of the friction coefficient evaluated for the pin-on-disc tests at RT. Materials: FM/2, LF1/2, LF2/2.

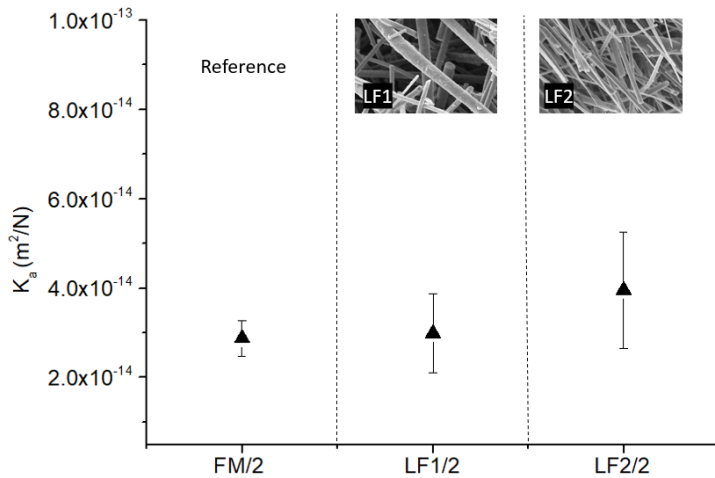


Fig. 7.12. Mean values of the specific wear coefficient (K_a) calculated for the pin-on-disc tests at RT. Materials: FM/2, LF1/2, LF2/2.

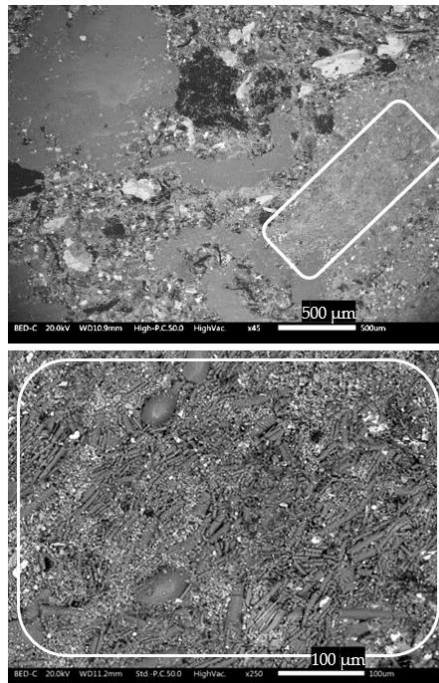


Fig. 7.13. SEM observations at different magnification of the worn pins. Material: LF2. The observation below is an enlargement.

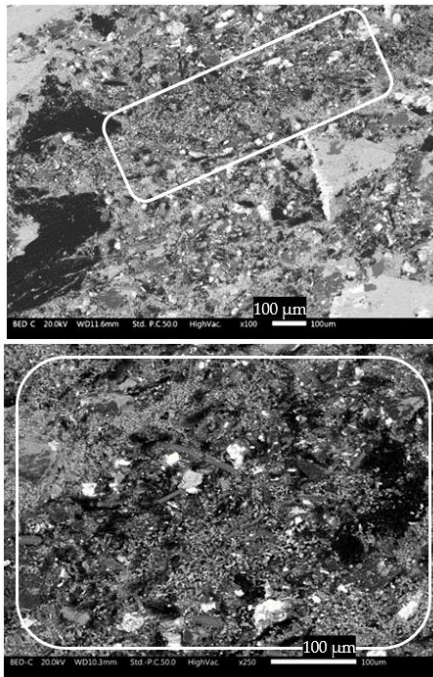


Fig. 7.14. SEM observations at different magnification of the worn pins. Material: LF1. The observation below is an enlargement (white box).

7.2.4 Main results

According to the experimental results, mineral fibres with different dimension and agglomeration, as well as surface treatments, influence the tribological properties of friction materials.

Fine agglomeration of fibres results to be far less problematic, and thus more advantageous than coarse agglomerates. Fine agglomerates are better distributed in the material and the fibres still act as anchoring spots for the wear debris. Moreover, the fibre surface treatment improves the adhesion with the binder in the friction material. It turns out that, the LF1 fibres increase the friction coefficient without affecting wear.

7.3 Phenolic resin

7.3.1 Background

In general, most of the friction materials used for automotive brakes are resin-based. Phenolic resins (PRs) are commonly used as binder in FM. The main disadvantages of the phenolic resins are the degradation with temperature and the instability during storage. Therefore, controlling the degradation phenomena occurring in friction material binder is important in several respects.

The critical temperatures for resin degradation are very important parameters to know. Thus, thermogravimetric analysis in association with FTIR of a resin (R1) were performed, before and after mixing the resin with all other pad constituents.

The other issue, i.e., the ageing of the resin, causes the deterioration of mechanical properties as well as its binder performances. Polymer degradation and storage stability studies have been profitably conducted using combined FTIR and differential scanning calorimetry (DSC) analyses [176][177][178]. Therefore, it was decided to use these two techniques to monitor polymer degradation and chemical changes as a function of time in the present investigation too.

7.3.2 Degradation

The thermal stability of the resin R1 was investigated, via TGA and FTIR spectroscopy, in order to detect the main degradation steps and the influence of friction material components (particularly metallic components) on the resin degradation. The resin was analysed in three different conditions: pristine (*A*, alone), in association with the other master-batch components (*B*, master-batch FM/2) and after the curing thermal treatment (*C*, namely in brake pad condition). The TGA shows four main thermally induced reactions (major detected mass loss steps). Samples of phenolic resin, according to the TGA curves, were isothermally heat treated at the temperatures: 200°C, 300°C, 500°C, 700°C, 1200°C.

The combination of the two techniques leads to the description of the phenolic resin degradation process summarized in Table 7.4.

Table 7.4. Process of the phenolic resin degradation summarized.

T (°C)	TGA	FTIR
100	Humidity loss	-
150-200	Resin polycondensation (mass loss: 3%).	Formation of CH ₂ methylene groups (bridging reaction between the phenolic rings) and C=O groups (oxidation process).
300	Significant mass loss with a pick at 422°C corresponding to the early stage of the resin degradation	Increase in the C=O groups and reduction of the C-C bonds. Increase of CH ₂ methylene groups and CH ₃ terminal groups (they probably form when the C-C chains break down).
Above 500	TG curve keeps decreasing, exhibiting a total mass loss of 40%.	Consistent reduction in peak intensity associated with CH ₂ and CH ₃ groups, that disappeared with the increase of temperature, indicating that the organic structure of the resin is progressively degrading.
1200	-	No traces of peaks due to complete resin degradation.

In summary, the degradation mechanism can be described as a sequence of two main steps:

- Above 300 °C, the cross-links gradually begin to break, and a fractioning of the methylene bridges is observed. The fracture of the bridges results in the release of the terminal groups and the formation of different volatile components (such as CO₂, H₂O [179] together with benzene, toluene, phenols and NH₃ [180]).
- Above 500 °C, there is a further fracture of the methylene bridges together with a collapse of the aromatic groups. The aromatic hydrogen and oxygen begin to be eliminated leading to the release of hydrocarbons, carbon oxides and hydrogen.

The resins in condition *B* and *C* have a very similar thermogravimetric curve to pristine resin (*A*). Both *B* and *C* show a further mass loss starting from 800°C which correlates with the graphite oxidation and the decomposition of the other constituents.

An interesting observation is related to the metal elements present in the master-batch. Metal fibres (iron), influence the polycondensation process as well as the resin degradation. The initial degradation temperature decreases from 354°C for the pure resin, to 303°C for the cured friction material. This reduction is of importance because of its relationship with the brake pad fading phenomenon.

Such effect is explained in literature [181] with a catalytic effect of metallic ions (e.g., Fe³⁺) that weakens the C-H bonds resulting in the breaking of molecular chains, with the formation of hydrogen radicals, very important for further resin degradation steps. The result is an anticipation of the oxidative resin degradation when it is heated in air. Among conditions *B* and *C*, the contact between the resin and the metals (closer in case *C*) is the only difference. This results in a small modification of the initial degradation temperature (346°C vs. 354°C). On the other hand, this behaviour is not observed in the presence of other constituents (e.g., carbon black [182], clay [183], silicon and boron [48]), which may have a stabilizing effect on the resin. There is, therefore, a synergic effect of added constituents with respect to phenolic resin degradation, although the properties of the resin itself are predominant.

A different study on two resins used in friction materials (*R1* and *R2*) was conducted to evaluate the degradation during storage, i.e., the natural ageing with time. The resins were in-door stored for fourteen months, under two different conditions: in a glass desiccator (normally exposed to natural light) and in a dark box (no light exposure, exposed to ambient humidity). A scanning calorimetry (DSC) run was performed every two months, to detect the glass transition temperatures (*T_g*). The changes in *T_g* over fourteen months are illustrated in Fig. 7.15.

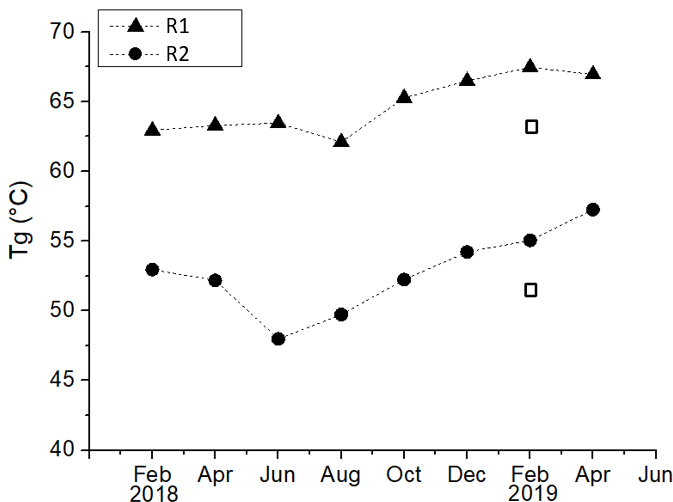


Fig. 7.15. Change in sample glass transition temperature (T_g) for the resin stored in a glass desiccator for 14 months. The white rectangles represent the T_g of the samples stored in the dark box after 12 months.

Both resins display a slightly increase in T_g , indicating the presence of structural changes; the resins, probably, begin a slow cross-linking process. R2 shows a faster increase than R1. Notably, resin samples stored in the dark (white rectangles in Fig. 7.15, after 12 months of storage) displayed no increase in glass transition temperature, clearly indicating that exposure to light has to be avoided.

Samples were also monitored via FTIR spectroscopy. Regretfully, FTIR data did not give specific information about chemical changes during storage, meaning that the magnitude of these changes is small. Anyway, the experimental results give important information to better characterize the behaviour of the resins and adopt better strategies to reduce their degradation kinetics, for instance, by avoiding exposure to light during storage.

7.3.3. Main results

The phenolic resin degradation has been studied considering two aspects: thermal stability and storage stability. As concerns the first one, two main steps of thermal degradation, correlate with different

chemical decomposition processes have been detected: above 300°C and above 500°C. Moreover, it was observed a reduction of the degradation temperature between the pure resin and the resin cured with the friction material of 51 °C. This phenomenon is related to the presence of the other ingredients, mainly metal components (Fe fibres). The study on storage stability was conducted monitoring the evolution of the glass transition temperature of two resins preserved in the laboratory. The detected slight increase of the T_g is an indication of the presence of a continuous cross-linking process. Furthermore, it was observed a negative effect of light exposure to storage stability.

Chapter 8

8. Conclusions and future perspectives

The states of California and Washington changed the law on brake pad certifications. This is causing the entire brake pad market to shift toward 'copper-free' formulations. In 2018, the Cu-free brake pads surpassed 50% of all granted certifications [101]. Many efforts were and still are being made by researchers to replace copper with other constituents. Satisfactory results have been achieved, although, based on state-of-the-art findings, none claimed success so far to achieve a complete Cu-free formulation efficient as Cu-full formulations. In this respect, several studies were performed to increase the knowledge about the role of copper in FMs, in view of its substitution.

Powder mixes of friction materials were used to produce pins for wear testing (pin-on-disc), so that the original formulations could be modified by adding or removing single components, using a little amount of material. Some targeted constituents have been considered and investigated with the aim of producing Cu-free formulations with comparable, or even better, performance than a reference Cu-full formulation. From the scientific point of view, the new formulations were evaluated considering the tribological properties (friction and wear), relevant to the mechanisms that take place at the materials interface, in order to fully understand them.

The starting point of the work was the validation of the methodology to produce the pins directly from the master-batch. These pins were compared to the pins extracted from a real brake pad produced with the same material. The "in house" produced pins resulted to be representative of the actual friction material properties. The approach is appropriate and strategic as a screening method for the selection of

pad constituents for novel formulations, since limited amounts only of powders are used. A minimum density of 2.2 g/cm^3 has to be achieved in the production of the samples in order to have a general improvement in friction material properties.

The study on the friction material formulations started with the investigation of the role of copper. It was removed from a reference commercial master-batch, and the performance of the material were compared with the original material. The removal of copper led to a reduction of the friction coefficient and an increase of wear. The SEM observations of the friction layer, which involves formation of primary and secondary plateaus, showed a coarse grain size and a low grade of compaction. Its observations (e.g. compaction, extension, composition) give hints on how to modify the composition to improve the tribological properties.

The commercial master-batch from which the copper was removed was used to produce novel Cu-free formulations. Copper fibres were replaced by steel fibres, as the formation mechanism of primary contact sites was proved to be the same. In this regard, the formation of a stable friction layer was guaranteed by adding barite in adequate concentrations. The use of barite instead of an otherwise environmentally critical material, like copper, into the formulation is advantageous because barite is considered fully inert and with no risk for human health. The Cu-free formulation, with the best combination of steel fibres and barite, displayed an improved wear behaviour and a stable friction coefficient, as compared to the reference Cu-full master-batch.

The investigation on balanced concentration of barite and steel fibres appeared promising also as regard to emissions. This result laid the basis for production of real brake pads in the ECOPADS project. In the project, novel formulations were developed, ranked and selected based on pin-on-disc test results, as concerns as both performance and emissions. The selected formulations were tested on a brake dynamometer and finally, the best material was tested on a real car. The project demonstrates the reliability of the experimental approach, which was used to obtain guidelines on how to develop the novel friction formulations.

Using the same experimental procedure, the work was extended to the study of the impact of other constituents, which were interesting from different aspects, in a Cu-free formulation. Fine natural graphite was proven to be strategic to form stable secondary plateaus, that provide favourable conditions for friction stabilization and improvements in wear performances. Fine agglomeration of mineral fibres increases the friction coefficient without affecting wear, and this could be promising to control the emissions. The investigation of the phenolic resin provided a better understanding of its degradation mechanisms, a fundamental aspect as concerns the detrimental effects on pad duration and particle emissions. It is observed that the temperature of the initial resin degradation is influenced by the constituents present in the formulation.

In brief, due to the many constituents in the brake friction materials, the complexity of the phenomena occurring at the contact interface between pad and disc is difficult to predict and interpret. Nevertheless, pads with good brake performance and eco-friendly properties can be developed balancing the constituents in effective concentrations, studying how each constituent contribute to the formation of the friction layer. A promising route to follow seems to be the attainment of the right balance between primary and secondary plateaus that together contribute to form a solid and tough friction layer.

The future of friction materials will be in the field of eco-friendly products, a critical selection of the constituents and the evaluation of emissions will have to be considered with increasing attention and concern.

References

- [1] H.P. Khairnar, V.M. Phalle, S.S. Mantha, Comparative frictional analysis of automobile drum and disc brakes, *Tribol. Ind.* 38 (2016) 11–23.
- [2] R.C. Dante, Friction materials, in: *Handb. Frict. Mater. Their Appl.*, Elsevier, 2016: pp. 1–6.
- [3] A. Rashid, Overview of disc brakes and related phenomena - A review, *Int. J. Veh. Noise Vib.* 10 (2014) 257–301.
- [4] G. Cueva, A. Sinatora, W.L. Guessser, A.P. Tschiptschin, Wear resistance of cast irons used in brake disc rotors, *Wear.* 255 (2003) 1256–1260.
- [5] S.W. Kim, K. Park, S.H. Lee, K.H. Kang, K.T. Lim, Thermophysical Properties of Automotive Metallic Brake Disk Materials, *Int. J. Thermophys.* 29 (2008) 2179–2188.
- [6] R. Renz, G. Seifert, W. Krenkel, Integration of CMC Brake Disks in Automotive Brake Systems, *Int. J. Appl. Ceram. Technol.* 9 (2012) 712–724.
- [7] A. Bonfanti, Low-impact friction materials for brake pads, University of Trento, 2016.
- [8] S.C. Lin, C.C. Guan, A.R.A. Bakar, M.R. Jamaluddin, Wan Mohd Musyris Wan Badri Abd, Disc Brake Squeal Suppression Through Chamfered and Slotted Pad, *Int. J. Veh. Struct. Syst.* 3 (2011) 28–35.
- [9] M. Nosonovsky, B. Bhushan, Multiscale friction mechanisms and hierarchical surfaces in nano- and bio-tribology, *Mater. Sci. Eng. R Reports.* 58 (2007) 162–193.
- [10] K.H. Zum Gahr, *Microstructure and Wear of Materials*, 1st ed., Tribology Series, Elsevier, Institute of Materials Technology, University of Siqen, 1987.
- [11] K.H. Czichos, K.H. Habig, *Handbook Tribologie, Reibung und Verschleiss*, 1992.
- [12] J.F. Archard, Contact and Rubbing of Flat Surfaces, *J. Appl. Phys.* 24 (1953) 981–988.
- [13] G. Straffellini, *Friction and Wear*, Springer International Publishing, Cham, 2015.
- [14] M.F. Ashby, J. Abulawi, H.S. Kong, Temperature Maps for Frictional Heating in Dry Sliding, *Tribol. Trans.* 34 (1991) 577–587.
- [15] F.E. Kennedy, Thermal and thermomechanical effects in dry sliding, *Wear.* 100 (1984) 453–476.

- [16] G. Sutter, N. Ranc, Flash temperature measurement during dry friction process at high sliding speed, *Wear*. 268 (2010) 1237–1242.
- [17] P.C. Verma, R. Ciudin, A. Bonfanti, P. Aswath, G. Straffelini, S. Gialanella, Role of the friction layer in the high-temperature pin-on-disc study of a brake material, *Wear*. 346–347 (2016) 56–65.
- [18] W. Österle, A.I. Dmitriev, Functionality of conventional brake friction materials – Perceptions from findings observed at different length scales, *Wear*. 271 (2011) 2198–2207.
- [19] M. Eriksson, S. Jacobson, Tribological surfaces of organic brake pads, *Tribol. Int.* 33 (2000) 817–827.
- [20] W. Österle, I. Dörfel, C. Prietzel, H. Rooch, A.-L. Cristol-Bulthé, G. Degallaix, Y. Desplanques, A comprehensive microscopic study of third body formation at the interface between a brake pad and brake disc during the final stage of a pin-on-disc test, *Wear*. 267 (2009) 781–788.
- [21] W. Österle, M. Griepentrog, T. Gross, I. Urban, Chemical and microstructural changes induced by friction and wear of brakes, *Wear*. 251 (2001) 1469–1476.
- [22] J. Kukutschová, V. Roubíček, K. Malachová, Z. Pavlíčková, R. Holuša, J. Kubačková, V. Mička, D. MacCrimmon, P. Filip, Wear mechanism in automotive brake materials, wear debris and its potential environmental impact, *Wear*. 267 (2009) 807–817.
- [23] P. Filip, Z. Weiss, D. Rafaja, On friction layer formation in polymer matrix composite materials for brake applications, *Wear*. 252 (2002) 189–198.
- [24] M. Eriksson, F. Bergman, S. Jacobson, On the nature of tribological contact in automotive brakes, *Wear*. 252 (2002) 26–36.
- [25] M. Eriksson, J. Lord, S. Jacobson, Wear and contact conditions of brake pads: dynamical in situ studies of pad on glass, *Wear*. 249 (2001) 272–278.
- [26] M.G. Jacko, P.H.S. Tsang, S.K. Rhee, Wear debris compaction and friction film formation of polymer composites, *Wear*. 133 (1989) 23–38.
- [27] W. Österle, I. Urban, Friction layers and friction films on PMC brake pads, *Wear*. 257 (2004) 215–226.
- [28] M. Eriksson, Friction and Contact Phenomena of Disc Brakes Related to Squeal, *Acta Univ. Ups.* (2000) 1–47.

- [29] P.J. Blau, H.M. Meyer, Characteristics of wear particles produced during friction tests of conventional and unconventional disc brake materials, *Wear*. 255 (2003) 1261–1269.
- [30] F. Eddoumy, H. Kasem, H. Dhieb, J.G. Buijsters, P. Dufrenoy, J.-P. Celis, Y. Desplanques, Role of constituents of friction materials on their sliding behavior between room temperature and 400°C, *Mater. Des.* 65 (2015) 179–186.
- [31] M. Federici, C. Menapace, A. Moscatelli, S. Gialanella, G. Straffelini, Pin-on-disc study of a friction material dry sliding against HVOF coated discs at room temperature and 300 °C, *Tribol. Int.* 115 (2017) 89–99.
- [32] J. Wahlström, V. Matejka, Y. Lyu, A. Söderberg, Contact Pressure and Sliding Velocity Maps of the Friction, Wear and Emission from a Low-Metallic/Cast-Iron Disc Brake Contact Pair, *Tribol. Ind.* 39 (2017) 460–470.
- [33] A. Heussaff, L. Dubar, T. Tison, M. Watremez, R.F. Nunes, A methodology for the modelling of the variability of brake lining surfaces, *Wear*. 289 (2012) 145–159.
- [34] D. Gultekin, M. Uysal, S. Aslan, M. Alaf, M.O. Guler, H. Akbulut, The effects of applied load on the coefficient of friction in Cu-MMC brake pad/Al-SiCp MMC brake disc system, *Wear*. 270 (2010) 73–82.
- [35] D. Chan, G.W. Stachowiak, Review of automotive brake friction materials, *Proc. Inst. Mech. Eng. Part D J. Automob. Eng.* 218 (2004) 953–966.
- [36] M. Arman, S. Singhal, P. Chopra, M. Sarkar, A review on material and wear analysis of automotive Break Pad, *Mater. Today Proc.* 5 (2018) 28305–28312.
- [37] V.V. Kumar, S.S. Kumaran, Friction material composite: types of brake friction material formulations and effects of various ingredients on brake performance—a review, *Mater. Res. Express.* 6 (2019) 082005.
- [38] K.L. Sundarkrishnaa, *Friction Material Composites*, 2nd ed., Springer International Publishing, 2015.
- [39] P. Filip, L. Kovarik, M.A. Wright, Automotive Brake Lining Characterization, in: *SAE Tech. Pap. Ser.*, 1997.
- [40] M. Eriksson, F. Bergman, S. Jacobson, Surface characterisation of brake pads after running under silent and squealing conditions, *Wear*. 232 (1999) 163–167.
- [41] J. Hwan Park, J. Oh Chung, H. Rae Kim, Friction

- characteristics of brake pads with aramid fiber and acrylic fiber, *Ind. Lubr. Tribol.* 62 (2010) 91–98.
- [42] N. Aranganathan, V. Mahale, J. Bijwe, Effects of aramid fiber concentration on the friction and wear characteristics of non-asbestos organic friction composites using standardized braking tests, *Wear.* 354–355 (2016) 69–77.
- [43] L. Mohammed, M.N.M. Ansari, G. Pua, M. Jawaid, M.S. Islam, A Review on Natural Fiber Reinforced Polymer Composite and Its Applications, *Int. J. Polym. Sci.* 2015 (2015) 1–15.
- [44] A.F. Gualtieri, E. Foresti, I.G. Lesci, N. Roveri, M.L. Gualtieri, M. Dondi, M. Zapparoli, The thermal transformation of Man Made Vitreous Fibers (MMVF) and safe recycling as secondary raw materials (SRM), *J. Hazard. Mater.* 162 (2009) 1494–1506.
- [45] J.-J. Lee, J.-A. Lee, S. Kwon, J.-J. Kim, Effect of different reinforcement materials on the formation of secondary plateaus and friction properties in friction materials for automobiles, *Tribol. Int.* 120 (2018) 70–79.
- [46] Y. Han, X. Tian, Y. Yin, Effects of ceramic fiber on the friction performance of automotive brake lining materials, *Tribol. Trans.* (2008).
- [47] P. Harrison, P. Holmes, R. Bevan, K. Kamps, L. Levy, H. Greim, Regulatory risk assessment approaches for synthetic mineral fibres, *Regul. Toxicol. Pharmacol.* 73 (2015) 425–441.
- [48] S. Li, F. Chen, B. Zhang, Z. Luo, H. Li, T. Zhao, Structure and improved thermal stability of phenolic resin containing silicon and boron elements, *Polym. Degrad. Stab.* 133 (2016) 321–329.
- [49] J. Kelly, I. Denry, Stabilized zirconia as a structural ceramic: An overview☆, *Dent. Mater.* 24 (2008) 289–298.
- [50] K.W. Hee, P. Filip, Performance of ceramic enhanced phenolic matrix brake lining materials for automotive brake linings, *Wear.* 259 (2005) 1088–1096.
- [51] J.-B. Donnet, E. Custodero, Reinforcement of Elastomers by Particulate Fillers, in: *Sci. Technol. Rubber*, Elsevier, 2013: pp. 383–416.
- [52] Y. Zhan, G. Zhang, Friction and wear behavior of copper matrix composites reinforced with SiC and graphite particles, *Tribol. Lett.* 17 (2004) 91–98.
- [53] H. Jang, K. Ko, S. Kim, R. Basch, J. Fash, The effect of metal fibers on the friction performance of automotive brake friction materials, *Wear.* 256 (2004) 406–414.
- [54] M. Kumar, J. Bijwe, Optimized selection of metallic fillers for

- best combination of performance properties of friction materials: A comprehensive study, *Wear*. 303 (2013) 569–583.
- [55] P. Cai, T. Wang, Q. Wang, Effect of several solid lubricants on the mechanical and tribological properties of phenolic resin-based composites, *Polym. Compos.* 36 (2015) 2203–2211.
- [56] R. Yun, S.G. Martynková, Y. Lu, Performance and evaluation of nonasbestos organic brake friction composites with SiC particles as an abrasive, *J. Compos. Mater.* 45 (2011) 1585–1593.
- [57] S. Venkatesh, K. Murugapoopathiraja, Scoping Review of Brake Friction Material for Automotive, *Mater. Today Proc.* 16 (2019) 927–933.
- [58] S.S. Kim, H.J. Hwang, M.W. Shin, H. Jang, Friction and vibration of automotive brake pads containing different abrasive particles, *Wear*. 271 (2011) 1194–1202.
- [59] IARC Working Group, Monographs on the Evaluation of Carcinogenic Risks to Humans. Man-made Vitreous Fibres, 2002.
- [60] W. Österle, A. Dmitriev, The Role of Solid Lubricants for Brake Friction Materials, *Lubricants*. 4 (2016) 5.
- [61] T.W. Scharf, S. V. Prasad, Solid lubricants: a review, *J. Mater. Sci.* 48 (2013) 511–531.
- [62] H. Wang, B. Xu, J. Liu, *Micro and Nano Sulfide Solid Lubrication*, Springer Berlin Heidelberg, Berlin, Heidelberg, 2012.
- [63] W. Österle, C. Prietzel, H. Kloß, A.I. Dmitriev, On the role of copper in brake friction materials, *Tribol. Int.* 43 (2010) 2317–2326.
- [64] K. Sathickbasha, A.S. Selvakumar, M.A.S. Balaji, B. Surya Rajan, The dual role of metal sulfides as lubricant and abrasive: an interface study in friction composite, *Mater. Res. Express*. 6 (2019) 045315.
- [65] L. Gudmand-Høyer, A. Bach, G.T. Nielsen, P. Morgen, Tribological properties of automotive disc brakes with solid lubricants, *Wear*. 232 (1999) 168–175.
- [66] A.R. Daei, D. Majumdar, P. Filip, Performance of Low-metallic Cu-free Brake Pads with Two Different Graphite Types, in: *SAE Tech. Pap. Ser.*, 2015.
- [67] M. Dienwiebel, N. Pradeep, G.S. Verhoeven, H.W. Zandbergen, J.W.M. Frenken, Model experiments of superlubricity of graphite, *Surf. Sci.* 576 (2005) 197–211.
- [68] N. Kumar, A.T. Kozakov, T.R. Ravindran, S. Dash, A.K. Tyagi,

- Load dependent friction coefficient of crystalline graphite and anomalous behavior of wear dimension, *Tribol. Int.* 88 (2015) 280–289.
- [69] O. von Uexküll, S. Skerfving, R. Doyle, M. Braungart, Antimony in brake pads-a carcinogenic component?, *J. Clean. Prod.* 13 (2005) 19–31.
- [70] J. Martinez, A.M. Echeberria, M. Zanon, A. Di Loreto, Characterization of the chemical reactions between solid lubricants and metal powders in low metallic brake pads during braking, *EuroBrake 2015.* (2015).
- [71] T. Peng, Q. Yan, Y. Zhang, X. Shi, M. Ba, Low-cost solid FeS lubricant as a possible alternative to MoS₂ for producing Fe-based friction materials, *Int. J. Miner. Metall. Mater.* 24 (2017) 115–121.
- [72] W. Österle, C. Deutsch, T. Gradt, G. Orts-Gil, T. Schneider, A.I. Dmitriev, Tribological screening tests for the selection of raw materials for automotive brake pad formulations, *Tribol. Int.* 73 (2014) 148–155.
- [73] X. Xiao, Y. Yin, J. Bao, L. Lu, X. Feng, Review on the friction and wear of brake materials, *Adv. Mech. Eng.* 8 (2016) 168781401664730.
- [74] B. Sugözü, B. Dağhan, Effect of BaSO₄ on Tribological Properties of Brake Friction Materials, *Int. J. Innov. Res. Sci. Eng. Technol.* 5 (2016) 30–35.
- [75] Y. LU, A combinatorial approach for automotive friction materials: Effects of ingredients on friction performance, *Compos. Sci. Technol.* 66 (2006) 591–598.
- [76] C. Cantoni, R. Cesarini, G. Mastinu, G. Rocca, R. Sicigliano, Brake comfort - A review, *Veh. Syst. Dyn.* 47 (2009) 901–947.
- [77] Factors Influencing Acoustic Performance of Sound Absorptive Materials, *Aust. J. Basic Appl. Sci.* (2009).
- [78] V.P. Sergienko, S.N. Bukharov, S.F. Mel'nikov, Vibration and noise in brake systems of mobile vehicles. Part 3: Forced low-frequency vibration (A Review), *J. Frict. Wear.* 33 (2012) 293–307.
- [79] R.C. Dante, Abrasives, ceramic, and inorganic materials, in: *Handb. Frict. Mater. Their Appl.*, Elsevier, 2016: pp. 105–121.
- [80] M. Křístková, Z. Weiss, P. Filip, Hydration properties of vermiculite in phenolic resin friction composites, *Appl. Clay Sci.* 25 (2004) 229–236.
- [81] R.C. Dante, *Handbook of Friction Materials and their*

- Applications, Elsevier, 2016.
- [82] B. Rodgers, W. Waddell, *The Science of Rubber Compounding*, in: *Sci. Technol. Rubber*, Elsevier, 2013: pp. 417–471.
- [83] L. Pilato, *Phenolic resins: 100Years and still going strong*, *React. Funct. Polym.* 73 (2013) 270–277.
- [84] U.S. Hong, S.L. Jung, K.H. Cho, M.H. Cho, S.J. Kim, H. Jang, *Wear mechanism of multiphase friction materials with different phenolic resin matrices*, *Wear.* 266 (2009) 739–744.
- [85] B. Strzemiescka, J. Zięba-Palus, A. Voelkel, T. Lachowicz, E. Socha, *Examination of the chemical changes in cured phenol-formaldehyde resins during storage*, *J. Chromatogr. A.* 1441 (2016) 106–115.
- [86] D. Ratna, *Handbook of Thermoset Resins*, 2009.
- [87] M. Asim, N. Saba, M. Jawaid, M. Nasir, M. Pervaiz, O. Y. Alothman, *A review on Phenolic resin and its Composites*, *Curr. Anal. Chem.* (2017).
- [88] F. Cardona, T. Aravinthan, C. Moscou, *Modified PF Resins for Composite Structures with Improved Mechanical Properties*, *Polym. Polym. Compos.* 18 (2010) 297–306.
- [89] D. Balgude, A.S. Sabnis, *CNSL: an environment friendly alternative for the modern coating industry*, *J. Coatings Technol. Res.* 11 (2014) 169–183.
- [90] J. Gao, Y. Liu, L. Yang, *Thermal stability of boron-containing phenol formaldehyde resin*, *Polym. Degrad. Stab.* 63 (1999) 19–22.
- [91] A.M. Kawamoto, L.C. Pardini, M.F. Diniz, V.L. Lourenço, M.F.K. Takahashi, *Synthesis of a boron modified phenolic resin*, *J. Aerosp. Technol. Manag.* 2 (2010) 169–182.
- [92] C. Li, Z. Ma, X. Zhang, H. Fan, J. Wan, *Silicone-modified phenolic resin: Relationships between molecular structure and curing behavior*, *Thermochim. Acta.* 639 (2016) 53–65.
- [93] A. Tejado, C. Peña, J. Labidi, J.M. Echeverria, I. Mondragon, *Physico-chemical characterization of lignins from different sources for use in phenol–formaldehyde resin synthesis*, *Bioresour. Technol.* 98 (2007) 1655–1663.
- [94] M. V. Alonso, M. Oliet, J.C. Domínguez, E. Rojo, F. Rodríguez, *Thermal degradation of lignin–phenol–formaldehyde and phenol–formaldehyde resol resins*, *J. Therm. Anal. Calorim.* 105 (2011) 349–356.
- [95] G. Nicholson, *Facts about friction*, P&W Price Enterprises, Inc.,

- Croydon, Pa., 1995.
- [96] Peter J. Blau, *Compositions, Functions, and Testing of Friction Brake Materials and Their Additives*, 2001. <http://www.ntis.gov/suppotVordernewabout.htm>.
- [97] C. Maltoni, Call for an international ban on asbestos, *Toxicol. Ind. Health*. 15 (1999) 529–531.
- [98] The Asbestos (Prohibitions) (Amendment) Regulations, (1999). <http://www.legislation.gov.uk/uksi/1999/2373/made>.
- [99] T. Ito, Hitachi Chemical Technical Report. *Automotive Parts for Environment, Safety and Comfort Performance*, (2013) 50–53. <https://www.hitachi-chem.co.jp/english/report/055.html>.
- [100] Brake friction material - Restrictions on use, substitute Senate Bill 6557, (2010).
- [101] Data portal for the State of Washington, <https://data.wa.gov/Natural-Resources-Environment/Better-Brakes-List-of-Certified-Parts/bv9x-jtbr>, (2018).
- [102] P.W. Lee, P. Filip, Friction and wear of Cu-free and Sb-free environmental friendly automotive brake materials, *Wear*. 302 (2013) 1404–1413.
- [103] M. Kumar, J. Bijwe, Non-asbestos organic (NAO) friction composites: Role of copper; its shape and amount, *Wear*. 270 (2011) 269–280.
- [104] P. Chandra Verma, L. Menapace, A. Bonfanti, R. Ciudin, S. Gialanella, G. Straffelini, Braking pad-disc system: Wear mechanisms and formation of wear fragments, *Wear*. 322–323 (2015) 251–258.
- [105] M. Kumar, J. Bijwe, NAO friction materials with various metal powders: Tribological evaluation on full-scale inertia dynamometer, *Wear*. 269 (2010) 826–837.
- [106] R. Gilardi, L. Alzati, M. Thiam, J.-F. Brunel, Y. Desplanques, P. Dufrénoy, S. Sharma, J. Bijwe, Copper Substitution and Noise Reduction in Brake Pads: Graphite Type Selection, *Materials (Basel)*. 5 (2012) 2258–2269.
- [107] G. Straffelini, R. Ciudin, A. Ciotti, S. Gialanella, Present knowledge and perspectives on the role of copper in brake materials and related environmental issues: A critical assessment, *Environ. Pollut.* 207 (2015) 211–219.
- [108] A.P. Davis, M. Shokouhian, S. Ni, Loading estimates of lead, copper, cadmium, and zinc in urban runoff from specific sources, *Chemosphere*. 44 (2001) 997–1009.
- [109] J. Wahlström, L. Olander, U. Olofsson, Size, Shape, and

- Elemental Composition of Airborne Wear Particles from Disc Brake Materials, *Tribol. Lett.* 38 (2010) 15–24.
- [110] C. Barlow, L.I. Bendell, C. Duckham, D. Faugeroux, V. Koo, Three-Dimensional Profiling Reveals Trace Metal Depositional Patterns in Sediments of Urban Aquatic Environments: A Case Study in Vancouver, British Columbia, Canada, *Water, Air, Soil Pollut.* 225 (2014) 1856.
- [111] J.F. Sandahl, D.H. Baldwin, J.J. Jenkins, N.L. Scholz, A Sensory System at the Interface between Urban Stormwater Runoff and Salmon Survival, *Environ. Sci. Technol.* 41 (2007) 2998–3004.
- [112] R. Franco, R. Sánchez-Olea, E.M. Reyes-Reyes, M.I. Panayiotidis, Environmental toxicity, oxidative stress and apoptosis: Ménage à Trois, *Mutat. Res. Toxicol. Environ. Mutagen.* 674 (2009) 3–22.
- [113] K.S. Rosselot, Copper Released from Brake Lining Wear in the San Francisco Bay Area, 2006.
- [114] A.K. Lund, J. Lucero, S. Lucas, M.C. Madden, J.D. McDonald, J.-C. Seagrave, T.L. Knuckles, M.J. Campen, Vehicular Emissions Induce Vascular MMP-9 Expression and Activity Associated With Endothelin-1-Mediated Pathways, *Arterioscler. Thromb. Vasc. Biol.* 29 (2009) 511–517.
- [115] J.A. Araujo, A.E. Nel, Particulate matter and atherosclerosis: role of particle size, composition and oxidative stress, *Part. Fibre Toxicol.* 6 (2009) 24.
- [116] M. Gasser, M. Riediker, L. Mueller, A. Perrenoud, F. Blank, P. Gehr, B. Rothen-Rutishauser, Toxic effects of brake wear particles on epithelial lung cells in vitro, *Part. Fibre Toxicol.* 6 (2009) 30.
- [117] Y.-C.T. Huang, A.J. Ghio, J. Stonehuerner, J. McGee, J.D. Carter, S.C. Grambow, R.B. Devlin, The Role of Soluble Components in Ambient Fine Particles-Induced Changes in Human Lungs and Blood, *Inhal. Toxicol.* 15 (2003) 327–342.
- [118] T. Grigoratos, G. Martini, Brake wear particle emissions: a review, *Environ. Sci. Pollut. Res.* 22 (2015) 2491–2504.
- [119] G. Knothe, C.A. Sharp, T.W. Ryan, Exhaust Emissions of Biodiesel, Petrodiesel, Neat Methyl Esters, and Alkanes in a New Technology Engine †, *Energy & Fuels.* 20 (2006) 403–408.
- [120] P. Pant, R.M. Harrison, Estimation of the contribution of road traffic emissions to particulate matter concentrations from field measurements: A review, *Atmos. Environ.* 77 (2013) 78–97.

- [121] G. Perricone, M. Alemani, J. Wahlström, U. Olofsson, A proposed driving cycle for brake emissions investigation for test stand, *Proc. Inst. Mech. Eng. Part D J. Automob. Eng.* (2019) 095440701984122.
- [122] G. Perricone, V. Matějka, M. Alemani, J. Wahlström, U. Olofsson, A Test Stand Study on the Volatile Emissions of a Passenger Car Brake Assembly, *Atmosphere (Basel)*. 10 (2019) 263.
- [123] J. Kukutschová, V. Roubíček, M. Mašláň, D. Jančík, V. Slovák, K. Malachová, Z. Pavlíčková, P. Filip, Wear performance and wear debris of semimetallic automotive brake materials, *Wear*. 268 (2010) 86–93.
- [124] V. Roubicek, H. Raclavska, D. Juchelkova, P. Filip, Wear and environmental aspects of composite materials for automotive braking industry, *Wear*. 265 (2008) 167–175.
- [125] C. Terzano, F. Di Stefano, V. Conti, E. Graziani, A. Petroianni, Air pollution ultrafine particles: toxicity beyond the lung, *Eur. Rev. Med. Pharmacol. Sci.* 14 (2010) 809–21.
- [126] M. Franchini, A. Guida, A. Tufano, A. Coppola, Air pollution, vascular disease and thrombosis: linking clinical data and pathogenic mechanisms, *J. Thromb. Haemost.* 10 (2012) 2438–2451.
- [127] B.D. Garg, S.H. Cadle, P.A. Mulawa, P.J. Groblicki, C. Laroo, G.A. Parr, Brake Wear Particulate Matter Emissions, *Environ. Sci. Technol.* 34 (2000) 4463–4469.
- [128] R.M. Harrison, A.M. Jones, J. Gietl, J. Yin, D.C. Green, Estimation of the Contributions of Brake Dust, Tire Wear, and Resuspension to Nonexhaust Traffic Particles Derived from Atmospheric Measurements, *Environ. Sci. Technol.* 46 (2012) 6523–6529.
- [129] F. Amato, M. Pandolfi, A. Escrig, X. Querol, A. Alastuey, J. Pey, N. Perez, P.K. Hopke, Quantifying road dust resuspension in urban environment by Multilinear Engine: A comparison with PMF2, *Atmos. Environ.* 43 (2009) 2770–2780.
- [130] V. Mahale, J. Bijwe, S. Sinha, Efforts towards green friction materials, *Tribol. Int.* 136 (2019) 196–206.
- [131] R. Yun, P. Filip, Y. Lu, Performance and evaluation of eco-friendly brake friction materials, *Tribol. Int.* 43 (2010) 2010–2019.
- [132] Y.H. Chang, B.S. Joo, S.M. Lee, H. Jang, Size effect of tire rubber particles on tribological properties of brake friction

- materials, *Wear*. 394–395 (2018) 80–86.
- [133] I. Rampin, M. Zanon, J. Echeberria, A.M. Martínez, A. Di Loreto, Development of copper-free low steel brake pads for passenger cars, *Proc. 2014 World Congr. Powder Metall. Part. Mater.* (2014).
- [134] S. Tiwari, J. Bijwe, S. Panier, Role of Nano-YbF₃-Treated Carbon Fabric on Improving Abrasive Wear Performance of Polyetherimide Composites, *Tribol. Lett.* 42 (2011) 293–300.
- [135] N. Aranganathan, J. Bijwe, Comparative performance evaluation of NAO friction materials containing natural graphite and thermo-graphite, *Wear*. 358–359 (2016) 17–22.
- [136] P. Fernao, T. Desirè, S. Razo, D. Adolfo, K. Arno, Bio-soluble mineral fibres: Alternative chemical compositions and the effect in disc pad applications, *Tech. Pap. Present. Published Eurobrake 2016, Milan, Italy.* (2016).
- [137] P.V. Gurunath, J. Bijwe, Friction and wear studies on brake-pad materials based on newly developed resin, *Wear*. 263 (2007) 1212–1219.
- [138] M.C. Lagel, L. Hai, A. Pizzi, M.C. Basso, L. Delmotte, S. Abdalla, A. Zahed, F.M. Al-Marzouki, Automotive brake pads made with a bioresin matrix, *Ind. Crops Prod.* 85 (2016) 372–381.
- [139] U.D. Idris, V.S. Aigbodion, I.J. Abubakar, C.I. Nwoye, Eco-friendly asbestos free brake-pad: Using banana peels, *J. King Saud Univ. - Eng. Sci.* 27 (2015) 185–192.
- [140] E. Omrani, P.L. Menezes, P.K. Rohatgi, State of the art on tribological behavior of polymer matrix composites reinforced with natural fibers in the green materials world, *Eng. Sci. Technol. an Int. J.* 19 (2016) 717–736.
- [141] L. Han, L. Huang, J. Zhang, Y. Lu, Optimization of ceramic friction materials, *Compos. Sci. Technol.* 66 (2006) 2895–2906.
- [142] J. Wahlström, A Factorial Design to Numerically Study the Effects of Brake Pad Properties on Friction and Wear Emissions, *Adv. Tribol.* 2016 (2016) 1–10.
- [143] M. Alemani, G. Perricone, U. Olofsson, A. Söderberg, A proposed dyno bench test cycle to study particle emissions from disc brakes, in: *Eurobrake 2014 Conf., Lille, France, 2014.*
- [144] M. Federici, M. Alemani, C. Menapace, S. Gialanella, G. Perricone, G. Straffelini, A critical comparison of dynamometer data with pin-on-disc data for the same two friction material pairs – A case study, *Wear*. 424–425 (2019) 40–

- [145] J. Wahlström, Y. Lyu, V. Matjeka, A. Söderberg, A pin-on-disc tribometer study of disc brake contact pairs with respect to wear and airborne particle emissions, *Wear*. 384–385 (2017) 124–130.
- [146] S., Hussain, M., Abdul Hamid, A., Mat Lazim, A.R. Abu Bakar, Brake Wear Particle Size and Shape Analysis of Non-Asbestos Organic (NAO) and Semi Metallic Brake Pad, *J. Teknol.* 71 (2014).
- [147] G. Perricone, V. Matějka, M. Alemani, G. Valota, A. Bonfanti, A. Ciotti, U. Olofsson, A. Söderberg, J. Wahlström, O. Nosko, G. Straffelini, S. Gialanella, M. Ibrahim, A concept for reducing PM 10 emissions for car brakes by 50%, *Wear*. 396–397 (2018) 135–145.
- [148] Lowbrasys, <http://www.lowbrasys.eu/en/>, (2019).
- [149] ECOPADS, <https://www.ecobrakes.eu/>, (2019).
- [150] MAUD, <http://maud.radiographema.eu/>, (2019).
- [151] T.S. Eyre, R.F. Iles, D.W. Gasson, Wear characteristics of flake and nodular graphite cast iron, *Wear*. 13 (1969) 229–245.
- [152] ASM, Vol 1: Properties and Selection: Irons, Steels, and High-Performance Alloys, ASM International, 1990.
- [153] A.C.P. Rodrigues, W. Österle, T. Gradt, C.R.F. Azevedo, Impact of copper nanoparticles on tribofilm formation determined by pin-on-disc tests with powder supply: Addition of artificial third body consisting of Fe₃O₄, Cu and graphite, *Tribol. Int.* 110 (2017) 103–112.
- [154] U. Olofsson, L. Olander, A. Jansson, A Study of Airborne Wear Particles Generated From a Sliding Contact, *J. Tribol.* 131 (2009).
- [155] L. Chasapidis, T. Grigoratos, A. Zygogianni, A. Tsakis, A.G. Konstandopoulos, Study of Brake Wear Particle Emissions of a Minivan on a Chassis Dynamometer, *Emiss. Control Sci. Technol.* 4 (2018) 271–278.
- [156] P.G. Sanders, T.M. Dalka, R.H. Basch, A reduced-scale brake dynamometer for friction characterization, *Tribol. Int.* 34 (2001) 609–615.
- [157] G. Perricone, J. Wahlström, U. Olofsson, Towards a test stand for standardized measurements of the brake emissions, *Proc. Inst. Mech. Eng. Part D J. Automob. Eng.* 230 (2016) 1521–1528.
- [158] V. Matějka, I. Metinöz, J. Wahlström, M. Alemani, G. Perricone, On the running-in of brake pads and discs for dyno

- bench tests, *Tribol. Int.* 115 (2017) 424–431.
- [159] S. Karabay, K. Baynal, C. İğdeli, Detecting Groan Sources in Drum Brakes of Commercial Vehicles by TVA-FMEA: A Case Study, *Strojniški Vestn. – J. Mech. Eng.* 57 (2013) 375–386.
- [160] P.D.D. Neis, N.F.F. Ferreira, G. Fekete, L.T.T. Matozo, D. Masotti, Towards a better understanding of the structures existing on the surface of brake pads, *Tribol. Int.* 105 (2017) 135–147.
- [161] N. Aranganathan, J. Bijwe, Development of copper-free eco-friendly brake-friction material using novel ingredients, *Wear.* 352–353 (2016) 79–91.
- [162] M. Kumar, J. Bijwe, Role of different metallic fillers in non-asbestos organic (NAO) friction composites for controlling sensitivity of coefficient of friction to load and speed, *Tribol. Int.* 43 (2010) 965–974.
- [163] D.A. Rigney, S. Karthikeyan, The Evolution of Tribomaterial During Sliding: A Brief Introduction, *Tribol. Lett.* 39 (2010) 3–7.
- [164] B. Venkataraman, G. Sundararajan, Correlation between the characteristics of the mechanically mixed layer and wear behaviour of aluminium, Al-7075 alloy and Al-MMCs, *Wear.* 245 (2000) 22–38.
- [165] W.. Rainforth, Microstructural evolution at the worn surface: a comparison of metals and ceramics, *Wear.* 245 (2000) 162–177.
- [166] D.. Rigney, Transfer, mixing and associated chemical and mechanical processes during the sliding of ductile materials, *Wear.* 245 (2000) 1–9.
- [167] N. Konduru, J. Keller, L. Ma-Hock, S. Gröters, R. Landsiedel, T.C. Donaghey, J.D. Brain, W. Wohlleben, R.M. Molina, Biokinetics and effects of barium sulfate nanoparticles, *Part. Fibre Toxicol.* (2014).
- [168] G.S. Abubakar, B.A. Yagana, M. Zarah, Environmental and health hazards associated with exploration of barite from Bukkuyum (Zamfara State), Nigeria, *ISABB J. Heal. Environ. Sci.* 2 (2015) 11–15.
- [169] N. Dureja, J. Bijwe, P.V. Gurunath, Role of Type and Amount of Resin on Performance Behavior of Non-asbestos Organic (NAO) Friction Materials, *J. Reinf. Plast. Compos.* 28 (2009) 489–497.
- [170] H. Yang, R. Luo, S. Han, M. Li, Effect of the ratio of

- graphite/pitch coke on the mechanical and tribological properties of copper-carbon composites, *Wear*. 268 (2010) 1337–1341.
- [171] P. Jayashree, M. Federici, L. Bresciani, S. Turani, R. Sicigliano, G. Straffelini, Effect of Steel Counterface on the Dry Sliding Behaviour of a Cu-Based Metal Matrix Composite, *Tribol. Lett.* 66 (2018) 123.
- [172] M. Federici, S. Gialanella, M. Leonardi, G. Perricone, G. Straffelini, A preliminary investigation on the use of the pin-on-disc test to simulate off-brake friction and wear characteristics of friction materials, *Wear*. 410–411 (2018) 202–209.
- [173] F. Persoon, D. Tegels, S. Razo, Diego Adolfo, A. Kerssemakers, Bio-soluble mineral fibres: alternative chemical compositions and the Effect in disc pad applications, *EuroBrake 2016, Milan, Italy*. (2016).
- [174] B.K. Satapathy, J. Bijwe, Influence of operating parameters on the performance of friction composites based on combinations of rock fibers and organic fibers, *J. Reinf. Plast. Compos.* 24 (2005) 579–595.
- [175] T. Singh, A. Patnaik, Performance assessment of lapinus-aramid based brake pad hybrid phenolic composites in friction braking, *Arch. Civ. Mech. Eng.* 15 (2015) 151–161.
- [176] B.M. deRonde, A.L. Carbone, K. Uhrich, Storage stability study of salicylate-based Poly(anhydride-esters), *Polym. Degrad. Stab.* 95 (2010) 1778–1782.
- [177] I. Janigová, I. Laciík, I. Chodák, Thermal degradation of plasticized poly(3-hydroxybutyrate) investigated by DSC, *Polym. Degrad. Stab.* 77 (2002) 35–41.
- [178] C.. Santos, B.. Freedman, K.. Leach, D.. Press, M. Scarpulla, E. Mathiowitz, Poly(fumaric-co-sebacic anhydride), *J. Control. Release.* 60 (1999) 11–22.
- [179] S. Ramousse, J.W. Høj, O.T. Sørensen, Thermal characteristic of brake pads, *J. Therm. Anal. Calorim.* 64 (2001) 933–943.
- [180] L. Di Gregorio, S. Ronchetti, B. Onida, Phenolic resins emissions upon thermal degradation, in: *EuroBrake, 4-6 May 2015, Dresden Germany, 2015*: pp. 4–6.
- [181] M. Křístková, P. Filip, Z. Weiss, R. Peter, Influence of metals on the phenol-formaldehyde resin degradation in friction composites, *Polym. Degrad. Stab.* 84 (2004) 49–60.
- [182] L. Asaro, D.A. D’Amico, V.A. Alvarez, E.S. Rodriguez, L.B.

- Manfredi, Impact of different nanoparticles on the thermal degradation kinetics of phenolic resin nanocomposites, *J. Therm. Anal. Calorim.* 128 (2017) 1463–1478.
- [183] L.B. Manfredi, D. Puglia, A. Tomasucci, J.M. Kenny, A. Vázquez, Influence of Clay Modification on the Properties of Resol Nanocomposites, *Macromol. Mater. Eng.* 293 (2008) 878–886.

Appendices

- I. List of publications.
- II. Participation to Congresses, Schools and Workshops.
- III. Acknowledgments.

I. List of publications

- Cinzia Menapace, Mara Leonardi, Guido Perricone, Mauro Bortolotti, Giovanni Straffelini, Stefano Gialanella. Pin-on-disc study of brake friction materials with ball-milled nanostructured components. *Materials and Design*, 115 (2017) 287–298.
- Cinzia Menapace, Mara Leonardi, Vlastimil Matějka, Stefano Gialanella, Giovanni Straffelini. Dry sliding behavior and friction layer formation in copper-free barite containing friction materials. *Wear*, 398–399 (2018) 191–200.
- Mara Leonardi, Cinzia Menapace, Vlastimil Matějka, Stefano Gialanella, Giovanni Straffelini. Pin-on-disc investigation on copper-free friction materials dry sliding against cast iron. *Tribology International*, 119 (2018) 73–81.
- Matteo Federici, Stefano Gialanella, Mara Leonardi, Guido Perricone, Giovanni Straffelini. A preliminary investigation on the use of the pin-on-disc test to simulate off-brake friction and wear characteristic of friction materials. *Wear*, 410–411 (2018) 202–209.
- Cinzia Menapace, Mara Leonardi, Maria Secchi, Andrea Bonfanti, Stefano Gialanella, Giovanni Straffelini. Thermal behavior of a phenolic resin for brake pad manufacturing. *Journal of Thermal Analysis and Calorimetry*, 137 (2019) 759–766.
- Yezhe Lyu, Mara Leonardi, Jens Wahlström, Stefano Gialanella, Ulf Olofsson. Friction, wear and airborne particle emission of Cu-free eco-friendly brake materials. *Tribology International*, 141 (2020) 105959.
- Mara Leonardi, Mattia Alemani, Giovanni Straffelini, Stefano Gialanella. A pin-on-disc study on the dry sliding behavior of a Cu-free friction material containing different types of natural graphite. *Wear*, 442–443 (2020) 203157.

Publications and presentations to congresses

- Mara Leonardi, Andrea Dorigato, Cinzia Menapace, Luca Menapace, Stefano Gialanella, Giovanni Straffelini. Disc brake pads regeneration: preliminary investigation of the re-use of worn friction materials. *Oral presentation*, EuroBrake 2019/EB2019-EBS-008, May 2019, Dresden, Germany.
- Yezhe Lyu, Mara Leonardi, Jijie Ma, Jens Wahlström, Stefano Gialanella, Ulf Olofsson. A pin-on-disc study on the friction, wear and airborne particle emission from recycled brake pad material. *Technical paper*, EuroBrake 2019/EB2019-FBR-028, May 2019, Dresden, Germany.
- Jijie Ma, Anna Hedlund Åström, Ulf Olofsson, Yezhe Lyu, Mara Leonardi, Jens Wahlström. Eco design of brake pads with recycled friction materials. *Technical paper*, EuroBrake 2019/EB2019-EBS-017, May 2019, Dresden, Germany.
- Mara Leonardi, Cinzia Menapace, Mattia Alemani, Giovanni Straffelini, Stefano Gialanella. Effect of density on the mechanical and wear behaviour of friction materials for braking systems. *Poster presentation*, 22nd International Conference on Wear of Materials, April 2019, Miami, Florida, USA.

II. Participation to Workshops, Schools and Congresses

- AIM course 'Tenacità e resistenza a fatica dei materiali metallici', June 6th-7th 2017, Milan, Italy;
- AIM course 'Prove meccaniche', June 20th-22nd 2017, Trento, Italy;
- LOWBRASYS Workshop: Simulation and Modelling in the field of brake systems, October 11th - 12th 2017, KTH, Stockholm, Sweden;
- Topstars 2017 Winter School, November 6th - 15th 2017, Trento, Italy;
- Workshop Cobra porta il cemento nei freni, March 27th 2018, Kilometro rosso innovation district, Bergamo, Italy;
- Eurobrake 2018, May 22nd - 24th 2018, Den Haag, Holland.
- EIT Raw materials SusCritMat (Sustainable Management of Critical Raw Materials) Autumn School for Professionals, October 24th-26th 2018, Delft, Netherlands;
- EIT Raw Materials Academy Bootcamp TNTM (Talk Nerdy To Me), July 2nd-4th 2018, Goslar, Germany;
- Bootstrap course 'Percorso di formazione imprenditoriale per lo sviluppo di idee innovative', Hub Innovation Trentino, September 19th 2018 - January 15th 2019, Trento, Italy;
- 22nd International Conference on Wear of Materials, April 14th - 18th 2019, Miami, Florida, USA;
- Eurobrake 2019, May 21st-23rd 2019, Dresden, Germany.
- ECOPADS Workshop 'Non-exhaust vehicular emissions', July 5th 2019, Riva del Garda, Italy;
- 7th International Biennial Conference 'Ultrafine Grained and Nanostructured Materials', September 1st-3rd 2019, Trento, Italy;
- AIM course 'Additive Metallurgy', September 16th-17th 2019, Milan, Italy;
- Winter School ECOPADS 2019 'From Linear to Circular Thinking', December 2nd - 6th 2019, Trento, Italy.

III. Acknowledgments

The research has received financial support by the EIT-Raw Materials through the EU Project: ECOPADS – Eliminating COpper from brake PADS & recycling. – n. 17182.

I would like to express my sincere gratitude to both my supervisors Prof. Stefano Gialanella and Prof. Giovanni Straffelini. I could not have had a better guide during my PhD.

Thanks to the people that work at the Department of Industrial Engineering. Thanks to Brembo S.p.A., Ing. Guido Perricone, Dr. Mattia Alemani and all the research team of the Advanced R&D Department. I found skilled people who have provided me with constant and precious support to carry on my research activity.

My heartfelt thankfulness goes to those who have sustained me side-by-side in my daily work. Thanks above all to Cinzia for her invaluable assistance; thanks to Matteo for having always tried to answer my questions; thanks to all my colleagues. Over the past few years, it has been nice to wake up in the morning and go to work!

Thanks to Marco for a long list of things, and Michela, a dear friend. Last but not the least, Massimo. I would give him most of the credit for getting here.

Finally, a thought to my family who is the inspiration for everything I do.

Grazie.